

## INFORMATION TO USERS

This manuscript has been reproduced from the microfilm master. UMI films the text directly from the original or copy submitted. Thus, some thesis and dissertation copies are in typewriter face, while others may be from any type of computer printer.

**The quality of this reproduction is dependent upon the quality of the copy submitted.** Broken or indistinct print, colored or poor quality illustrations and photographs, print bleedthrough, substandard margins, and improper alignment can adversely affect reproduction.

In the unlikely event that the author did not send UMI a complete manuscript and there are missing pages, these will be noted. Also, if unauthorized copyright material had to be removed, a note will indicate the deletion.

Oversize materials (e.g., maps, drawings, charts) are reproduced by sectioning the original, beginning at the upper left-hand corner and continuing from left to right in equal sections with small overlaps. Each original is also photographed in one exposure and is included in reduced form at the back of the book.

Photographs included in the original manuscript have been reproduced xerographically in this copy. Higher quality 6" x 9" black and white photographic prints are available for any photographs or illustrations appearing in this copy for an additional charge. Contact UMI directly to order.

# UMI

A Bell & Howell Information Company  
300 North Zeeb Road, Ann Arbor MI 48106-1346 USA  
313/761-4700 800/521-0600



**MODEL-ORDER REDUCTION TECHNIQUES FOR CIRCUITS  
AND INTERCONNECTS SIMULATION**

BY

WENDEMAGEGNEHU TSEGAYE BEYENE

B.S., Columbia University, 1988

M.S., Columbia University, 1991

THESIS

Submitted in partial fulfillment of the requirements  
for the degree of Doctor of Philosophy in Electrical Engineering  
in the Graduate College of the  
University of Illinois at Urbana-Champaign, 1997

Urbana, Illinois

**UMI Number: 9737051**

---

**UMI Microform 9737051**  
**Copyright 1997, by UMI Company. All rights reserved.**

**This microform edition is protected against unauthorized  
copying under Title 17, United States Code.**

---

**UMI**  
**300 North Zeeb Road**  
**Ann Arbor, MI 48103**

© Copyright by Wendemagegnehu Tsegaye Beyene, 1997

UNIVERSITY OF ILLINOIS AT URBANA-CHAMPAIGN  
THE GRADUATE COLLEGE

FEBRUARY 1997  
(date)

WE HEREBY RECOMMEND THAT THE THESIS BY

WENDEMAGEGNEHU TSEGAYE BEYENE

ENTITLED MODEL-ORDER REDUCTION TECHNIQUES FOR CIRCUITS

AND INTERCONNECTS SIMULATION

BE ACCEPTED IN PARTIAL FULFILLMENT OF THE REQUIREMENTS FOR

THE DEGREE OF DOCTOR OF PHILOSOPHY

*Jose E. Schutt-Aine*

Director of Thesis Research

*G. W. Kang*

Head of Department

Committee on Final Examination†

*Jose E. Schutt-Aine*

Chairperson

*W. C. Crou*

*Donald Haff*

*Paul Snyper*

† Required for doctor's degree but not for master's.

# MODEL-ORDER REDUCTION TECHNIQUES FOR CIRCUITS AND INTERCONNECTS SIMULATION

**Wendemagegnehu Tsegaye Beyene, Ph.D.**  
**Department of Electrical and Computer Engineering**  
**University of Illinois at Urbana-Champaign, 1997**  
**José E. Schutt-Ainé, Advisor**

This dissertation addresses model-order reduction techniques for use in analog circuit simulation. Efficient yet accurate modeling and simulation methods of circuits and interconnects are developed. Particularly, charge carrier diffusion in  $p$ - $n$  junction devices and wave propagation in frequency-dependent electromagnetic systems are solved.

Recently, Padé synthesis has been applied to analyze large, linear networks, and an efficiency of two- to three-orders of magnitude in speed over conventional methods has been obtained. The miniaturization of the devices and the increase in operating frequency of integrated circuits have placed more emphasis not only on the efficiency of the simulation methods, but also on the accuracy of the synthesis techniques. It has become increasingly apparent that the traditional, equivalent circuit representations are not adequate to deal with the intricate physical effects that become more prominent with the reducing dimension, growing packing density, and increasing frequency of operation. Therefore, methods that are solely based on Padé synthesis cannot guarantee the accurate simulation of complex networks. Advanced simulation techniques and powerful models are indispensable in the design of future systems.

The basic goal of this dissertation is to extend the use of order-reduction techniques as accurate methods for analyzing complex electronic systems. The theoretical and practical aspects of moment-matching, Krylov subspace-based methods, and rational approximations techniques are studied. The moment-matching techniques are directly applied to  $p$ - $n$  junction device equations to accurately model the carrier dynamic in the junctions. A robust approximation technique that uses Householder orthogonalization techniques is developed to generate macromodels of electromagnetic systems, such as frequency-dependent coupled transmission lines. A pole-clustering technique with inverse distance-measure criterion is

used to further reduce the models. This allows the efficient accurate simulation of frequency-dependent coupled transmission lines characterized by scattering parameters and an optimal reference system. The heterogeneous reduction techniques are woven into a unified method by using network partitioning techniques. Recursive convolution is used to speedup the transient simulation. The method does not suffer from aliasing or round-off errors caused by nonband-limited frequency responses, nor by numerical transforms of a large number of points, respectively.



## **DEDICATION**

*To the Memory of my Father,  
Tsegaye Beyene.*

## ACKNOWLEDGMENTS

I would like to thank my advisor, Professor José E. Schutt-Ainé, for providing an ideal environment for my research and for his guidance throughout the course of my graduate study at the University of Illinois.

I would like to thank Professors Weng Chew, Ibrahim Hajj and Paul Saylor for serving on my preliminary and final examination committees, and for their many useful suggestions during my research. I am also thankful to Professor Kyle A. Gallivan and Dr. Dmitri Kuznetsov for many fruitful discussions related to this dissertation. I acknowledge my colleagues and friends at the Center for Computational Electromagnetics for many technical discussions.

I owe a great deal of thanks to my colleagues and friends at IBM Corp. The friendships of Mr. Ching Tong, Mr. Ali Sarfaraz and Dr. Peter VanDyke are appreciated. I am grateful to Mr. Harvey Hamel, who was an invaluable resource throughout my years at IBM. He always impressed me with his knowledge, and his ability and willingness to share it with others. The encouragement and caring that I received from my former manager, Mr. Harsaran Bhatia, is highly appreciated. I would like to express my regard and respect for Professor Fung-Yuel Chang whom I was fortunate to work with.

I would like to thank the University of Illinois, the SURGE fellowship program, NSF, and AFSOR (via the MURI program) for their financial support. Special thanks goes to the director of SURGE fellowship program, Professor Preston Ransom.

Last, but not least, I express my deepest gratitude and love to my mother, Elfenish Gebre-Tsadik, and my sisters who have been a constant source of love and support. I will always be grateful to them for encouraging me to pursue my ideals. Finally, it is with love and appreciation that I thank my wife Yewubdar Legesse, whose love, friendship and understanding were invaluable to the timely completion of this dissertation.

## TABLE OF CONTENTS

| CHAPTER  | PAGE |
|--|------|
| <b>1 INTRODUCTION</b> .....  | 1    |
| 1.1 Background.....  | 1    |
| 1.2 Overview.....  | 3    |
| <b>2 REVIEW OF CIRCUIT SIMULATION TECHNIQUES</b> .....                                 | 7    |
| 2.1 Introduction.....  | 7    |
| 2.2 Traditional Simulation Techniques.....   | 8    |
| 2.3 Waveform Relaxation Techniques.....  | 9    |
| 2.4 Modeling and Simulation of Distributed Systems.....                                | 10   |
| 2.5 Padé Synthesis.....  | 13   |
| 2.5.1 Moment-matching methods.....   | 15   |
| 2.5.2 Krylov subspace-based methods.....   | 16   |
| 2.6 Rational Approximation Techniques.....   | 17   |
| <b>3 PADÉ ANALYSIS VIA MOMENT-MATCHING AND KRYLOV<br/>SUBSPACE-BASED METHODS</b> ..... | 18   |
| 3.1 Introduction.....  | 18   |
| 3.2 Frequency-Domain Analysis.....   | 20   |
| 3.3 Moment-Matching Methods.....   | 22   |
| 3.3.1 Moment calculation.....  | 22   |
| 3.3.2 Moment matching.....   | 25   |
| 3.3.3 Frequency shifting.....  | 27   |
| 3.3.4 Frequency scaling.....   | 27   |
| 3.3.5 Complexity.....  | 28   |
| 3.3.6 Stability.....   | 29   |
| 3.3.7 Advances in moment-matching techniques.....                                      | 30   |
| 3.4 Krylov Subspace-Based Methods.....   | 32   |
| 3.4.1 Krylov subspace method.....  | 33   |
| 3.4.2 Arnoldi algorithm.....   | 35   |
| 3.4.3 Lanczos algorithm.....   | 37   |
| 3.4.4 Computing poles and residues.....  | 39   |
| 3.5 Applications.....  | 42   |
| 3.5.1 Example 3.1: RLC circuit.....  | 43   |
| 3.5.2 Example 3.2: RLC interconnect network.....                                       | 47   |
| 3.5.3 Example 3.3: Coaxial cable with skin effect.....                                 | 49   |
| 3.5.4 Example 3.3: An example of RC-ladder network.....                                | 51   |
| 3.6 Conclusions.....   | 53   |

|  |     |
|--|-----|
| <b>4 ACCURATE ANALYSIS OF DIODE SWITCHING CHARACTERISTICS USING ASYMPTOTIC WAVEFORM EVALUATION</b> ..... | 55  |
| 4.1 Introduction.....  | 55  |
| 4.2 AWE Diode Modeling.....  | 58  |
| 4.3 Numerical Results.....   | 65  |
| 4.4 Conclusions.....   | 73  |
| <br>   |     |
| <b>5 FREQUENCY-DOMAIN MODELING AND SIMULATION TECHNIQUES</b> .....                                       | 74  |
| 5.1 Introduction.....  | 74  |
| 5.2 Multiport Network.....   | 77  |
| 5.3 Approximation.....   | 79  |
| 5.3.1 Interpolation by rational functions .....  | 81  |
| 5.3.2 Approximation of a network function .....  | 83  |
| 5.3.3 Numerical considerations .....   | 86  |
| 5.4 Model-Order Reduction Using Pole-Clustering Technique .....  | 90  |
| 5.5 Recursive Convolution .....  | 94  |
| 5.5.1 Derivation of recursive convolution equations.....   | 95  |
| 5.6 Numerical Results.....   | 97  |
| 5.6.1 Example 5.1: Linear network.....   | 98  |
| 5.6.1 Example 5.2: Nonlinear network.....  | 104 |
| 5.7 Conclusions.....   | 106 |
| <br>   |     |
| <b>6 ANALYSIS OF FREQUENCY-DEPENDENT COUPLED TRANSMISSION LINES</b> .....                                | 107 |
| 6.1 Introduction.....  | 107 |
| 6.2 Transmission Line Equations.....   | 109 |
| 6.3 Scattering Parameters Formulation.....   | 111 |
| 6.4 Simulation Techniques .....  | 115 |
| 6.5 Numerical Results.....   | 116 |
| 6.5.1 Example 6.1: Lossless coupled transmission lines.....  | 117 |
| 6.5.2 Example 6.2: Coaxial cable with skin effect .....  | 122 |
| 6.6 Conclusions.....   | 126 |
| <br>   |     |
| <b>7 CONCLUSIONS</b> .....   | 127 |
| 7.1 Summary of Research .....  | 127 |
| 7.2 Suggestions for Further Studies.....   | 129 |
| <br>   |     |
| <b>APPENDIX A</b> .....  | 130 |
| <br>   |     |
| <b>REFERENCES</b> .....  | 133 |
| <br>   |     |
| <b>CURRICULUM VITAE</b> .....  | 145 |

## LIST OF TABLES

| Table  | Page |
|--|------|
| 3.1: Expansion moments. ....                                   | 44   |
| 3.2: Approximate poles for Example 3.1. ....                   | 45   |
| 3.3: Approximate residues for Example 3.1. ...                 | 45   |
| 3.4: Approximate poles for Example 3.4. ....                   | 52   |
| 3.5: Absolute errors of approximate poles for Example 3.4. ... | 52   |
| 4.1: Actual and scaled expansion moments. ....                 | 67   |
| 4.2: Approximate residues. ....                                | 67   |
| 4.3: Approximate poles. ....                                   | 68   |

## LIST OF FIGURES

| Figure   | Page |
|--|------|
| 1.1: Circuit model of an interconnect network. ....  | 2    |
| 3.1: RLC circuit. ....   | 43   |
| 3.2: Input waveform for RLC Example 3.1. ....  | 43   |
| 3.3: Transient response: First-order approximation. ....   | 46   |
| 3.4: Output waveform: Second-order approximation. ....   | 46   |
| 3.5: Output waveform: Sixth-order approximation & SPICE. ....  | 47   |
| 3.6: Interconnect network of Example 3.2. ....   | 48   |
| 3.7: Response waveform at node 29. ....  | 48   |
| 3.8: Response waveform at node 20. ....  | 49   |
| 3.9: Example 3.3, a coaxial line. ....   | 50   |
| 3.10: Example 3.3: Near-end voltage waveform, exact method (solid) and<br>moment-matching (dashed). ....                           | 50   |
| 3.11: Example 3.3: Near-end voltage waveform, exact method (solid) and<br>moment-matching (dashed). ....                           | 51   |
| 3.12: Example 3.4: An example of RC-ladder network. ....   | 52   |
| 4.1: $p$ - $n$ Junction diode. ....  | 59   |
| 4.2: A biasing diode circuit. ....   | 66   |
| 4.3: Charge buildup during turn-on phase. ....   | 70   |
| 4.4: Stored charge decay during turn-off phase. ....   | 70   |
| 4.5: The diode voltage waveforms, one to four orders of approximations. ....   | 71   |
| 4.6: The diode current waveforms, one to four orders of approximations. ....   | 71   |
| 4.7: Input waveforms and diode voltage response. AWE method (---) versus<br>conventional quasi-static model (—). ....              | 72   |
| 4.8: Diode current response. AWE method (---) versus<br>conventional quasi-static model (—). ....                                  | 72   |
| 5.1: Partitioned multiports subnetworks. ....  | 78   |
| 5.2: Location of poles of original system (diamond) and the cluster-centers for<br>reduced-model (star) in the complex plane. .... | 93   |
| 5.3: Magnitude plots of $S_{12}$ , the measured data and the 24th-order<br>rational approximation. ....                            | 99   |
| 5.4: Phase plots of $S_{12}$ , the measured data and the 24th-order<br>rational approximation. ....                                | 99   |
| 5.5: Magnitude plots of $S_{11}$ , the measured data and the 27th-order<br>rational approximation. ....                            | 100  |

|   |     |
|---|-----|
| <b>5.6:</b> Phase plots of $S_{11}$ , the measured data and the 27th-order rational approximation. ....   | 100 |
| <b>5.7:</b> (a) Magnitude plots of the errors , the 41st-order rational approximation using the method in [19] (gray line), and the proposed method (dark line),<br>(b) magnitude plots of the errors , the 60th-order rational approximation using the proposed method (dark line). .... | 101 |
| <b>5.8:</b> Example 5.1, interconnect network with measured component. ....   | 102 |
| <b>5.9:</b> Example 5.1, transient response at node $x$ . ....  | 103 |
| <b>5.10:</b> Example 5.1, transient response at node $y$ . ....   | 103 |
| <b>5.11:</b> Example 5.2, diode-pair terminated network,<br>(the 5 K $\Omega$ resistor replaces the diode-pair). ....   | 104 |
| <b>5.12:</b> Example 5.2, transient response at node $x$ . ....   | 105 |
| <b>5.13:</b> Example 5.2, transient response at node $y$ . ....   | 105 |
| <b>6.1:</b> General representation of an $n$ -coupled transmission line system. ....  | 114 |
| <b>6.2:</b> A network of $n$ -coupled transmission line system, reference system,<br>and arbitrary networks. ....   | 114 |
| <b>6.3:</b> Norton-equivalent representation of Equation (6.13) at $t_n$ . ....   | 116 |
| <b>6.4:</b> (a) Dimensions of a three-conductor microstrip system, (b) network<br>of the three-conductor microstrip system. ....  | 118 |
| <b>6.5:</b> Approximated input waveform. ....   | 119 |
| <b>6.6:</b> The near-end voltage transient waveform on conductor 1,<br>measurements (solid) and simulation (dashed). ....   | 119 |
| <b>6.7:</b> The far-end voltage transient waveform on conductor 1,<br>measurements (solid) and simulation (dashed). ....  | 120 |
| <b>6.8:</b> The near-end voltage transient waveform on conductor 2,<br>measurements (solid) and simulation (dashed). ....   | 120 |
| <b>6.9:</b> The near-end voltage transient waveform on conductor 3,<br>measurements (solid) and simulation (dashed). ....   | 121 |
| <b>6.10:</b> The far-end voltage transient waveform on conductor 3,<br>measurements (solid) and simulation (dashed). ....   | 121 |
| <b>6.11:</b> Example 6.2, a coaxial line. ....  | 122 |
| <b>6.12:</b> The magnitude of $S_{12}$ , for 50 $\Omega$ (solid) and 100 $\Omega$ (dashed)<br>reference impedances. ....  | 123 |
| <b>6.13:</b> The magnitude of $S_{11}$ , for 50 $\Omega$ (solid) and 100 $\Omega$ (dashed)<br>reference impedances. ....  | 123 |
| <b>6.14:</b> Example 6.2: Near-end simulated voltage waveform.....  | 124 |
| <b>6.15:</b> Example 6.2: Near-end measured voltage waveform.....   | 124 |
| <b>6.16:</b> Example 6.2: Far-end simulated voltage waveform .....  | 125 |
| <b>6.17:</b> Example 6.2: Far-end measured voltage waveform .....   | 125 |

# CHAPTER 1

## INTRODUCTION

### 1.1 Background

Advances in VLSI circuitry have brought about an enormous growth in the scale and complexity of integrated circuits and electronic packages. Integrated circuits are now being produced with millions of transistors, and electronic packages are being designed with thousands of interconnects. The fabrication and test of prototypes is very costly and time consuming, and computer simulation is becoming more essential to determine the performance of the VLSI circuits and the packages before they are built. The increase in circuit size makes performance verification of current systems using standard simulators such as SPICE [1], ASTAP [2], and Saber [3] computationally impractical. In addition, the reduction in size of the devices and interconnection structures requires powerful modeling and advanced capabilities of synthesis techniques in order to analyze them accurately. Higher-order and previously neglected effects must be considered. Device models need to be valid over a wide frequency range [4], [5]. The interconnects' frequency-dependent behaviors become more important in determining the performance of systems. As a result, the demand for alternate CAD tools that can efficiently and accurately analyze current complex systems has generated the search for new methods of circuit simulation.



The complexity of new technology and the increase in clock speed directs the search for modeling and simulation toward more accurate methods, whereas the size of current VLSI circuits push the approach away to less accurate approximation methods. Such conflicting requirements also arise in signal integrity analysis of high speed systems. Often, detailed analyses of large interconnect networks at chip, board or system levels need the analyses of complex interconnect networks that consist of inhomogeneous media, solid and perforated power planes, vias, bends and pads, nonlinear drivers and terminations. A typical network representation of a signal path in an electronic package is shown in Figure 1.1.

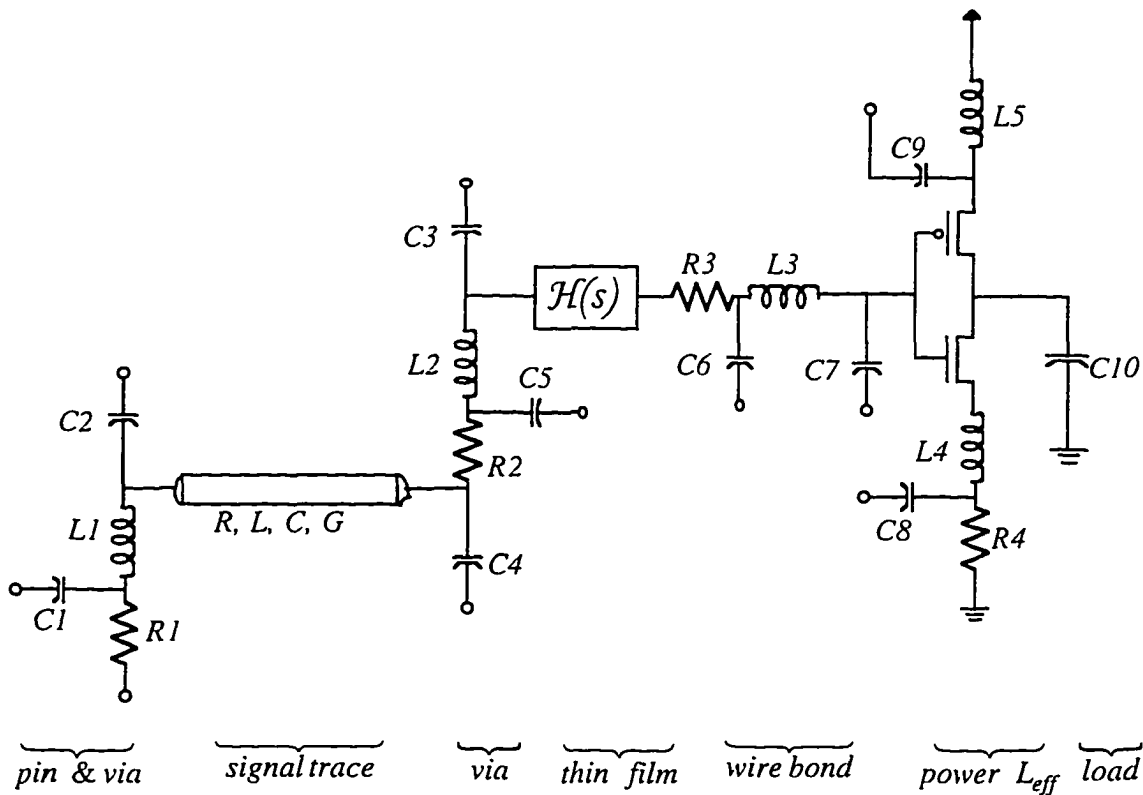


**Figure 1.1:** Circuit model of an interconnect network.

All  $R_i$ 's,  $C_i$ 's, and  $L_i$ 's in Figure 1.1 are resistance, capacitance and inductance matrices of the lumped system, respectively. The  $R(j\omega)$ ,  $L(j\omega)$ ,  $C(j\omega)$ , and  $G(j\omega)$  are resis-

tance, capacitance, inductance, and conductance per-unit-length of the distributed system, respectively. The  $H(s)$  is a matrix of fundamental parameters in analytical or tabular form characterizing nonuniform interconnects. The impulse response of such a network is so complex that a detailed analysis using conventional methods is time consuming. The simulator needs to be capable of dealing with distributed, frequency-dependent networks and systems characterized by sampled data. The direct method of analyzing a system using numerical transforms such as the FFT and nonlinear convolution is extremely time consuming. The traditional methods require low-pass filtering of frequency-domain data that are nonband limited. For example, the reflections and couplings of a coupled interconnect system approaches unity as frequency tends toward infinity.

Although recent circuit simulation techniques, such as asymptotic waveform evaluation (AWE) [6]-[10], complex frequency hopping (CFH) [11]-[12], and Padé via Lanczos (PVL) [13]-[15] reduce computational complexity, the stability and accuracy of these approaches when applied to complex networks still remain issues of concern.

## 1.2 Overview

This dissertation focuses on developing a more accurate and efficient methodology of model-order reduction techniques for circuits, interconnects and package simulation. The research investigates the application of model-order reduction techniques for the solutions of the equations describing circuits, devices, and electromagnetic systems. This dissertation attempts to bring together the two conflicting requirements of CAD tools, efficiency and accuracy, by improving the accuracy and robustness of model-order reduction techniques. The dissertation develops the methodology for the construction of pole-zero models to represent complex effects of distributed systems or system responses obtained from field

solvers and measurements. The models are compatible to conventional simulators and can be integrated to estimate the response of a system.

The reduced-order model of a system is obtained by directly approximating the solution of the partial differential equations or the response of the system in a very efficient way. The reduced-order model method accurately represents the dynamics of complex systems, such as carrier diffusion in  $p$ - $n$  diode and wave propagation in electromagnetic systems, that are difficult to account for using circuit elements and analytical models. The simpler, low-order models are analyzed substantially faster.

Most methods generate a reduced model by attempting to retain the leading moments or the dominant eigenvalues of the system and calculate the remaining parameters of the low-order model in such a way that its response to certain inputs is a close approximation to the response of the original system. For example, Padé approximation techniques [6]-[15] are based on matching the moments of the response of the system to extract the dominant poles. An attractive feature of these approaches is that they retain the physical meaning and require much less computation.

A simplified model of a large network can also be obtained by finding an optimum approximation of the original system without the constraints of matching the moments or the locations of the eigenvalues. The method involves a constrained curve-fitting that minimizes the error between the original model and the reduced-order model. Most of the computational procedures usually require high computational efforts and can be very costly for applications in circuit simulation. Although the method suffers from the drawback that the physical significance of the reduced variables is lost, the approach is more general and can give better approximations than single and multipoint, moment-matching methods. The recent works on the direct representation of lossy transmission lines using transfer functions have regenerated considerable interest in the possibility of direct determination of the poles and zeros from the time-domain or frequency-domain response [16]-[20]. The characteristics of the transmission lines can be approximated using a stable rational function in a pole-

residue or pole-zero form or as a ratio of polynomials. Once the poles and zeros are obtained, the model can be reduced by using pole-clustering techniques.

In Chapter 2, circuit simulation techniques are reviewed. Some of the recent methods that are proposed to improve the speed of circuit simulation are discussed. The basic ideas that made these methods different from the conventional methods are described and their merits will be examined.

In Chapter 3, Padé approximation using the moment-matching technique and Krylov subspace-based methods, such as the Arnoldi algorithm and the Lanczos algorithm, are studied. The two methods are compared and the strengths and the weaknesses of the methods are presented. Examples are given to show their similarities and differences.

In Chapter 4, asymptotic waveform evaluation technique is applied to  $p$ - $n$  junction devices. The AWE is used to accurately model the transient behavior and high frequency characteristics of junction diodes. It is demonstrated that the method can accurately analyze the diode forward and reverse recovery effects and high-frequency behavior of a diode. This phenomena cannot be analyzed in conventional circuit simulation. An example of diode switching circuit is given and the results are compared with SPICE and other published simulations.

In Chapter 5, a robust rational interpolation technique is presented for synthesizing electromagnetic systems over a wide frequency range. Rational synthesis is a very effective technique for generating a finite-order model of complex, infinite-dimension systems. The method is used to obtain rational approximations for systems with relatively complicated transfer functions having a large fluctuation in the waveform. The method is a curve-fitting procedure based on the Householder QR orthogonalization to obtain a very accurate solution for the coefficients of a constrained stable function that minimizes the error between the original model and the approximate model. The pole-clustering technique is used to further reduce the model of the intermediate, large-order system obtained through rational approximation of the original system. For most practical cases, the order of approximation

can be selected to directly obtain a reduced model. The method can be used with complex systems described by partial differential equations or systems expressed by sampled data. General transmission lines and complex interconnect systems are analyzed using this method. The simulation results are compared with results using other methods.

In Chapter 6, the rational synthesis is used to analyze frequency-dependent coupled transmission lines. Scattering parameter formulations are used to characterize the transmission lines. By using an optimal reference system that makes the scattering parameters smooth and simpler to approximate, low-order rational functions are generated. These low-order rational approximations of the scattering parameters are used to obtain the time-domain response of the coupled transmission line system for arbitrary excitation using recursive convolution. The method does not suffer from aliasing or round-off errors caused by nonband-limited frequency-domain data, or by numerical transforms of a large number of points, respectively. The low-order frequency-domain modeling of a transmission line system using scattering parameters and appropriate reference system combined with recursive convolution is used to reduce the simulation time.

# CHAPTER 2

## REVIEW OF CIRCUIT SIMULATION TECHNIQUES

### 2.1 Introduction

Circuit simulation programs are important tools in the design and testing of electronic systems. They provide an inexpensive and fast means of verifying and optimizing designs without building prototypes. Prototypes require too much time to build and test, and cannot accurately represent all the electrical parameters of the actual products. Circuit simulation provides the timing details of the circuit, as well as signal levels. In addition, circuit simulation is advantageous over actual measurement because one can probe any node in a network and observe the response in time or frequency domain without overloading the circuit.

In the following sections, general circuit simulation programs are reviewed. Three approaches of circuit simulation: direct method, waveform-relaxation method and Padé synthesis are discussed. The modeling and simulation of distribute systems are also reviewed.

## 2.2 Traditional Simulation Techniques

Conventional circuit simulators such as SPICE, ASTAP, and Saber [1]-[3] are general purpose simulators that can provide time-domain transient analysis, dc solutions, frequency-domain ac analysis, sensitivity analysis, and noise and distortion analysis. The algorithms of these simulators are based on the construction of differential equations by representing electronic devices with analytical functions. The modified nodal admittance (MNA), a matrix formulation used by circuit simulation [21], matrix equation of any lumped network can be written using Kirchoff current and voltage laws and the constitutive or branch equations of each element as

$$C \frac{d}{dt} v(t) + Gv(t) + F(v(t)) = e(t) \quad (2.1)$$

where  $v(t)$  is a vector of nodal voltages appended by an independent voltage source current, linear inductor current, nonlinear capacitor charge, and nonlinear inductor flux;  $F(v(t))$  is a function describing the nonlinear elements in the network;  $e(t)$  is the independent source vector; and  $C$  and  $G$  are matrices describing the network. The nonlinear differential equations in (2.1) are converted into algebraic equations using stiffly stable integration methods. The multistep integration formula of the form

$$x_{n+1} = \sum_{i=0}^p a_i x_{n-i} + h_n \sum_{i=1}^p b_i f(x_{n-i}, t_{n-1}) \quad (2.2)$$

is often applied to Equation (2.1). The  $x_k$ 's are the approximated solution at time  $t_k$ , and  $h_k = t_k - t_{k-1}$  is the discretization time step, with  $a_i$ 's,  $b_i$ 's and  $p$  chosen to satisfy a certain relationship between the accuracy and the stability within the order of the formula [22], [23]. The nonlinear algebraic equations are solved iteratively using the Newton-Raphson method. For  $n$  nonlinear equations in  $n$  unknowns defined by

$$f_i(x_1, x_2, \dots, x_n) = 0, \quad i=1, 2, 3, \dots, n \quad (2.3)$$

a new iterate  $x_n^{k+1}$  at time  $t_n$  can be obtained from past values of  $x_n$  solving

$$x_n^{k+1} = x_n^k - [J(x_n^k)]^{-1} f(x_n^k) \quad (2.4)$$

where  $J(x_j) = \partial f(x_j) / \partial x_j$  is the Jacobian matrix. Finally, at each iteration point a system of linear equation of the form

$$Ax = b \quad (2.5)$$

is solved.

Although this algorithm leads to accurate solutions, the computing time grows super-linearly with circuit size, practically limiting its applications to small-sized circuits. Recently, a number of specialized circuit simulators have been developed by abandoning one or more of the above paradigms in order to speed up the analysis. Simulation programs, such as MOTIS [24], SPLICE [25], DIANA [26], [27], and ILLIADS [28] are among the few new simulators that traded the accuracy of their analyses for computational speed [29].

## 2.3 Waveform-Relaxation Techniques

The main reason why the conventional technique is inefficient for large circuits is that the solution time grows super-linearly with the size of the problem. Methods based on tearing, decomposition and partitioning techniques have improved the speed of simulation while maintaining the accuracy of the solutions [29]-[31]. A relatively new simulation algorithm, known as waveform relaxation [32]-[34], analyzes large circuits by partitioning them into manageable pieces to reduce simulation time. The method takes advantage of the unique properties of MOS circuits that transistors switching activity tends to propagate through the circuits in unidirectional waves. While some switches are generally in transition, others can be idle. The gates of MOS devices also have little effect on the portions of the circuit connected to their inputs. The delays on the transmission lines act as natural boundaries for the partitions [35]. The waveform-relaxation algorithm, based on



these observations, partitions the circuit into small pieces to take advantage of these latency behaviors. Each piece is analyzed independently following the direction of signal propagation. This partitioned analysis is repeated a number of times to gradually take into account the full interaction among the subnetworks.

The relaxation can be applied at different levels. When applied to the linear system of Equation (2.5), the Gauss-Jacobi and Gauss-Seidel algorithm gives

$$Dx^{k+1} = b - (L + U)x^k \quad (2.6a)$$

$$(L + D)x^{k+1} = b - Ux^k \quad (2.6b)$$

respectively. The matrix  $A$  is decomposed into  $A=L+D+U$ , where  $L$ ,  $D$ , and  $U$  are nonsingular, strictly lower-triangular, diagonal, and strictly upper-triangular matrices, respectively. While the method has extended the size of circuits that can be simulated to thousands of transistors and interconnects, the method is limited to certain classes of technology and falls short in satisfying the current demand.

## 2.4 Modeling and Simulation of Distributed Systems

Conventional circuit simulators, such as SPICE, ASTAP and its derivatives such as RELAX [34] are primarily discrete or lumped-element simulators. The transient simulation of high-speed analog and digital integrated circuits requires the analysis of distributed components. The interconnect structures, such as wirebonds, tape automated bonds (TAB's), pins, connectors, and pads, have to be represented as distributed components to determine the performance of the systems. The interconnect discontinuities, dispersions, conductor and dielectric losses can be accurately represented by transmission line systems rather than by equivalent circuits. The accurate determinations of losses, delays, and noise on interconnects in high-speed integrated circuits requires transmission line models.

Arbitrary transmission lines are distributed systems, unlike lumped networks, and cannot be described by the ordinary-differential equations in (2.1). The voltages and currents of an RLCG transmission line system are functions of time and space. They are infinite-order systems described by coupled partial-differential equations, known as the telegrapher's equations given by

$$\begin{aligned}\frac{\partial}{\partial x}v(x,t) &= -R i(x,t) - L \frac{\partial}{\partial t}i(x,t) \\ \frac{\partial}{\partial x}i(x,t) &= -G v(x,t) - C \frac{\partial}{\partial t}v(x,t)\end{aligned}\tag{2.7}$$

where  $R$ ,  $L$ ,  $G$ , and  $C$  are the resistance, inductance, conductance, and capacitance  $n \times n$  matrices per unit length, and  $v(x,t)$  and  $i(x,t)$  are  $n \times 1$  voltage and current vectors, respectively.

The method of characteristics can be used to transform Equation (2.7) into two ordinary differential equations using the equations

$$\begin{aligned}\frac{dx}{dt} &= \frac{1}{\sqrt{LC}} \\ \frac{dx}{dt} &= -\frac{1}{\sqrt{LC}}\end{aligned}\tag{2.8}$$

as forward and backward characteristic curves, respectively [36]. By combining Equations (2.7) and (2.8), the two differential equations along the forward and backward characteristic curves are given by

$$\begin{aligned}\sqrt{\frac{L}{C}} di(x,t) + \left( Ri(x,t) + \sqrt{\frac{L}{C}} G v(x,t) \right) dx + d v(x,t) &= 0 \\ -\sqrt{\frac{L}{C}} di(x,t) + \left( Ri(x,t) - \sqrt{\frac{L}{C}} G v(x,t) \right) dx + d v(x,t) &= 0\end{aligned}\tag{2.9}$$

respectively.

The method of characteristics was first used to simulate lossless transmission lines in time domain by Branin [37]. For lossless transmission line systems, where  $R=0$  and  $G=0$ , and distortionless line systems, where  $R/L = G/C$ , Equation (2.9) can be directly

integrated [38]. The method can be used to analyze general uniform lossless  $n$ -coupled transmission lines in [39] and [40]. The inductance,  $L$ , and the capacitance,  $C$ , matrices are diagonalized and the set of  $2n$  uncoupled ordinary-differential equations are solved in a similar fashion as a single line case. However, general transmission lines are solved by numerical techniques; therefore, the analysis of lossy lines is very involved [41]. The method cannot be easily applied to analyze frequency-dependent behaviors such as skin effects and dielectric losses.

Traditionally, a transmission line is modeled by cascading a large number of resistors, inductors and capacitors. The method introduces a large number of nodes that increase the simulation time substantially. This lumped-element circuit model introduces excessive ringing and can give accurate results only within a limited frequency range. The lumped-element circuit models must be supplemented to account for frequency-dependent effects in transmission lines.

The most general approach for the simulation of transmission lines is based on the convolution method. The impulse responses of transmission line systems are used to solve the nonlinear convolution equations governing the interconnects and nonlinear drivers and terminations [42]-[44]. The convolution requires the inverse transforms and band-limit filtering of a large number of points in order to minimize aliasing and unwanted ringing [45]. This method is computationally expensive. In the recent version of SPICE, *SPICE3* convolution formulas for single lossless transmission lines and simple lossy transmission lines, with constant  $R$ ,  $L$  and  $C$ , are used to reduce simulation time [46]. These analytical models are not general and do not consider frequency-dependent phenomena such as the skin effect.

Recently, in order to be able to analyze arbitrary interconnect structures with nonlinear loads, research has been directed to integrate the distributed electromagnetic networks and circuit simulations into one platform. The approach can be categorized in two groups. The first approach is to extend the existing electromagnetic techniques by

introducing the concept of a lumped-device model to handle circuit components that represent passive and active devices [47]-[50]. Resistors and capacitors are implemented as three-dimensional block resistors and parallel-plate capacitors with selected conductance and the permittivity of the regions. The semiconductor devices are implemented either as analytical grid models or by using the concepts of voltage-variable resistors and capacitors. Although this method performs the most accurate simulation, it is limited to very small systems. The second approach concentrates on integrating the characteristic parameters into a circuit environment. The fundamental parameters, such as impedance, admittance or scattering parameters, are directly used in circuit simulation to solve the terminal voltages and currents in networks using convolution. The convolution and the numerical transform required to obtain the response of a system are time consuming. An alternative approach is to extract equivalent circuit representations directly from simulated or measured time- or frequency-domain data [51]-[54]. The time-domain approximation of an impulse response involves costly optimization and the method does not guarantee physically meaningful positive values for the circuit elements. Often, the automatic extraction of circuit element values fails to give useful information to practical problems [52].

Recently, methods that are based on Padé synthesis have been applied to improve the simulation efficiency of distributed networks. AWE, CFH and PVL, have been used successfully to analyze interconnect systems [9]-[12], [55]-[59]. Typical efficiency gains of two- to three-orders of magnitude over traditional methods have been reported. These methods are reviewed in the following section.

## 2.5 Padé Synthesis

The direct analyses of VLSI circuits and electronic packages, as discussed in Section 2.2, are computationally expensive. The simulation of such systems, however, can

be carried out less expensively by replacing the high-order systems with simplified low-order systems that closely approximate the original systems. Padé approximation can be used to generate these low-order approximations.

In 1948, Elmore [60] proposed an expression for approximating the time at which the transient step response would reach 50% of its final value of monotonic waveforms. The waveforms are restricted to monotonic unit step responses, and initial conditions are not allowed. The timing delay, known as Elmore delay,  $T_D$  obtained in terms of the first moment of the derivative of the step response  $v(t)$  is

$$T_D = \int_0^{\infty} t \underbrace{\left( \frac{\partial v(t)}{\partial t} \right)}_{h(t)} dt \quad (2.7)$$

This expression represents the first moment, or mean, of the impulse response,  $h(t)$ , provided that the circuit is initially in equilibrium, i.e., the capacitors are discharged. Rubenstein, Penfield, and Horowitz [61] applied the Elmore delay as a dominant time constant approximation to determine the nominal delay in linear RC-tree circuits, which are networks consisting of resistive chains with capacitance-to-ground at each node [62], [63]. The approximation was refined by developing second-order RC-tree methods as an extension of the previous RC-tree methods. A transfer function with two poles and one zero,

$$H(s) = \frac{a_0 + a_1 s}{1 + b_1 s + b_2 s^2} \quad (2.8)$$

is used to approximate the voltages at the nodes. Zukowski [64] extended the method to a general class of RC-trees. He derived rigorous bounds on the behavior of the digital MOS circuits using RC-trees. The RC-tree approaches to timing estimation have been used successfully for timing analysis and timing simulation of low- to mid-frequency MOS digital-integrated circuits. The MOS gates are modeled as linear capacitors and the channels as linear resistors that are determined as functions of process parameters and voltage changes which are to appear across the gates. The interconnects are also modeled by

RC-tree networks [65]. While extremely large circuits can be analyzed with such an approach, crucial information about their behavior is often lost because very simplified circuit models are used to predict circuit responses. The method considers only one or two moments of the impulse response of the system and only works for monotonic waveforms.

### **2.5.1 Moment-matching methods**

The RC-tree method has limited applications. The method cannot model capacitive coupling or resistance-to-ground effects. Recently, asymptotic waveform evaluation (AWE), method based on the moment-matching technique has been used for the analyses of large linear networks and interconnect structures [9]-[12], [55]-[59]. Unlike the RC-tree method, AWE handles more complex networks, non-tree structures and inductances without increasing computational complexity.

McCormick and Allen [6] showed that the moments of an electrical network could be used to form a low-order approximate response. They developed a moment representation method to simplify the analysis of linear circuits and interconnects. Pillage, Wolff and Rohrer [7] used a form of the RLC network equations to generate the network moments in an efficient manner and extracted an approximation set of network poles. They demonstrated that the resultant low-order model was a generalization of the simpler one or two-pole, RC-tree approximation method. Typical efficiency gains of two to three orders of magnitude speedup over traditional simulation techniques have been reported. The accuracy of the analysis can be improved by increasing the number of poles used in the approximation.

## 2.5.2 Krylov subspace-based methods

Recently, iterative methods have become standard tools for solving large linear systems. Many iterative methods are based on Krylov subspace methods which are particularly more effective for partial eigensolution, for determining few eigenvalues and the corresponding eigenvectors of a matrix [66]-[68].

The use of Krylov subspace-based methods to obtain dominant eigenvalues has various advantages. The Krylov subspace-based methods avoid the magnification of the dominant eigenvector component that is inherent in the moment-matching method by using a set of vectors that describes the same vector space as the moment matrix but are mutually orthogonal. This method allows the extraction of the desired number of poles to capture the dominant features of the original input-to-output mapping. The Krylov subspace-based method, unlike the moment-matching method, provides a methodology to measure the error between the original model and the reduced-order model. The link between the Lanczos method and the moment-matching analysis has been studied in [67]. Recent papers [13]-[15], [59] have applied the Lanczos process for linear network simulations.

The synthesis of transmission lines with long delays are problematic. The selection of expansion points that guarantee stable Padé approximations of highly coupled lossy interconnects with complex impulse responses is heuristic. In an effort to overcome some of these concerns, the direct representation of lossy transmission lines using the transfer functions obtained from curve-fitting of time- or frequency-domain response has regenerated considerable interest [19], [69]. Thus, the poles and zeros of the transmission line systems are directly determined from the transfer functions.

## 2.6 Rational Approximation Techniques

A simplified model of a large, lumped and distributed network can be obtained by finding an optimum approximation, in some sense, of the original system without the constraints of matching the eigenvalues or the moments. The method involves a constrained curve-fitting that minimizes the error between the original system and the approximation. The approach is more general and can give better approximations than the single-or multi-point moment-matching methods. The recent works on the direct representation of lossy transmission lines using transfer functions have regenerated considerable interest in the possibility of direct determination of the poles and zeros from the time- and frequency-domain response. The characteristics of the transmission lines can be approximated using a stable rational function in a pole-residue or pole-zero form or as a ratio of polynomials [18], [19], [69]-[71]. Once the poles and zeros are obtained, a reduced-order model can be obtained using one of the standard techniques for an efficient time- or frequency-domain simulation.

The computational procedure to determine a rational approximation requires the solutions of ill-conditioned systems. The accurate calculation of poles and zeros often involves costly optimization [73].



## CHAPTER 3

# PADÉ ANALYSIS VIA MOMENT-MATCHING AND KRYLOV SUBSPACE-BASED METHODS

### 3.1 Introduction

The idea of obtaining a low-order model from a high-order linear system characterized by a set of differential or difference equations is quite mature. It has been long recognized as an important tool to reduce computational complexity and simplify large systems. The topic has been studied extensively in the control and system fields for many years, and consequently, a wide variety of approaches has been proposed [74]-[75].

Recently, asymptotic waveform evaluation (AWE) and its derivatives, which are based on moment-matching methods, are successfully used for the simulation of large-lumped and distributed systems. The reduced-order models of large-scale systems have been used to generate fast-timing analyses of PCB and MCM interconnects. A typical efficiency gain of more than two orders of magnitude speedup over traditional simulation techniques has been attained [6]-[10], [55], [56].

AWE is a form of Padé approximation that uses the moment-matching method for extracting dominant poles and zeros of linear(ized) networks. These dominant poles and zeros form low-order models that can be used for efficient transient-response

approximations. The low-order models are constructed by first expanding the networks transfer functions by the Taylor series, and then matching as many coefficients as necessary in terms of low-order approximate functions. Recently, AWE technique and its derivatives that are based on moment-matching methods have been applied to circuit simulation successfully.

The increase in signal and clock speed has put an additional demand for accurate simulation of VLSI circuits and package interconnections. The emphasis is placed not only on efficiency, but also on accuracy and generality of the simulation algorithms. The AWE analysis, despite its success, fails to guarantee improved approximation when the order of the approximation is increased. These shortcomings are inherent to the moment-matching techniques that the current AWE-based simulators employ. The moment-generation process is very sensitive to numerical accuracy, and the resulting moment matrix, despite some remedial techniques such as scaling and frequency shifting, is very ill-conditioned. Consequently, a very small error in moment value leads to a large error in pole-residue calculation. This error is more probable when the order of approximation is increased. The fact that moments are generated by iterating the original system matrix results in the magnification of the dominant eigenvector component and the loss of information contained by the eigenvectors that correspond to the smaller eigenvalues. As the number of iterations is increased, the moment vectors become increasingly parallel to each other, forcing the approximation to remain stagnant despite the increase in order.

Recently, iterative methods have become standard tools for solving large linear systems. Many iterative methods are based on Krylov-subspace methods. Krylov-subspace methods are particularly effective for partial eigensolutions, determining few eigenvalues and the corresponding eigenvectors of a matrix [67]-[68]. In [74]-[77], Krylov-subspace methods are used to construct a reduced-order state-space control by projecting the system onto expanding subspaces generated by the original matrix.

The Arnoldi and Lanczos algorithms are two popular Krylov methods that are used for partial eigenvalue problems [78]-[81]. The use of these methods for model-order reduction has manifold advantages. The Krylov-based methods avoid the magnification of a dominant eigenvector component that is inherent in the moment-matching method by using a set of vectors that describes the same vector space as the moment matrix, but is mutually orthogonal. This vector space allows the extraction of the desired number of poles to capture the dominant features of the original input-to-output mapping. These methods, unlike the moment-matching method, provide a methodology to measure the error between the original model and the reduced-order model. The link between the Lanczos method and the moment-matching analysis has been studied in [14],[67]. Recent papers [13],[15] have applied the Lanczos method to AWE-like circuit simulations.

In this chapter, moment-matching and the Krylov-subspace methods are presented for the analysis of linear networks using modified nodal analysis formulation. The frequency-domain analysis is discussed in Section 3.2 as the motivation for the use of Padé synthesis. The moment-matching method and its implementation details are presented in Section 3.3. In Section 3.4, Krylov-subspace methods are introduced and Arnoldi and Lanczos algorithms are applied for solving the partial eigenvalue, respectively. The moment-matching and Krylov subspace-based methods are compared in Section 3.5. Finally, the conclusion is given in Section 3.6.

## **3.2 Frequency-Domain Analysis**

The response of a linear circuit can be calculated efficiently in the frequency domain by using the transfer function of the circuit. The transfer function of a linear circuit is defined as the ratio of the output and input waveforms and is expressed as

$$H(s) = \frac{V_{out}(s)}{V_{in}(s)} \quad (3.1)$$

where  $V_{in}(s)$  and  $V_{out}(s)$  are the Fourier transforms of the input and the output waveforms, respectively. For sufficiently small signals, a nonlinear network may be linearized in a small region around the operating point, and a transfer function can also be defined.

The transfer function of order  $[m,n]$  of a linear-lumped network can be written as a ratio of two polynomial functions of  $s$  or as a product of factors containing the poles and the zeros:

$$H(s) = \frac{\sum_{i=0}^m a_i s^i}{1 + \sum_{i=1}^n b_i s^i} = K \frac{\prod_{i=1}^m (s - z_i)}{\prod_{i=1}^n (s - p_i)} \quad (3.2)$$

where the  $a_i$ 's and  $b_i$ 's are real coefficients, the  $z_i$ 's are the zeros or the roots of the numerator polynomial, and the  $p_i$ 's are the poles or the roots of the denominator polynomial.

A convenient expression for the circuit transfer function  $H(s)$  is in terms of its partial fraction expansion. For the case of  $n$  distinct poles, and  $m \leq n$ , the transfer function can be expressed as

$$H(s) = k_\infty + \sum_{i=1}^n \frac{k_i}{s - p_i} \quad (3.3)$$

where  $k_i$  is the residue that corresponds to the pole  $p_i$  of the circuit. Once we determine the circuit function  $H(s)$  and its poles, it is easy to calculate the time-domain response of the function using Laplace transformation. Equation (3.3) is convenient for an inversion of the Laplace transform, and the time-domain impulse response is given in a closed form in terms of the poles and residues as

$$h(t) = k_\infty \delta(t) + \sum_{i=1}^n k_i e^{p_i t} \quad (3.4)$$

Thus, the poles and zeros play a pivotal role in the analysis and understanding of a linear circuit. Unfortunately, the computation of the poles and zeros, even for a small

circuit, is computationally complex [123]; therefore, the analysis of a network by extracting its poles is a formidable task and cannot be used for large circuits.

### 3.3 Moment-Matching Methods

Finding all of the poles of a large circuit is computationally inefficient, especially because some of the poles make an insignificant contribution to the circuit performance. Instead, we attempt to find an effective approximate transfer function by obtaining those few *dominant poles* that may adequately characterize the circuit behavior.

#### 3.3.1 Moment calculation

The modified nodal admittance (MNA) [21] is one of the simplest, most general, and convenient methods of formulation for the analysis of circuits. The standard description of a network using the MNA formulation can be written as

$$C \frac{d}{dt} v(t) + Gv(t) + F(v(t)) = e(t) \quad (3.5)$$

where  $v(t)$  is a vector of nodal voltages appended by independent voltage source current, linear inductor current, nonlinear capacitor charge, and nonlinear inductor flux;  $F(v(t))$  is a function describing the nonlinear elements in the network;  $e(t)$  is the independent source vector; and  $C$  and  $G$  are matrices describing the network.

For linear networks, the solution of (3.5) is given in the Laplace domain as

$$V(s) = [Y(s)]^{-1} E(s) \quad (3.6)$$

where  $Y(s)=(G+sC)$  is the transfer function. To approximate the solution of (3.6),  $V(s)$  can be expanded in a Maclaurin series as

$$V(s) = ([Y^{-1}]_0 + s[Y^{-1}]_1 + s^2[Y^{-1}]_2 + s^3[Y^{-1}]_3 + \dots)E(s) \quad (3.7)$$

The coefficients of expansion in (3.7) are known as moments because they are related to the moments of the impulse response as

$$V(s) = \sum_{n=0}^{\infty} M_n s^n$$

where

$$M_n = \frac{\left[ \frac{\partial^n Y(s)}{\partial s^n} \right]_{s=0}}{n!} E(s) \quad (3.8)$$

The derivative of  $Y^{-1}(s)$  can be expressed in terms of  $Y$  using a recursive relation [12] given as

$$[Y]_{s=0} \left[ \frac{\partial^n Y^{-1}}{\partial s^n} \right]_{s=0} = - \sum_{r=1}^n \left[ \frac{\partial^r Y}{\partial s^r} \right]_{s=0} \left[ \frac{\partial^{(n-r)} Y^{-1}}{\partial s^{(n-r)}} \right]_{s=0} \quad (3.9)$$

Using (3.8) and (3.9), the recursive equation for the calculation of the moments is

$$Y_0 M_n = - \sum_{r=1}^n \frac{\left[ \frac{\partial^r Y(s)}{\partial s^r} \right]_{s=0} M_{n-r}}{r!} \quad (3.10)$$

with

$$Y_0 M_0 = E$$

The moment approach can also be viewed from the definition of the Laplace transform:

$$V(s) = \int_0^{\infty} e^{-st} v(t) dt = \sum_{k=0}^{\infty} \frac{(-s)^k}{k!} \int_0^{\infty} t^k v(t) dt$$

The integral terms are identical to the moments in the probability density function, and they are given as

$$M_k = \frac{(-1)^k}{k!} \int_0^{\infty} t^k v(t) dt \quad (3.11)$$

The moments provide a measure of delay and rise times. For example, the Elmore delay for any system with a transfer function  $H(s)$  is the first moment that is [60]

$$T_D = \int_0^{\infty} t h(t) dt = -\dot{H}(0) \quad (3.12)$$

This first moment of the impulse response is often a good, time-constant approximation if a single pole dominates the low frequency behavior of a circuit. When there is more than one dominant pole, the higher order moments of  $h(t)$  are also important. The more moments that we calculate, the more we know about the behavior of the circuit around the expansion frequency point.

To generate higher approximations of order  $[l, q]$ , the first  $l+q$  moments of each variable  $V$  are matched to a lower-order frequency domain function of the form

$$V(s) = k_{\infty} + \sum_{i=1}^q \frac{k_i}{s - p_i} \quad (3.13)$$

where the  $p_i$ 's and  $k_i$ 's are the complex approximating poles of the system and residues of each variable, respectively. It is equivalent to matching the time-domain moments to an approximating function of the form

$$v(t) = k_{\infty} \delta(t) + \sum_{i=1}^q k_i e^{p_i t} \quad (3.14)$$

For an impulse excitation  $e(t)$ , Equations (3.13) and (3.14) become the transfer function  $H(s)$  and impulse response  $h(t)$  of the system, respectively. Note that as long as the circuit is asymptotically stable,  $h(t)$  is comprised of exponentials in time with negative real parts in the exponents, so the above defined moments exist for all values of  $q$ . If we can calculate these moment values efficiently, we may be able to better predict the low-frequency response behavior. The choices of  $l$  and  $q$  determine the accuracy of the approximations, and often the choices  $l=q$  and  $l=q-1$  are used.

Therefore, the moment-generation process is a simple process by which the MNA matrix is expanded using the Taylor series, and the coefficients of expansion are obtained recursively using Equation (3.10).

### 3.3.2 Moment matching

Once we have obtained the moments efficiently by using the recursive relationship in (3.10), we can match the moments of the original system to those of a lower-order approximate system.

The approximation of a transfer function of a system is obtained by matching the various Maclaurin series coefficients of the system function to a low-order rational approximation. Matching the rational function to the Maclaurin series of Equation (3.8) as

$$\frac{a_0 + a_1s + a_2s^2 + \dots + a_l s^l}{1 + b_1s + b_2s^2 + \dots + b_q s^q} = M_0 + M_1s + M_2s^2 + \dots + M_{l+q} s^{l+q}$$

(3.15) and cross-multiplying, we find

$$\begin{aligned} (a_0 + a_1s + a_2s^2 + \dots + a_l s^l) &= (M_0 + M_1s + M_2s^2 + \dots + M_{l+q-1} s^{l+q-1}) \\ &\quad \times (1 + b_1s + b_2s^2 + \dots + b_q s^q) \end{aligned}$$

Matching the coefficients of  $s^0, s^1, \dots, s^{l+q}$  yields to the following systems of equations:

$$\begin{cases} a_0 = M_0 \\ a_1 = M_1 + M_1 b_1 \\ a_2 = M_2 + M_1 b_1 + M_0 b_2 \\ \vdots \\ a_l = M_l + M_{l-1} b_1 + \dots + M_1 b_{l-1} + M_0 b_l \\ 0 = M_{l+1} + M_l b_1 + \dots + M_{l-q+2} b_{q-1} + M_{l-q+1} b_l \\ 0 = M_{l+2} + M_{l+1} b_1 + \dots + M_{l-q+3} b_{q-1} + M_{l-q+2} b_l \\ \vdots \\ 0 = M_{l+q} + M_{l+q-1} b_1 + \dots + M_{l+1} b_{q-1} + M_l b_l \end{cases} \quad (3.16)$$

The last set of  $q$  equations in (3.16) can be written in matrix form as



$$\begin{bmatrix} M_l & M_{l-1} & \cdot & \cdot & \cdot & M_{l-q+1} \\ M_{l+1} & M_l & \cdot & \cdot & \cdot & M_{l-q+2} \\ \cdot & \cdot & & & & \cdot \\ \cdot & \cdot & & & & \cdot \\ \cdot & \cdot & & & & \cdot \\ M_{l+q-1} & M_{l+q-2} & \cdot & \cdot & \cdot & M_l \end{bmatrix} \begin{bmatrix} b_1 \\ b_2 \\ \cdot \\ \cdot \\ \cdot \\ b_q \end{bmatrix} = - \begin{bmatrix} M_{l+1} \\ M_{l+2} \\ \cdot \\ \cdot \\ \cdot \\ M_{l+q} \end{bmatrix} \quad (3.17)$$

Once the coefficients of the denominator polynomial are obtained from Equation (3.17), the roots of the denominator polynomial are calculated from

$$b_q p^{-q} + b_{q-1} p^{-q+1} + \dots + b_2 p^{-2} + b_1 p^{-1} + 1 = 0 \quad (3.18)$$

Instead of obtaining the coefficients of the numerator polynomial directly, it is more convenient to generate the partial fraction expansions in terms of the  $q$  poles, roots of (3.18). For  $l \leq q$ , the transfer function can be written as

$$H(s) = k_\infty + \sum_{i=1}^q \frac{k_i}{s - p_i} \quad (3.19)$$

The residues  $c_i$ 's in (3.19) are obtained by matching the moments in (3.15) using the higher derivatives as

$$M_n = \frac{\partial^n}{\partial s^n} \left[ k_\infty + \sum_{i=1}^q \frac{k_i}{s - p_i} \right]_{s=0} \quad (3.20a)$$

The residues are obtained from the solution of

$$\begin{bmatrix} 1 & p_1^{-1} & \cdot & \cdot & \cdot & p_{q-1}^{-1} & p_q^{-1} \\ 0 & p_1^{-2} & \cdot & \cdot & \cdot & p_{q-1}^{-2} & p_q^{-2} \\ \cdot & \cdot & & & & \cdot & \cdot \\ \cdot & \cdot & & & & \cdot & \cdot \\ \cdot & \cdot & & & & \cdot & \cdot \\ 0 & p_1^{-q} & \cdot & \cdot & \cdot & p_{q-1}^{-q} & p_q^{-q} \\ 0 & p_1^{-q-1} & \cdot & \cdot & \cdot & p_{q-1}^{-q-1} & p_q^{-q-1} \end{bmatrix} \begin{bmatrix} k_\infty \\ k_1 \\ \cdot \\ \cdot \\ \cdot \\ k_{q-1} \\ k_q \end{bmatrix} = - \begin{bmatrix} M_0 \\ M_1 \\ \cdot \\ \cdot \\ \cdot \\ M_{q-1} \\ M_q \end{bmatrix} \quad (3.20b)$$

The computational cost associated with solving Equations (3.16) and (3.20), which are Toeplitz and Vandermonde-like matrices, respectively, is negligible because for most practical cases, the matrix size is very small. In practice, we start from a one- or two-pole

approximation depending on the size of the circuit and proceed to higher orders until the approximation is accurate enough for the purpose at hand. The above discussed procedure of obtaining the coefficients of the numerator and denominator polynomials or determining the residues and poles through partial expansion from the coefficients of a series is known as the Padé approximation [82]. A serious problem with the method is that it may yield unstable poles.

### 3.3.3 Frequency shifting

One approach to avoiding instability is by using frequency shifting in the calculation of the moments. From Equation (3.20), we see that the higher-order moments are increasingly determined by the first pole or the first few poles. As a result, the higher-order poles do not contribute to the moments, and the higher-order moments do not add useful information to the model. This problem can be solved through real frequency shifting. By moving the  $j\omega$  axis to the right, we have reduced the ratio  $k_i/p_i$ .

The frequency shifting can also be achieved by adding proportional resistors in parallel or in series to capacitance and inductances, respectively. Of course, approximate dominant poles that are obtained for the altered circuit must be shifted back to the right to obtain the actual poles.

### 3.3.4 Frequency scaling

A small deviation in the calculation of moments can cause a large deviation in the poles. Because the moments are computed with finite accuracy, the round-off error can spoil the Padé approximation and, consequently, the poles and the residues. When the eigenvalues of  $Y^{-1}$  are not close to unity, the powers of  $Y^{-1}$  in Equation (3.6), and therefore

the moment, change very rapidly. The large variation in moment values causes the moment matrix in Equation (3.17) to become ill-conditioned and near singular. This problem is easily circumvented if we adopt a new frequency scale where the poles assume a more manageable range. If a normalization factor  $\gamma = M_0/M_1$  is used in (3.8), the expansion

$$Y(s) = \hat{M}_0 + \hat{M}_1 s + \hat{M}_2 s^2 + \hat{M}_3 s^3 + \dots + \hat{M}_{l+q} s^{l+q} \quad (3.21)$$

is obtained by replacing  $s$  with  $\gamma \hat{s}$ , and  $\gamma^j$  is absorbed in  $\hat{M}_j$ ; the scaled moments,  $\hat{M}_j$ , have similar magnitude. The scaling can also be achieved by scaling the capacitance and inductance. Once we obtain the normalized residues and poles, we need to scale the poles and residues back to retrieve the actual poles and residues. This method is found to be necessary in obtaining higher-order poles and residues.

### 3.3.5 Complexity

The computation of the power of  $Y^l(s)$  to obtain the moments (9) may look to be more complicated than it actually is. In general, the  $Y$  matrix for a lumped, linear, time invariant circuit can be reordered to improve the condition of the matrix.

In the special case, where the network contains lumped components only,

$$\frac{\partial^r Y}{\partial s^r} = 0 \quad (r \geq 2) \quad (3.22)$$

and can be reduced to

$$[Y]_{s=0} M_n = - \left[ \frac{\partial Y}{\partial s} \right]_{s=0} M_{n-1} \quad (3.23)$$

Therefore, once the  $Y$  matrix is  $LU$ -decomposed, the major task in computing even higher moments is the repeated back substitutions of these  $LU$ -factors. For lumped elements, we need only one  $LU$  decomposition and  $l+q$  forward and back substitutions. The cost for polynomial factorization is less than that for moment calculation.

The complexity of AWE increases linearly with the desired order of approximation, while the simulation time of the traditional method increases super-linearly with MNA matrix size.

### 3.3.6 Stability

Circuits composed of passive elements, positive-valued  $R$ ,  $L$ , and  $C$  [83] are always stable. The poles lie in the left half plane. Because  $v(t)$  is the response of  $h(t)$  to finite input, the integral of  $v(t)$  in Equation (3.11) exists, guaranteeing the stability of low-order approximations.

Experience, however, has shown that the Padé approximation yields *bogus poles* when higher orders of approximation are undertaken [7]-[9]. For passive circuits, without feedback and dependent sources, we can categorically reject all unstable poles.

There are instances, however, where the selected order of approximation cannot match the response waveform. When the response waveform is nonmonotonic and a first-order approximation is required, a single exponential function cannot match the waveform. If a network is strongly resistive, i.e., small resistors in parallel with  $L$  and large resistors in series with  $L$ , then the circuit operates essentially as an  $RC$  circuit with small inductance effects. Or, if the network has larger resistors across the capacitors and small resistors in series with capacitors, then the circuit behaves as an  $RL$  circuit with small capacitance effects. An even-order approximation may not match the waveform. Similarly, if a network is weakly resistive, it essentially behaves as an  $LC$  network with complex conjugate pairs. Then, an odd-order approximation cannot produce the response waveform. As a result, AWE approximation may prove, in such cases, to have no solution or may generate a positive approximating pole in an effort to match the waveform. These situations are easily

remedied by moving to a higher order of approximation. Of course, the order of the approximation need not be higher than the order of the network.

### 3.3.7 Advances in moment-matching techniques

As described in preceding sections, AWE is an efficient method to approximate the frequency-domain and time-domain responses of linear(ized) circuits. The method is found to be two to three orders of magnitude faster than the conventional circuit simulation methods. This does not mean, however, that the method will always work. The Padé approximation can generate unstable *bogus poles*. AWE cannot reliably be applied to analyze complex networks. It cannot model pure delay very well, even with higher-order approximations. The use of complex exponentials to approximate pure delays in the transmission lines leads to spurious ringing.

Nevertheless, the results obtained from AWE are too good to abandon. Since the inception of AWE [6]-[8], different improvements have been suggested to make the method more flexible, more stable, and more accurate [9]-[12], [55]-[58].

Bracken, Raghavan, and Rohrer [56] and Lin and Kuh [57] extended the method for simulating distributed elements with long delays using the method of characteristics. The method overcomes the problem by factoring out pure delay, and applying moment-matching methods to approximate the remaining characteristic admittance and propagation function. In [56], a partitioning technique is used to incorporate nonlinearities into AWE. Tang and Nakhla [10] generalized AWE for transient analysis of lossy, coupled transmission lines network with nonlinear elements. The response of the linear subnetwork to arbitrary piecewise linear signal is expressed in a recursive relation and is used in the reduced MNA matrix of the global network equation. Chiprout and Nakhla [11] introduced the complex frequency hopping technique (CFH) or multipoint Padé approximation to extract

accurate dominant poles of a linear network within the frequency range of interest. This constrained search of system poles in the left half plane improves the methods' capability to detect some of the high-frequency dominant poles that lie far from the expansion points. Recently, Sanaie and Nakhla [16], [58] introduced a method for incorporating subnetworks characterized by measurement data in AWE. In [20], a rational approximation technique is used to generate the moments from the measured data. However, the moments calculated by differentiating the approximating rational functions are order dependent and violate the definition of the Taylor series.

The addition of the above described techniques has converted AWE into a general purpose simulator that can be used frequency and time-domain analysis, sensitivity analysis, and symbolic analysis. These improvements, however, have been achieved at the cost of reducing the speed and increasing the complexity of AWE. Nonlinear elements are handled using partitioning and macromodeling that are implemented in the context of a traditional simulation using implicit integration methods. The admittance macromodel is solved in time-marching fashion with the Newton-Raphson iteration to update coefficients. Pre-processing of subnetworks is also required before constructing the admittance macromodel. The CFH methods require the expansion of system functions at several points in search of good candidates for dominant poles. Although these additional operations increased the complexity of AWE, the method remains very efficient for analyzing electronic packages, performance-driven routing, and timing analysis of VLSI circuits.

**Algorithm 3.1:** Moment-matching method

1. *Compute the moments:*

$$M_n = \frac{\left[ \frac{\partial^n Y(s)}{\partial s^n} \right]_{s=0}}{n!} E(s)$$

2. *Compute the denominator polynomial coefficients,  $b_i$ 's:*

$$\begin{bmatrix} M_l & M_{l-1} & \cdot & \cdot & \cdot & M_{l-q+1} \\ M_{l+1} & M_l & \cdot & \cdot & \cdot & M_{l-q+2} \\ \cdot & \cdot & \cdot & \cdot & \cdot & \cdot \\ \cdot & \cdot & \cdot & \cdot & \cdot & \cdot \\ \cdot & \cdot & \cdot & \cdot & \cdot & \cdot \\ M_{l+q-1} & M_{l+q-2} & \cdot & \cdot & \cdot & M_l \end{bmatrix} \begin{bmatrix} b_1 \\ b_2 \\ \cdot \\ \cdot \\ \cdot \\ b_q \end{bmatrix} = - \begin{bmatrix} M_{l+1} \\ M_{l+2} \\ \cdot \\ \cdot \\ \cdot \\ M_{l+q} \end{bmatrix}$$

3. Compute (poles) the roots of the denominator polynomial,  $p_i$ 's:

$$b_q p^{-q} + b_{q-1} p^{-q+1} + \dots + b_2 p^{-2} + b_1 p^{-1} + 1 = 0$$

4. Compute the residues:

$$\begin{bmatrix} 1 & p_1^{-1} & \cdot & \cdot & \cdot & p_{q-1}^{-1} & p_q^{-1} \\ 0 & p_1^{-2} & \cdot & \cdot & \cdot & p_{q-1}^{-2} & p_q^{-2} \\ \cdot & \cdot & \cdot & \cdot & \cdot & \cdot & \cdot \\ \cdot & \cdot & \cdot & \cdot & \cdot & \cdot & \cdot \\ \cdot & \cdot & \cdot & \cdot & \cdot & \cdot & \cdot \\ 0 & p_1^{-q} & \cdot & \cdot & \cdot & p_{q-1}^{-q} & p_q^{-q} \\ 0 & p_1^{-q-1} & \cdot & \cdot & \cdot & p_{q-1}^{-q-1} & p_q^{-q-1} \end{bmatrix} \begin{bmatrix} k_\infty \\ k_1 \\ \cdot \\ \cdot \\ \cdot \\ k_{q-1} \\ k_q \end{bmatrix} = - \begin{bmatrix} M_0 \\ M_1 \\ \cdot \\ \cdot \\ \cdot \\ M_{q-1} \\ M_q \end{bmatrix}$$

5. Construct reduced-order model:

$$H(s) = k_\infty + \sum_{i=1}^q \frac{k_i}{s - p_i}$$

### 3.4 Krylov Subspace-Based Methods

Methods based on Krylov projectors can be used to generate reduced-order models of large systems. The Krylov subspace methods are more stable than moment-matching methods because the solution of an ill-conditioned, moment matrix is not needed to calculate the dominant poles. Two variants of these methods, Arnoldi and Lanczos processes,

are discussed in this chapter. Both methods construct the reduced-order models in a computationally efficient manner by recursively operating on the original system. The methods are applied successfully for time and frequency-response approximations of large-lumped networks. The Arnoldi and Lanczos methods compare favorably to the moment-matching technique in their numerical stability and accuracy. Illustrative examples are also given to study the methods' performance and accuracy.

### 3.4.1 Krylov subspace method

The numerical calculations of all eigenvalues of a matrix, even for a matrix of moderate size, are prohibitively expensive. The Krylov method allows us to estimate some or all of the eigenvalues of a matrix without solving a large eigenvalue problem. The method takes advantage of the sparsity of the matrix, which makes it particularly attractive for circuit-simulation problems.

The Krylov subspace method simplifies the computation of the characteristic equation of a matrix,  $Y$ , by transforming the equation

$$p(s) = \begin{vmatrix} y_{11} - s & y_{12} & \dots & y_{1n} \\ y_{21} & y_{22} - s & \dots & y_{2n} \\ \dots & \dots & \dots & \dots \\ y_{n1} & y_{n2} & \dots & y_{nn} - s \end{vmatrix} = 0 \quad (3.24)$$

to an equivalent equation

$$q(s) = \begin{vmatrix} a_{11} - s & a_{12} & \dots & a_{1n} \\ a_{21} - s^2 & a_{22} & \dots & a_{2n} \\ \dots & \dots & \dots & \dots \\ a_{n1} - s^n & a_{n2} & \dots & a_{nn} \end{vmatrix} = 0 \quad (3.25)$$

The expansion of (3.25) in the power of  $s$  is accomplished with little effort by expanding the determinant in terms of minors of one row or one column [84].



The coefficients,  $a_{ij}$ , in (3.25) are determined by the recurrent formulas

$$\begin{aligned} a_{1j} &= y_{1j} \\ a_{ij} &= \sum_{k=1}^n a_{i-1,k} y_{kj} \quad (i=2, \dots, n; \quad j=1, \dots, n) \end{aligned} \quad (3.26)$$

For a nonsingular system, the polynomials  $p(s)$  and  $q(s)$  have identical roots. The polynomial  $q(s)$  differs from the desired characteristic polynomial  $p(s)$  by only a numerical factor

$$q(s) = \alpha p(s) \quad (3.27)$$

The numerical factor for an initial vector  $A_0 = (1, 0, \dots, 0)^H$  is given by

$$\alpha = \begin{vmatrix} 1 & 0 & \dots & 0 \\ a_{11} & a_{12} & \dots & a_{1n} \\ \cdot & \cdot & \dots & \cdot \\ a_{n-1,1} & a_{n-1,2} & \dots & a_{n-1,n} \end{vmatrix} \quad (3.28)$$

Equation (3.26) can be written as a matrix-vector product of the form

$$a_i = A a_{i-1}, \quad (i=1, 2, \dots, n) \quad (3.29)$$

where  $A$  is the transpose of the given matrix,  $Y$ , obtained from the topology of the network and  $a_i = (a_{i1}, a_{i2}, \dots, a_{in})^H$  is a column vector. Equation (3.28) can also be written as

$$a_i = A^i a_0, \quad (i=1, 2, \dots, n) \quad (3.30)$$

The sequence of vectors generated by the recurrent Equation (3.29) is called the Krylov sequence. For  $\alpha \neq 0$ , the vectors  $a_0, a_1, \dots, a_{k-1}$  form a basis of the Krylov subspace generated by (3.29) and (3.30), i.e., the subspace of the form

$$K_k(A, a_0) = (a_0 \quad A a_0 \quad A^2 a_0 \quad \dots \quad A^{k-1} a_0) = (a_0 \quad a_1 \quad a_2 \quad \dots \quad a_{k-1}) \quad (3.31)$$

For the smallest integer  $k$ , where the matrix  $K_k(A, a_0)$  is not full column rank, the vectors  $a_0, a_1, \dots, a_k$  are not linearly independent. Therefore, the vector  $a_k$  can be written as a linear combination

$$a_k = c_1 a_{k-1} + \dots + c_k a_0 \quad (3.32)$$

where the  $a_i$ 's are determined by Equation (3.29) and  $c_i$ 's are the coefficients of the characteristic polynomial. Thus the Krylov method makes it possible to determine the coefficients of the characteristic polynomial without solving an eigenvalue problem.

The particular Krylov subspace methods that we consider are the Arnoldi and Lanczos methods. The Arnoldi and Lanczos methods reduce a matrix into lower-order Hessenberg and tridiagonal matrices, respectively.

### 3.4.2 Arnoldi algorithm

The Arnoldi algorithm is used to generate a reduced-order model of a large system. The method is based on the orthogonal projection of a system onto a subspace spanned by  $K_k(A, v_0)$ , where  $v_0$  is an initial vector. The Arnoldi algorithm generates the Krylov sequence of vectors  $v_i$  using the Gram-Schmidt process. The vectors  $v_i$ 's are mutually orthonormal and have the property that

$$\text{span}\{v_0, v_1, \dots, v_{k-1}\} = K_j(A, v_0) = \text{span}\{v_0, Av_0, \dots, A^{k-1}v_0\} \quad (3.33)$$

The results of the Arnoldi process are a reduced  $r \times r$  upper Hessenberg matrix  $H$  and a set of  $N \times r$  Krylov vectors such that

$$\begin{aligned} AV &= VH \\ V^H V &= I \end{aligned} \quad (3.34)$$

Given a starting nonzero vector  $v_0$ , the procedure generates the orthonormal basis,  $V$ . The constructed orthogonal basis of the Krylov subspace generates a reduced Hessenberg matrix  $H_k$  whose entries are obtained by

$$h_{i,j} = \begin{cases} \|v_{i+1}^H\|_2, & \text{if } i = j+1 \\ v_i^H A v_j, & \text{elsewhere} \end{cases} \quad (3.35)$$

Then, the eigenvalues of  $H_k$ , can be used as approximations for the eigenvalues of  $A$ . If  $A$  is symmetric, then  $H_k$  is a tridiagonal matrix. In this case, the Arnoldi method reduces to the Lanczos method described in the next section. Furthermore, if  $A$  is symmetric, the reduced matrix  $H_k$  is built using only three-term recurrences.

The pseudo-code for the Arnoldi algorithm is given in Algorithm 3.2.

**Algorithm 3.2:** Arnoldi Algorithm

1) Choose  $v_1$  with  $\|v_1\|_2 = 1$

For  $n=1,2,\dots$ , do:

2) For  $k = 1, 2, \dots, n$ , compute

$$h_{kn} = v_k^H A v_n$$

3) Set

$$\tilde{v}_{n+1} = A v_n - \sum_{k=1}^n h_{kn} v_k$$

4) Compute

$$h_{n+1,n} = \|\tilde{v}_{n+1}\|_2$$

5) If  $h_{n+1,n} = 0$ , stop.

Otherwise, set

$$v_{n+1} = \frac{\tilde{v}_{n+1}}{h_{n+1,n}}$$

The third step can be written in a matrix form as follows:

$$A V_n = V_{n+1} \tilde{H}_n$$

where

$$V_n = [v_1 \quad v_2 \quad \dots \quad v_n]$$

has orthonormal columns, and

$$\tilde{H}_n = \begin{bmatrix} h_{11} & h_{12} & \dots & h_{1n} \\ h_{21} & h_{22} & \dots & \cdot \\ 0 & h_{32} & \dots & \vdots \\ \vdots & \dots & h_{n,n-1} & h_{nn} \\ 0 & \dots & 0 & h_{n+1,n} \end{bmatrix}$$

is an upper Hessenberg matrix of full rank  $n$ .  $H_n$  is obtained by removing the last row of  $\tilde{H}_n$ .

### 3.4.3 Lanczos algorithm

The Lanczos method reduces an arbitrary large nonsymmetric matrix  $A$  to a tridiagonal matrix  $T_k$  using two biorthogonal Krylov spaces whose columns are recursively filled using the matrix  $A$  and two initial vectors. Given two nonzero initial vectors, the generated biorthogonal basis vectors

$$\begin{aligned} V_k &= (v_0 \quad v_1 \quad \dots \quad v_{k-1}) \\ W_k &= (w_0 \quad w_1 \quad \dots \quad w_{k-1}) \end{aligned}$$

satisfy  $W_k^H V_k = I$ , and they are related to  $A$ -invariant and  $A^H$ -invariant Krylov subspace,  $K_k$ , in that

$$\begin{aligned} \text{span}(V_k) &= K_k(A, v_0) = \text{span}(v_0, Av_0, \dots, A^{k-1}v_0) \\ \text{span}(W_k) &= K_k(A^H, w_0) = \text{span}(w_0, A^H w_0, \dots, (A^H)^{k-1}w_0) \end{aligned} \tag{3.36}$$

The  $V_k$  and  $W_k$  are constructed based on three-term recurrences given as

$$v_{n+1} = Av_n - \alpha_n v_n - \beta_n v_{n-1}$$

$$w_{n+1} = A^H w_n - \alpha_n w_n - \gamma_n w_{n-1}$$

where  $\alpha_n = \frac{w_n^T A v_n}{\delta_n}$ ,  $\beta_n = \frac{\delta_n}{\delta_{n-1}} \eta_n$ , and  $\gamma_n = \frac{\delta_n}{\delta_{n-1}} \rho_n$  are the diagonal, upper, and lower off-diagonal elements of the reduced tridiagonal matrix  $T$ , respectively. The results,  $V$ ,  $W$ , and  $T$  matrices, satisfy

$$AV = W^H T$$

$$W^H V = I$$

The best  $k \times k$  approximation to  $A$  that can be obtained using the information from the two Krylov spaces is the matrix  $T_k$ . These two bases can be built only with three-term recurrences, thus requiring only inner-products and matrix-vector multiplication. The methods also take advantage of the sparsity of the  $A$  matrix to generate the reduced triangular matrix quite efficiently. If the rows of  $A$  have  $m$  nonzero entries, the matrix-vector product  $Av_i$  uses only  $mn$  multiplications. The whole iteration step can take only  $mn+4n$  products.

Then, the eigenvalues of  $T_k$  can be used as approximations for the eigenvalues of  $A$ . The nonsymmetric Lanczos algorithm is given in Algorithm 3.3. Typically, the spectrum of  $T_n$  offers good approximations to some of the eigenvalues of  $A$  after relatively few iterations, i.e., for  $n \ll N$ . The reduced tridiagonal matrix  $T_n$  is obtained by removing the last row of  $\tilde{T}_n$ .

**Algorithm 3.3:** Lanczos Algorithm

*Lanczos*( $A, v_1, w_1, r$ )

1) For a given pair,  $v_1, w_1$  such that  $v_1, w_1 \neq 0$

Set  $v_0 = w_0 = 0$ , and  $\delta_0 = 1$ .

For  $n=1,2,\dots,r$ , do:

2) Compute  $\delta_n = \tilde{w}_n^H \tilde{v}_n$ , if  $\delta_n = 0$ , stop,

else compute  $\alpha_n = \frac{w_n^T A v_n}{\delta_n}$ ,  $\beta_n = \frac{\delta_n}{\delta_{n-1}} \eta_n$ , and  $\gamma_n = \frac{\delta_n}{\delta_{n-1}} \rho_n$ .

3) Compute

$$\begin{aligned} v_{n+1} &= A v_n - \alpha_n v_n - \beta_n v_{n-1} \\ w_{n+1} &= A^H w_n - \alpha_n w_n - \gamma_n w_{n-1}. \end{aligned}$$

4) Set  $\rho_{n+1} = \|v\|_2$ ,  $\eta_{n+1} = \|w\|_2$ ,

$$v_{n+1} = \frac{v}{\rho_{n+1}} \text{ and } w_{n+1} = \frac{w}{\eta_{n+1}}.$$

The coefficients  $\alpha_n, \beta_n$ , and  $\gamma_n$  form the reduced tridiagonal matrix

$$\tilde{T}_n = \begin{bmatrix} \alpha_1 & \beta_2 & 0 & \dots & 0 \\ \gamma_2 & \alpha_2 & \cdot & \dots & \vdots \\ 0 & \cdot & \cdot & \dots & 0 \\ \vdots & \cdot & \cdot & \cdot & \beta_n \\ 0 & \dots & 0 & \gamma_n & \alpha_n \\ 0 & \dots & \dots & 0 & \gamma_{n+1} \end{bmatrix}$$

### 3.4.4 Computing poles and residues

If the network consists of only linear elements, the Equation (3.5) can be written in Laplace domain as

$$(sC + G)V(s) = J(s) \quad (3.37)$$

The frequency response of the network for the  $i$ th variable is

$$H(s) = e_i (sC + G)^{-1} J(s) \quad (3.38)$$

where  $e_i$  is a unit vector with a one on the  $i$ th position and zero elsewhere.

The reduced transfer function of the system in (3.38) can be written in the form

$$H(s) = k_{\infty} + \sum_{i=1}^r \frac{k_i}{s - p_i} \quad (3.39)$$

where the  $p_i$ 's and  $k_i$ 's are the poles and residues of the reduced system, respectively. The Arnoldi and Lanczos methods can generate the reduced-order transfer function equivalent to (3.38) by operating on the system matrix  $A$  and on the two initial vectors  $\tilde{v}_0$  and  $\tilde{w}_0$  that are obtained from the topology of the network given by

$$A = -(G + s_0 C)^{-1} C, \quad (3.40a)$$

$$\tilde{v}_0 = (G + s_0)^{-1} J, \quad (3.40b)$$

$$\tilde{w}_0 = e_i \quad (3.40c)$$

where  $e_i$  selects the output variable of interest.

Let the matrices  $V_r$  and  $W_r$  be the results of two separate Arnoldi methods or one Lanczos method run with initial vectors. Both methods produce the Krylov bases,  $K(A, \tilde{v}_0)$  and  $K(A, \tilde{w}_0)$ , with approximately the same complexity. The Arnoldi method, in general, more reliable than the Lanczos method. Although there is no guarantee for the stability of the Arnoldi-reduced matrix  $H_r$  and Lanczos-reduced matrix  $T_r$ , the Lanczos method is often used because of the existence of some techniques, such as restarted Lanczos method to insure the stability of Lanczos-reduced model [124].

The eigen-decomposition of the reduced matrix  $T_r$  or  $H_r$  is easily computed using one of the standard methods [64] to give

$$T_r = S_r \Lambda S_r^{-1} \quad (3.41)$$

where  $\Lambda$  and  $S_r$  are the diagonal matrix and the eigenvector matrix, respectively. The poles are obtained from the eigenvalues as

$$p_i = \lambda_i^{-1} \quad (3.42)$$

and the residues are calculated from

$$\begin{aligned}
k_i &= \frac{e_i \bar{v}_0 \cdot (S_i^T e_1)(S_i^{-1} e_1)}{\lambda_i} \\
k_\infty &= \sum_{\substack{i=1 \\ \lambda_i=0}}^r e_i \bar{v}_0 \cdot (S_i^T e_1)(S_i^{-1} e_1)
\end{aligned} \tag{3.43}$$

where  $S_i$  is the eigenvector belonging to  $\lambda_i$  and  $e_i = [1, 0, \dots, 0]^T$ .

Padé via Arnoldi (PVA) and Padé via Lanczos (PVL) methods for calculating reduced order model of linear lumped using Arnoldi and Lanczos are given in Algorithms 3.4 and 3.5, respectively.

**Algorithm 3.4:** Padé via Arnoldi

*PVA(G, C, s<sub>0</sub>, r, i)*

1) Define  $A = -(G + s_0 C)^{-1} C$ ,  $v_0 = (G + s_0)^{-1} J$ , and  $e_i$

2)  $T_r = \text{Arnoldi}(A, r, v_0)$

3) Compute an eigen-decomposition of the reduced matrix  $H_r$ ,

$$H_r = S_r \Lambda S_r^{-1}$$

4) Calculate the poles and the residues

$$p_i = \lambda_i^{-1}$$

$$k_i = \frac{e_i v_0 \cdot (S_i^T e_1)(S_i^{-1} e_1)}{\lambda_i}$$

$$k_\infty = \sum_{\substack{i=1 \\ \lambda_i=0}}^r e_i v_0 \cdot (S_i^T e_1)(S_i^{-1} e_1)$$

where  $S_i$  is the eigenvector belonging to  $\lambda_i$  and  $e_i = [1, 0, \dots, 0]^T$ .



**Algorithm 3.5: Padé via Lanczos**

$$PVL(G, C, s_0, r, i)$$

1) Define  $A = -(G + s_0 C)^{-1} C$ ,  $v_0 = (G + s_0)^{-1} J$ , and  $w_0 = e_i$

2)  $T_r = \text{Lanczos}(A, r, v_0, w_0)$

3) Compute an eigen-decomposition of the reduced matrix  $T_r$

$$T_r = S_r \Lambda S_r^{-1}$$

4) Calculate the poles and the residues

$$p_i = \lambda_i^{-1}$$

$$k_i = \frac{e_i v_0 \cdot (S_i^T e_1)(S_i^{-1} e_1)}{\lambda_i}$$

$$k_\infty = \sum_{\substack{i=1 \\ \lambda_i=0}}^r e_i v_0 \cdot (S_i^T e_1)(S_i^{-1} e_1)$$

where  $S_i$  is the eigenvector belonging to  $\lambda_i$  and  $e_1 = [1, 0, \dots, 0]^T$ .

In the following section, moment-matching and Lanczos methods are applied in a Padé analysis to approximate the responses of linear circuits.

### 3.5 Applications

The Padé synthesis of linear networks using the moment-matching and Krylov-subspace methods are compared. For illustration purposes, the moment values before and after scaling are given. The poles and the residues of various orders of approximation are also tabulated. Response waveforms for various orders of approximations are given, and a comparison with traditional methods is also given.

### 3.5.1 Example 3.1: RLC circuit

Consider the RLC circuit shown in Figure 3.1. A pulse waveform of  $0.1 \text{ ns}$  rise and fall times and  $0.5 \text{ ns}$  pulse duration, shown in Figure 3.2, is used as an input. Both the Lanczos and moment-matching methods are applied to extract the poles of the circuit. The approximation is done at  $s=0$  in order to compare the results with published work [12].

The moments generated vary considerably in scale. The moment matrix formed using these values is ill-conditioned. To avoid this problem, moment scaling is applied. The actual and the scaled moments are shown in Table 3.1.

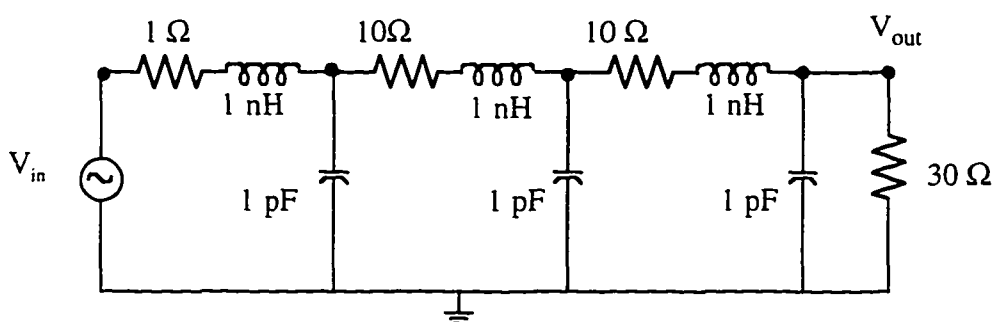


Figure 3.1: RLC circuit.

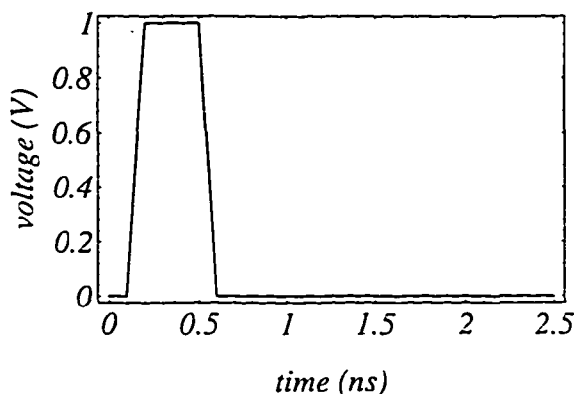


Figure 3.2: Input waveform for RLC Example 3.1.

The approximated poles converge to the actual poles of the network. Using the poles and residues, the time-domain response can be obtained by applying a recursive convolution that is discussed in Chapter 5.

**Table 3.1:** Expansion moments.

| Order    | Actual moments                        | Scaled moments                       |
|----------|---------------------------------------|--------------------------------------|
| $M_0$    | 0.2127827084259825                    | $-1.192217128472535 \times 10^{-11}$ |
| $M_1$    | $-1.192217128472535 \times 10^{-11}$  | $-1.192217128472535 \times 10^{-11}$ |
| $M_2$    | $-1.478364899656193 \times 10^{-22}$  | $2.638533534523005 \times 10^{-11}$  |
| $M_3$    | $3.111527518808308 \times 10^{-32}$   | $9.91141355227619 \times 10^{-12}$   |
| $M_4$    | $-3.388034280475733 \times 10^{-43}$  | $1.926152738770375 \times 10^{-12}$  |
| $M_5$    | $-6.607005742449817 \times 10^{-53}$  | $-6.703916347266424 \times 10^{-12}$ |
| $M_6$    | $2.284754958651971 \times 10^{-63}$   | $-1.192217128472535 \times 10^{-11}$ |
| $M_7$    | $1.038643408885756 \times 10^{-73}$   | $4.137561920769726 \times 10^{-12}$  |
| $M_8$    | $-7.692418404174678 \times 10^{-83}$  | $-3.357007586637437 \times 10^{-12}$ |
| $M_9$    | $-7.119239194301306 \times 10^{-93}$  | $-4.43741172989366 \times 10^{-12}$  |
| $M_{10}$ | $1.964689820995303 \times 10^{-103}$  | $7.329618812040346 \times 10^{-13}$  |
| $M_{11}$ | $-2.736497219579782 \times 10^{-113}$ | $3.610129450868341 \times 10^{-12}$  |

The reduced-order approximation of the RLC circuit via both the moment-matching and Lanczos methods gave correct and completely identical results. The various orders approximations of the poles and residues are given in Tables 3.2 and 3.3, respectively. Exceptionally good agreements, of more than eight-digit accuracy, are obtained for the poles and residues of this circuit. The first-order approximation shown in Figure 3.3 exhibits an error that may be unacceptable for some delay applications. This approximation corresponds to the Elmore delay. Higher-order approximations are found at incremental cost to the first-order approximation. As shown in Figures 3.4 and 3.5, the approximations are approaching the exact solution as the order increases. As shown in Figure 3.4, the second-order approximation gives an acceptable solution. The higher-order, fourth, fifth,

and sixth approximations are identical as shown in Figures 3.5 to the SPICE simulation results.

**Table 3.2.** Approximate poles for Example 3.1.

| order | poles $\times 10^{-10}$  |   |
|-------|--|---|
|       | Lanczos  | Moment matching   |
| 1     | -1.784764732   | -1.784764732  |
| 2     | -0.6183868387 $\pm j$ 2.0091873  | -0.6183868387 $\pm j$ 2.0091873   |
| 3     | -0.4687361814 $\pm j$ 2.002331794<br>-25.78293771  | -0.4687361816 $\pm j$ 2.002331794<br>-25.78293771   |
| 4     | -0.4718456316 $\pm j$ 2.005063915<br>-1.612961139<br>-43.33257593  | -0.4718464207 $\pm j$ 2.005063523<br>-1.61296114<br>-43.33335495  |
| 5     | -0.4780826222 $\pm j$ 2.008306882<br>-0.4439703289 $+ j$ 4.880644709<br>-0.6769398962                    | -0.4780841212 $\pm j$ 2.008308277<br>-0.4439702273 $+ j$ 4.880644925<br>-0.6769413692                   |
| 6     | -0.4780053243 $\pm j$ 2.008347166<br>-0.109034219 $\pm j$ 5.103524657<br>-6.227593083 $\pm j$ 1.77018153 | 0.4780055759 $\pm j$ 2.00834756<br>-0.109030158 $\pm j$ 5.103524513<br>-6.227591408 $\pm j$ 1.770180524 |

**Table 3.3.** Approximate residues for Example 3.1.

| order | residues   |  |
|-------|--|--|
|       | Lanczos  | Moment matching  |
| 1     | -0.2127827084  | -0.2127827084  |
| 2     | -0.1063913542 $\pm j$ 0.09836983483  | -0.1063913542 $\pm j$ 0.09836983483  |
| 3     | -0.0865486481 $\pm j$ 0.1040156707<br>-0.03968541224   | -0.0865486481 $\pm j$ 0.1040156707<br>-0.0396854122 - $j$ 7.452440653 $\times 10^{-19}$  |
| 4     | -0.08737105511 $\pm j$ 0.1045046772<br>-0.0002349088457 - $j$ 3.924641704 $\times 10^{-20}$<br>-0.0396854122 - $j$ 1.530094936 $\times 10^{-18}$ | -0.08737113831 $\pm j$ 0.104504651<br>-0.0002349080725 - $j$ 7.208607347 $\times 10^{-18}$<br>-0.03780552373 - $j$ 1.530094936 $\times 10^{-17}$ |
| 5     | 0.001689814954 $\pm j$ 0.01290704296<br>-0.09005050001 $\pm j$ 0.105044178<br>-0.03606133831 - $j$ 8.537363593 $\times 10^{-19}$                 | 0.001689840368 $\pm j$ 0.01290703191<br>-0.09005049554 $\pm j$ 0.1050443185<br>-0.03606139808 - $j$ 8.303899626 $\times 10^{-17}$                |
| 6     | -0.09001543714 $\pm j$ 0.1050821952<br>0.0007452615687 $\pm j$ 0.01464729719<br>-0.01712117864 $\pm j$ 0.007333778404                            | -0.09001543843 $\pm j$ 0.1050822346<br>0.0007452604444 $\pm j$ 0.0146473104<br>-0.01712117623 $\pm j$ 0.00733375678                              |

Because reduced-order models will ultimately be used for nonlinear simulations, the final comparison between the full and reduced-order models is done in the time domain. Not surprisingly, the time responses of the output for the two methods are indistinguishable. Figure 3.5 is the output waveform for the sixth-order approximation, respectively. The sixth-order approximations of both methods are exactly identical to the SPICE result.

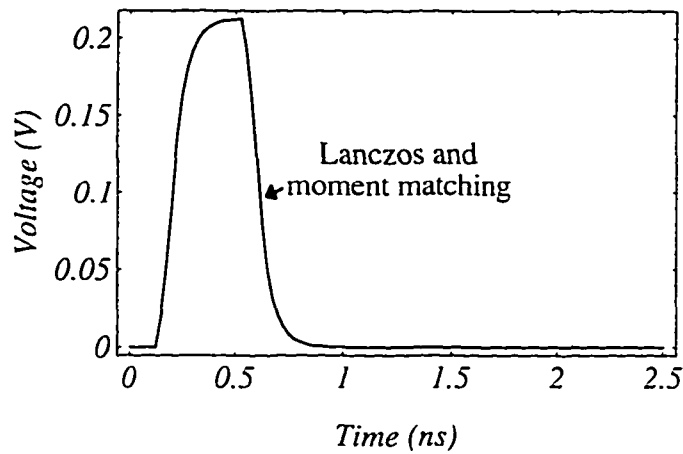


**Figure 3.3:** Transient response: First-order approximation.

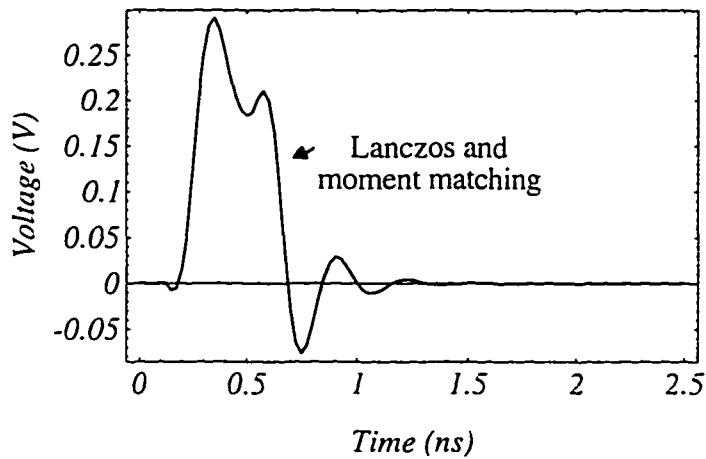


**Figure 3.4:** Output waveform: Second-order approximation.

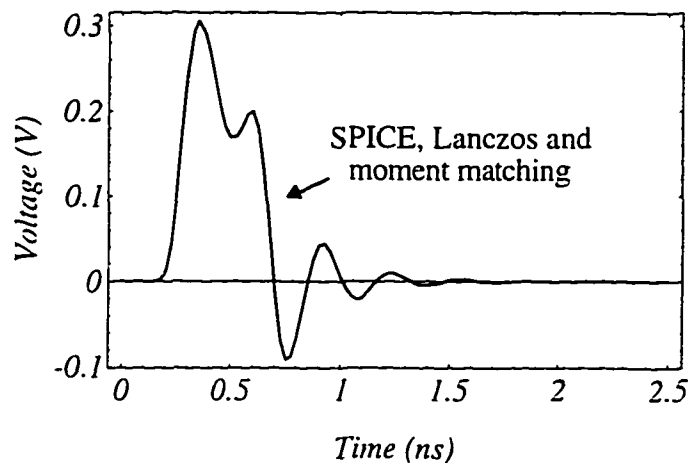


**Figure 3.5:** Output waveform: Sixth-order approximation and SPICE.

### 3.5.2 Example 3.2: RLC interconnect network

Consider a large, interconnect tree network shown in Figure 3.6. The uniform interconnects are modeled with a lumped RLC model. A pulse waveform of  $0.1 \text{ ns}$  rise and fall times and  $0.5 \text{ ns}$  pulse is applied at the input. The transient response is obtained by applying Lanczos and moment-matching methods.

Single-point expansion, Lanczos and moment-matching methods are performed to extract the poles and residues. The moment-matching method can only extract stable poles up to the eighth order. An improved approximation using the moment-matching method requires a multipoint expansion. On the other hand, the Lanczos method is able to extract stable, higher-order approximations. The comparison of the moment-matching method and the Lanczos approximations for the responses  $V_{29}$  and  $V_{20}$  are shown in Figures 3.7 and 3.8, respectively.

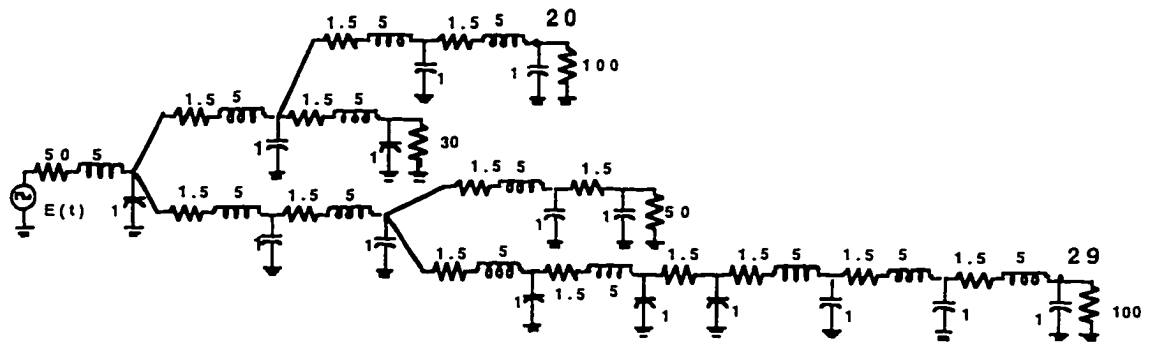


Figure 3.6: Interconnect network of Example 3.2 (all units are in  $\Omega$ ,  $nH$ , and  $pF$ ).

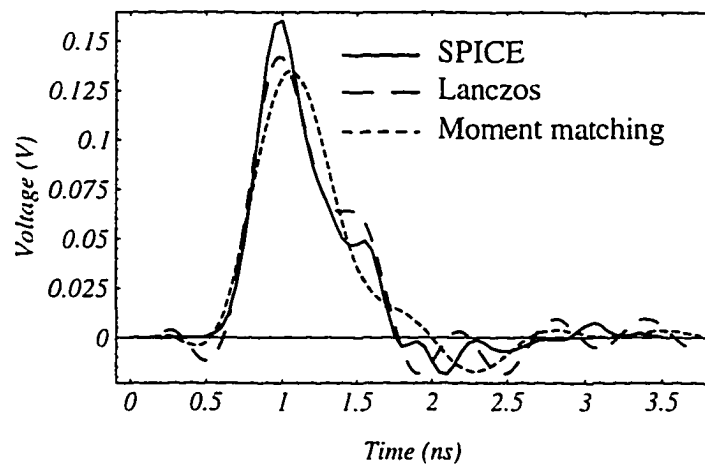
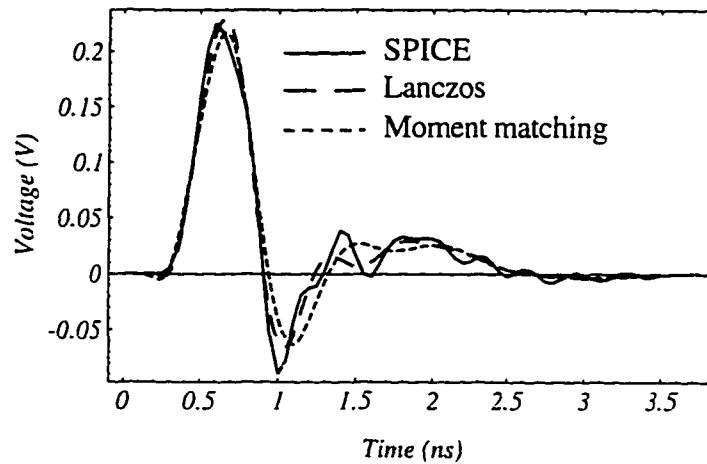


Figure 3.7: Response waveform at node 29.



**Figure 3.8:** Response waveform at node 20.

### 3.5.3 Example 3.3: Coaxial cable with skin effect

A lossy coaxial line is simulated using moment-matching and the accuracy of the method is studied. A 100 m long coaxial cable, shown in Figure 3.9, has the following characteristic parameters of transmission line:  $L=476 \text{ nH/m}$ ,  $C=0.0476 \text{ nF/m}$ ,  $G=0$ , and the resistance is characterized with a skin effect model described in [85] as

$$R(s) = A + B(s)^\alpha$$

where  $R$  is the overall resistance in ohms per meter,  $A=0$ ,  $B= 15.384$ ,  $\alpha=0.48288$ , and  $s=j2\pi f$ , where  $f$  is the frequency in GHz. The line is not terminated at the far end. A 3 V pulse of 2 ns rise / fall and a duration of 58 ns is placed at the input.



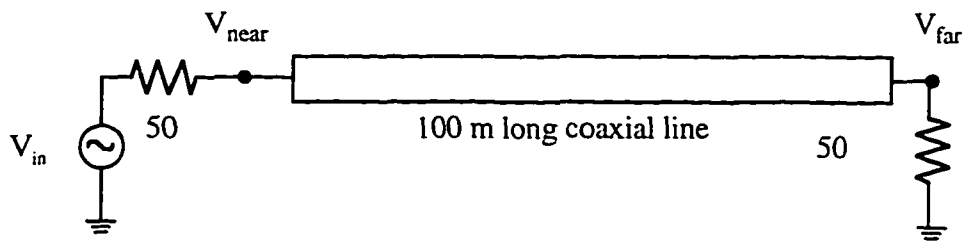


**Figure 3.9:** Example 3.3, a coaxial line.

The exact, transient response waveforms are obtained using the Fourier transform of 8192 points. The AWE technique with the method of characteristic [56] is applied to approximate the response. A single-point, moment-matching method is used to extract ten poles. The solutions are compared to the exact solutions obtained using frequency-domain analysis and IFFT. As shown in Figures 3.10 and 3.11, the reduced-model solutions are indistinguishable from the exact solutions while the moment-matching method shows considerable error.

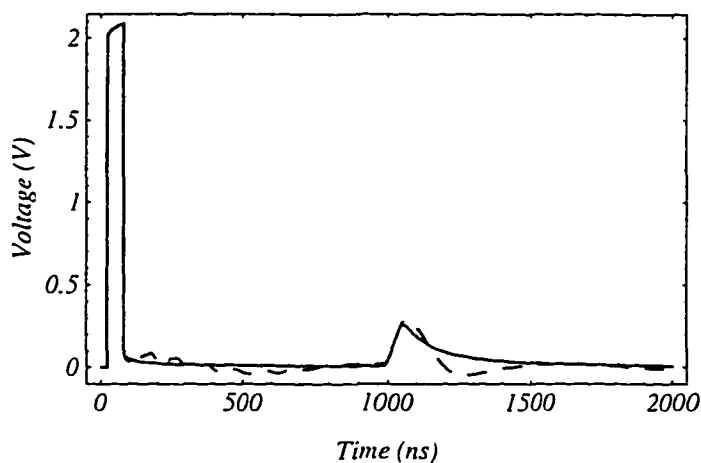


**Figure 3.10:** Example 3.3: Near-end voltage waveform, exact method (solid) and moment-matching (dashed).

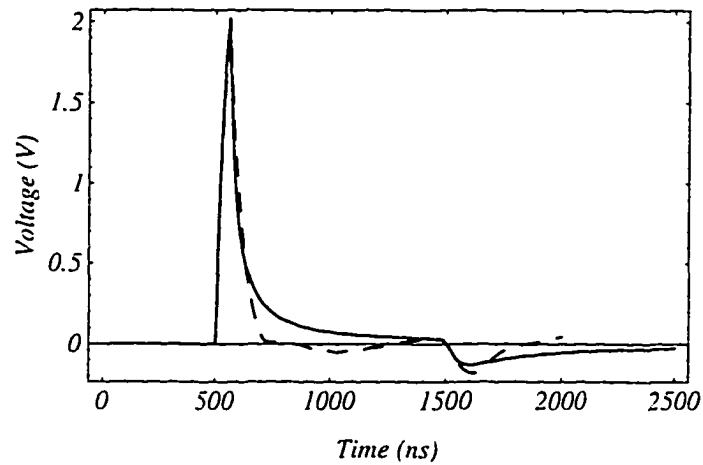


**Figure 3.11:** Example 3.3: Far-end voltage waveform, exact method (solid) and moment-matching (dashed).

### 3.5.4 Example 3.4: An example of RC-ladder network

Padé analysis is applied to analyze a simple stiff RC-ladder network shown in Figure 3.12. The moment-matching and the Lanczos methods are used to extract the eigenvalues of the system. A single-point expansion is used around the origin. As shown in Table 3.4, the moment-matching method is able to estimate only the two eigenvalues of the circuit. On the other hand, the Lanczos method gives all eigenvalues accurately. The comparison of the percentage errors for the moment-matching and Lanczos are given in Table 3.5.

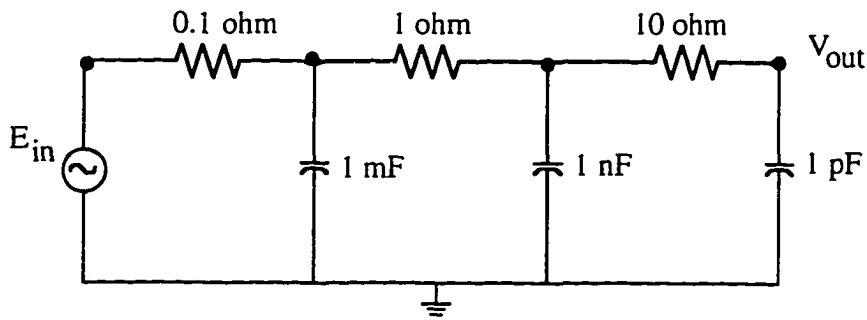


Figure 3.12: Example 3.4: An example of RC-ladder network

Table 3.4: Approximate poles for Example 3.4.

| order | Poles                         |                               |
|-------|-------------------------------|-------------------------------|
|       | Lanczos                       | Moment matching               |
| 1     | $-9.89011 \times 10^6$        | $-9.89011 \times 10^6$        |
| 2     | $-9.9899 \times 10^6$         | $-9.9899 \times 10^6$         |
|       | $-9.99901 \times 10^8$        | $-9.99901 \times 10^8$        |
| 3     | $-9.989899102 \times 10^6$    | $-9.989899102 \times 10^6$    |
|       | $-1.000001019 \times 10^9$    | $-1.000001008 \times 10^9$    |
|       | $-1.001010143 \times 10^{11}$ | $-1.013426214 \times 10^{11}$ |

Table 3.5: Absolute errors of approximate poles for Example 3.4.

| Exact poles                   | % error                  |                          |
|-------------------------------|--------------------------|--------------------------|
|                               | Lanczos                  | Moment matching          |
| $-9.989899102 \times 10^6$    | $3.5215 \times 10^{-9}$  | $3.617 \times 10^{-9}$   |
| $-1.000001023 \times 10^9$    | $3.525 \times 10^{-7}$   | $1.45307 \times 10^{-6}$ |
| $-1.001010091 \times 10^{11}$ | $5.25066 \times 10^{-6}$ | 1.24036                  |

### 3.6 Conclusions

Direct simulation methods are far too slow to consider the simulation of the entire chip with the electronic package that is needed for adequate circuit performance verification. As a result, many specialized methods that are based model-order reduction methodologies are applied to circuit simulations to tackle these problems. Methods based on Padé synthesis, such as AWE, CFH, PVL and PVA techniques are by far the most efficient analysis methods for systems with a large number of passive elements.

Padé approximation can also be efficiently applied to the analysis of transmission lines. The accuracy of the estimation is improved by merely increasing the order of approximation. Methods, such as AWE, CFH, PVL and PVA techniques give a two- to three-order magnitude savings in simulation time over the traditional methods when applied to a large system.

Both moment-matching and Krylov-subspace methods have shown to be computationally efficient. The Krylov subspace-based methods, and Arnoldi and Lanczos algorithms compare favorably to the moment-matching methods when analyzing linear lumped networks. For low-order systems, the moment-matching method and the Lanczos algorithm have identical accuracy. However, for stiff systems and large networks where high-order approximations are sought, the Krylov-subspace method is found to be superior.

The moment-matching, however, is direct and more efficient than the Krylov subspace-based method when analyzing distributed systems. The moments of a transmission line system can be calculated analytically and matched to obtain partial Padé approximation. However, for Krylov subspace-based methods, such as PVA and PVL, the transmission line system has to be approximated by a finite-order system. In [59], [86], and [87], the spatial variation of the transmission system is approximated by cosine and Chebyshev functions. The Arnoldi or Lanczos methods can be applied to the approximated

finite system to find a reduced model. The intermediate spatial approximation can introduce error.

Although the methods based on Padé approximations, such as AWE, CFH, PVA, and PVL reduce the simulation time for interconnect networks, the stability of the reduced model still remains an issue of concern. In Chapter 5, a guaranteed stable reduce-order modeling technique is described.

## CHAPTER 4

# ACCURATE ANALYSIS OF DIODE- SWITCHING CHARACTERISTICS USING ASYMPTOTIC WAVEFORM EVALUATION

### 4.1 Introduction

In this chapter, an accurate diode model that represents the transient behavior and high-frequency characteristics of a semiconductor diode is derived using the asymptotic waveform evaluation technique. The AWE technique is directly applied to the diffusion equation to construct a reduced pole-residue model that describes the dynamic process occurring in a  $p$ - $n$  junction. The model is derived by directly solving the carrier continuity equations in an analogous manner to that of the AWE solution to transmission line equations. The method efficiently calculates the poles and the residues of the diode model efficiently accurately by recursively generating the moments of the carrier concentration. The method simulates the excess carrier redistribution phenomenon in a diode junction using a reduced-order model. It simulates accurately the diode forward and reverse recovery phenomena in high-speed and power electronics. The model is capable of providing an increasingly accurate approximation to the characteristics of the device under all operating conditions.

The method reduces the computational cost by an order of magnitude over that for Linvill's multisection model [88] of ladder or lattice networks [89], [90] of many lumped elements used to model carrier diffusion and the recombination process. The diode recovery phenomenon is simulated for illustration, and the improved accuracy is verified by comparisons with results from conventional methods and published works.

For most applications, the transient simulation of integrated, diode-switching circuits can be carried out using conventional circuit simulators such as SPICE and ASTAP. However, under high-frequency operations, the compact analytical device models used in the traditional simulators cannot predict the true behavior of terminal currents and charges caused by the dynamic process of carrier diffusion and recombination in the diodes. The conventional charge-control model [91] that is derived with a quasi-static approximation produces unsatisfactory results when used for the transient analysis of switching circuits. For example, the diode reverse-recovery phenomenon and, consequently, the power dissipation during the diode turn-off process are often miscalculated.

More powerful and accurate models for diodes have been the topic of active research for many years [88], [89], [92]-[94]. In particular, the reverse-recovery phenomenon has been discussed in a number of recent papers [4], [90], [95]-[98]. Linvill in [88] showed that the diffusion process in junction transistors can be modeled by a ladder network consisting of many lumped elements. The physical model was modified by Wang and Branin [89] for simulating the diode recovery phenomenon in a circuit analysis environment. Although the incorporation of such elaborate models into a conventional circuit simulation program such as SPICE improves the accuracy of the analysis, the size of the problems increases several fold due to the introduction of many nodes to interconnect the lumped elements. A large number of circuit elements are necessary to account for the distributed nature of the carrier diffusion process in order to accurately predict the dynamic

behavior of a  $p$ - $n$  junction diode. Consequently, the method did not gain attention as an accurate modeling technique.

In [4], Chua and Chang proposed a diode model using higher-order dynamic elements. The method accurately represents the diode; however, the potential of the model has not been exploited fully because dynamic elements cannot easily be implemented in SPICE-like simulators. As a result, recent research efforts have been focused on improving the conventional model using additional circuit elements and macro-model circuits [95]-[97]. Most recently, Chang [90] has used a time-varying diode characteristic model for accurate analysis of diode-switching behavior.

In Chapter 3, Asymptotic waveform evaluation, and its derivatives, which are based on asymptotic waveform evaluation and other moment-matching techniques, have shown to be useful in the analysis of large, linear distributed systems described by partial differential equations. The AWE has been shown to be an efficient method to analyze large distributed networks with a gain of three orders of magnitude speed over that for traditional simulators. It provided a suitable platform for efficiently handling large RLC networks and distributed systems. The multisection, physical diode model [88], [89] can be efficiently implemented using AWE. The carrier-continuity equations describing the dynamic process in the diode junction can also be solved in a similar manner as for the AWE solution of the transmission line equations. First, the moments of the solutions of the continuity equations are computed recursively. The Padé approximation is applied to obtain a reduced-order model. Then, the resulting transfer parameters are expressed as a pole-residue model that can be used for time-domain simulations. Recursive convolution is used to obtain the transient response of diode-switching circuits.

In Section 4.2, we briefly outline the physical principles and the basic equations that govern the behavior of charge carriers in the presence of time-varying fields. Then the AWE technique for solving such a system of equations is discussed, and recursive relationships to generate moments of the solution of continuity equations are discussed. In



Section 4.3, simulation results and implementation issues are discussed via an example of diode-recovery analysis. The accuracy of the method is verified using conventional methods and published results of the exact numerical simulation using mixed-level circuit simulation [90]. Finally, a conclusion is given in Section 4.4.

## 4.2 AWE Diode Modeling

Consider a one-dimensional  $p$ - $n$  diode shown in Figure 4.1 with  $\{D_n, D_p\}$  and  $\{\tau_n, \tau_p\}$ , the electron and hole diffusion constants and life times, respectively. Under a quasi-neutral assumption, the dynamic behavior of excess minority-carrier concentrations  $n(x, t)$  and  $p(x, t)$  in the  $n$ -region and  $p$ -region, respectively, are governed by the continuity equation [98]

$$\begin{aligned} \frac{\partial n(\bar{x}, t)}{\partial t} &= D_n \frac{\partial^2 n(\bar{x}, t)}{\partial \bar{x}^2} - \frac{n(\bar{x}, t)}{\tau_n} & (0 \leq \bar{x} \leq W_p) \\ \frac{\partial p(x, t)}{\partial t} &= D_p \frac{\partial^2 p(x, t)}{\partial x^2} - \frac{p(x, t)}{\tau_p} & (0 \leq x \leq W_n) \end{aligned} \quad (4.1)$$

where  $\{W_p, W_n\}$  are the junction widths of the  $n$ -region and  $p$ -region, respectively. The total current, under the quasi-neutral approximation, can be approximated by the diffusion current at the junction interface  $x=0$ , i.e.,

$$\begin{aligned} i_n(t) &= -AqD_n \left. \frac{\partial n(\bar{x}, t)}{\partial \bar{x}} \right|_{\bar{x}=0} \\ i_p(t) &= -AqD_p \left. \frac{\partial p(x, t)}{\partial x} \right|_{x=0} \end{aligned} \quad (4.2)$$

where  $q$  is the charge and  $A$  is the junction area. To obtain the solutions of the partial differential Equation (4.1), we define the corresponding boundary conditions for excess carrier distributions

$$\begin{aligned}
 n(0,t) &= n_{p0} (e^{v(t)/V_T} - 1) \\
 p(0,t) &= p_{n0} (e^{v(t)/V_T} - 1)
 \end{aligned}
 \tag{4.3}$$

where  $\{n_{p0}, p_{n0}\}$ ,  $v(t)$ , and  $V_T$  are the equilibrium carrier concentrations, the diode junction voltage, and the thermal voltage, respectively.

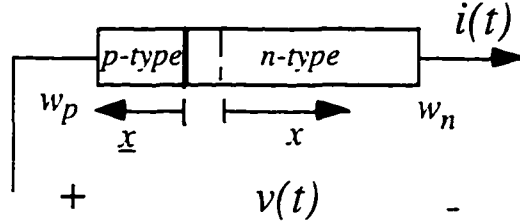


**Figure 4.1:** *p-n* Junction diode.

Identifying the continuity Equation (4.1) as an analogous to the transmission-line equation, the excess minority-carrier concentrations can be considered as the voltages and currents, with the diffusion constants, electron and hole life times, and width of the base acting as the transmission line parameters [88], [90]. The solution of (4.1) can be implemented very efficiently using the AWE technique without any synthesis and explicitly calculating any circuit element for a ladder or lattice network.

We start the solution process<sup>1</sup> by taking the Laplace transform of (4.1) that yields

$$sP(x,s) = D_p \frac{\partial^2 P(x,s)}{\partial x^2} - \frac{P(x,s)}{\tau_p}
 \tag{4.4}$$

Now let  $P(x,s)$  be expanded in a power series as

$$P(x,s) = P_0(x,s) + sP_1(x,s) + s^2P_2(x,s) + s^3P_3(x,s) + \dots
 \tag{4.5}$$

Inserting (4.5) into (4.4) yields

---

<sup>1</sup> The solution for electron concentration,  $n(x,t)$ , can be obtained in a similar manner.

$$sP_0(x,s) + s^2P_1(x,s) + s^3P_2(x,s) + \dots = D_p \left[ \frac{\partial^2 P_0(x,s)}{\partial x^2} + s \frac{\partial^2 P_1(x,s)}{\partial x^2} + s^2 \frac{\partial^2 P_2(x,s)}{\partial x^2} + \dots \right] - \frac{[P_0(x,s) + sP_1(x,s) + s^2P_2(x,s) + \dots]}{\tau_p} \quad (4.6)$$

Matching the corresponding powers of  $s$ , the following set of equations is obtained.

The zeroth-order equation is

$$0 = D_p \frac{\partial^2 P_0(x,s)}{\partial x^2} - \frac{P_0(x,s)}{\tau_p} \quad (4.7)$$

The first-order diffusion equation is

$$P_0(x,s) = D_p \frac{\partial^2 P_1(x,s)}{\partial x^2} - \frac{P_1(x,s)}{\tau_p} \quad (4.8)$$

and, in general, the  $n$ th -order diffusion equation is

$$P_{n-1}(x,s) = D_p \frac{\partial^2 P_n(x,s)}{\partial x^2} - \frac{P_n(x,s)}{\tau_p} \quad (4.9)$$

For convenience in exposition, a long base ( $W_n \rightarrow \infty$ ) is considered first. The initial and boundary conditions are

$$P_0(x,0) = P_{no} \tilde{V}(s) e^{-x/L_r} \Big|_{s=0} \quad (4.10.a)$$

$$\begin{aligned} P_0(0,s) &= P_{no} \tilde{V}(s) \\ P_n(x,0) &= 0 \\ P_n(0,s) &= 0 \end{aligned} \quad (4.10.b)$$

where  $n = 1, 2, 3, \dots$  and  $\tilde{V}(s)$  is the Laplace transform of  $\tilde{v}(t) = e^{v(t)/v_r} - 1$ .

To generate the moments of  $P(x,s)$ , the same system of differential equations must be solved repeatedly; the forcing functions on the right-hand side are the only changing parameters. First,  $P_0(x,s)$  is determined from (4.7). Then, (4.8) is used to find  $P_1(x,s)$ , and so forth, until  $2q$  moments have been found. All terms in moments, therefore, can be evaluated in succession by solving only the simpler differential equations. In [4], Chua and

Chang used quasi-static expansion to transform the partial differential Equations (4.1) into differential equations and to obtain a series of solutions in the time domain.

The zeroth-order solution for a long-base diode is given as

$$P_0(x, s) = P_{no} \tilde{V}(s) e^{-x/L_p} \quad (4.11)$$

The higher-order solutions of  $P_n(x, s)$ ,  $n=1, 2, 3, \dots$  are found to be

$$\begin{aligned} P_1(x, s) &= -\frac{\tau_p P_{no}}{2L_p} s [\tilde{V}(s) - \frac{\tilde{v}(0)}{s}] x e^{-x/L_p} \\ P_2(x, s) &= \frac{\tau_p^2 P_{no}}{8L_p} s^2 [\tilde{V}(s) - \frac{\tilde{v}(0)}{s}] (x + \frac{x^2}{L_p}) e^{-x/L_p} \\ P_3(x, s) &= -\frac{\tau_p^3 P_{no}}{16L_p} s^3 [\tilde{V}(s) - \frac{\tilde{v}(0)}{s}] (x + \frac{x^2}{L_p} + \frac{x^3}{3L_p^2}) e^{-x/L_p} \\ P_4(x, s) &= -\frac{\tau_p^4 P_{no}}{64L_p} s^3 [\tilde{V}(s) - \frac{\tilde{v}(0)}{s}] (\frac{5x}{2} + \frac{5x^2}{2L_p} + \frac{x^3}{L_p^2} + \frac{x^4}{6L_p^3}) e^{-x/L_p} \\ &\vdots \\ &\vdots \\ &\vdots \end{aligned} \quad (4.12)$$

The higher-order solutions are summarized in a matrix form as

$$\begin{bmatrix} P_1(x, s) \\ P_2(x, s) \\ P_3(x, s) \\ P_4(x, s) \\ P_5(x, s) \\ \vdots \\ P_n(x, s) \end{bmatrix} = \begin{bmatrix} \frac{-P_{no}\tau_p}{2L_p} & 0 & 0 & 0 & 0 & \dots \\ \frac{P_{no}\tau_p^2}{8L_p} & \frac{P_{no}\tau_p^2}{8L_p^2} & 0 & 0 & 0 & \dots \\ -\frac{P_{no}\tau_p^3}{16L_p} & -\frac{P_{no}\tau_p^3}{16L_p^2} & -\frac{P_{no}\tau_p^3}{48L_p^3} & 0 & 0 & \dots \\ \frac{5P_{no}\tau_p^4}{128L_p} & \frac{5P_{no}\tau_p^4}{128L_p^2} & \frac{P_{no}\tau_p^4}{64L_p^3} & \frac{P_{no}\tau_p^4}{384L_p^4} & 0 & \dots \\ -\frac{7P_{no}\tau_p^5}{256L_p} & -\frac{7P_{no}\tau_p^5}{256L_p^2} & -\frac{3P_{no}\tau_p^5}{256L_p^3} & -\frac{P_{no}\tau_p^5}{384L_p^4} & -\frac{P_{no}\tau_p^5}{3840L_p^5} & \dots \\ \vdots & \vdots & \vdots & \vdots & \vdots & \dots \end{bmatrix} \begin{bmatrix} x \\ x^2 \\ x^3 \\ x^4 \\ x^5 \\ \vdots \\ x^n \end{bmatrix} (\tilde{V}(s) - \frac{\tilde{v}(0)}{s}) e^{-x/L_p} \quad (4.13)$$

Here,  $v(t)$  is assumed to reach a steady-state value for  $t < 0$ . The general expression for the  $m$ th-order carrier distribution can be derived by induction as

$$P_m(x, s) = (C_n^m x^n + C_{n-1}^m x^{n-1} + \dots + C_1^m x + C_0^m) \left( \bar{V}(s) - \frac{\bar{v}(0)}{s} \right) e^{-x/L_p} \quad (4.14)$$

where  $C_n^m$  is the entry in the  $m$ th row and  $n$ th column of the triangular matrix in (4.13), henceforth referred to as matrix  $C$ .

Efficient recursive relationships to generate the higher-order moments are thus obtained from the entries of the matrix  $C$  of (4.13) as

$$\begin{aligned} C_n^m &= L_p \frac{C_{n+1}^m (n+1)}{2} - \frac{\tau_p C_{n-1}^{m-1}}{2L_p n} && \{for\ m > n \neq 1\} \\ C_n^m &= -\frac{\tau_p C_{n-1}^{m-1}}{2L_p n} && \{for\ m = n\} \\ C_n^m &= 0 && \{for\ n > m\} \end{aligned} \quad (4.15)$$

starting from

$$P_0(x, s) = P_{no} \bar{V}(s) e^{-x/L_p} \Rightarrow C_0^0 = P_{no}$$

Therefore, the higher-order solution of (1) for a finite-width base diode can be written in the form of

$$P(x, s) = (Ae^{-x/L_p} + Be^{x/L_p}) \left( \bar{V}(s) - \frac{\bar{v}(0)}{s} \right) \quad (4.16)$$

where  $P(x, s)$  is a column vector of higher-order solution  $P_n(x, s)$ ,  $n=1, 2, 3, \dots$ , and  $A$  and  $B$  are triangular matrices similar to matrix  $C$  of (4.13). The general expression for the  $m$ th-order carrier distribution can be similarly derived by induction from the entries of matrices  $A$  and  $B$ :

$$\begin{aligned} P_m(x, s) &= \left[ (a_n^m x^n + a_{n-1}^m x^{n-1} + \dots + a_1^m x + a_0^m) e^{-x/L_p} + (b_n^m x^n + b_{n-1}^m x^{n-1} + \dots + b_1^m x + a_0^m) e^{x/L_p} \right] \\ &\quad \times \left( \bar{V}(s) - \frac{\bar{v}(0)}{s} \right) \end{aligned} \quad (4.17)$$

where  $a_n^m$  and  $b_n^m$  are the entries in the  $m$ th row and  $n$ th column of the matrices  $A$  and  $B$ , respectively.

The efficient, recursive relationship to generate the higher-order moments is similarly derived:

$$\begin{aligned}
 a_n^m &= \frac{-L_p a_{n-1}^{m-1}}{2D_p n} && \{for\ m=n\} \\
 b_{ni}^m &= \frac{L_p b_{n-1}^{m-1}}{2D_p n} \\
 a_n^m &= \frac{-L}{2D_p n} [-D_p n(n-1)a_{m+1}^m + a_{n-1}^{m-1}] \\
 b_n^m &= \frac{-L}{2D_p n} [-D_p n(n-1)b_{m+1}^m + b_{n-1}^{m-1}] && \{for\ m > n \neq 1\} \quad (4.18) \\
 a_n^m &= \frac{-W_n}{1 - e^{-zW_n/L_p}} \left[ \sum_{j=1}^m a_j^m W_n^{j-1} + e^{-zW_n/L_p} \sum_{j=1}^m b_j^m W_n^{j-1} \right] \\
 b_n^m &= \frac{W_n}{1 - e^{-zW_n/L_p}} \left[ \sum_{j=1}^m a_j^m W_n^{j-1} + e^{-zW_n/L_p} \sum_{j=1}^m b_j^m W_n^{j-1} \right] && \{for\ n=1\}
 \end{aligned}$$

Therefore,

$$b_n^m = -a_n^m \quad \{for\ n=1\}$$

$$\text{and } a_n^m = b_n^m = 0 \quad \{for\ m < n\}$$

where

$$\begin{aligned}
 a_0^0 &= \frac{P_{no} e^{-zW_n/L_p}}{e^{-zW_n/L_p} - 1} \\
 b_0^0 &= \frac{P_{no}}{1 - e^{-zW_n/L_p}}
 \end{aligned} \quad (4.19)$$

Next, the  $r$ th -order excess hole density, the solution to (4.1), is given by the power series

$$\begin{aligned}
 P(x, s) &= \sum_{k=0}^r s^k P_k(x, s) \\
 N(x, s) &= \sum_{k=0}^r s^k N_k(x, s)
 \end{aligned} \quad (4.20)$$

The diode current can be found in (4.2)

$$I_0(s) + sI_1(s) + s^2I_2(s) + \dots = -AqD_p \left. \frac{\partial P(x,s)}{\partial x} \right|_{x=0} \quad (4.21)$$

By substituting (4.20) into (4.21), the current for a long-base diode ( $W_n \rightarrow \infty$ ) can be expressed as [4]

$$I(s) = I_s \tilde{V}(s) + I_s \left[ \frac{\tau_p s}{2} - \frac{\tau_p^2 s^2}{8} + \frac{\tau_p^3 s^3}{16} - \frac{\tau_p^4 s^4}{128} + \frac{7\tau_p^5 s^5}{256} - \dots \right] \left( \tilde{V}(s) - \frac{\tilde{v}(0)}{s} \right) \quad (4.22)$$

The above series also converges at the rate  $\tau_p \approx 10^{-7}$ .

If we define a *virtual admittance* as  $\tilde{Y}(s) = \frac{I(s)}{\tilde{V}(s)}$  and assume that  $\tilde{v}(0) = 0$  without any loss of generality, then

$$\tilde{Y}(s) = I_s \left[ 1 + \frac{\tau_p s}{2} - \frac{\tau_p^2 s^2}{8} + \frac{\tau_p^3 s^3}{16} - \frac{\tau_p^4 s^4}{128} + \frac{7\tau_p^5 s^5}{256} - \dots \right] \quad (4.23)$$

Thus, the procedure above allows one to compute the moments of the *virtual admittance*  $\tilde{Y}(s)$  for a *p-n* diode:

$$\tilde{Y}(s) = \tilde{Y}_0(s) + s\tilde{Y}_1(s) + s^2\tilde{Y}_2(s) + s^3\tilde{Y}_3(s) + \dots \quad (4.24)$$

Once the moments are found, the Padé approximation is carried out to convert the  $2q$  low-order moments into a  $q$  pole-residue rational function. The *virtual admittance* can be written in the form

$$a_0 + \sum_{i=1}^q \frac{a_i}{1 + \frac{s}{p_i}} = \tilde{Y}_0(s) + s\tilde{Y}_1(s) + s^2\tilde{Y}_2(s) + s^3\tilde{Y}_3(s) + \dots + s^{2q}\tilde{Y}_{2q}(s) \quad (4.25)$$

where the  $p_i$ 's are the poles of the approximation, and the  $a_i$ 's are the products of the corresponding residues and poles.

Recursive convolution is used to construct a macromodel that can be implemented as a conductance and a time-dependent current source. Recursive convolution is discussed

in Chapter 5. The current and voltage relationship for piecewise constant excitation is given as

$$i[n\Delta T] = a_0 \tilde{v}[n\Delta T] + \sum_{k=1}^q i_k[n\Delta T] \quad (4.26)$$

where  $i_k[n\Delta T] = a_i(1 - e^{-p_i \Delta T})\tilde{v}[(n-1)\Delta T] + e^{-p_i \Delta T} i_k[(n-1)\Delta T]$

Equation (4.26) can be incorporated in the MNA matrix [21] to be analyzed with other nonlinear network using conventional Newton-Raphson and numerical integration routines. This equation provides the capability for integrating the diode reduced-order model into SPICE-type simulators.

Thus, AWE provides an efficient means representing a diode with the pole-residue model either in the time or frequency domain. An important advantage of this type of model is that it is easy to implement and is very fast to evaluate. The poles and the residues need to be calculated from device parameters only once and will be used during simulation when needed. The model is restricted not only to predicting terminal characteristics, but also to providing additional information on the transport phenomena that is valid under all operating conditions.

### 4.3 Numerical Results

In this section, we will show that the diode model derived in the preceding section can be used to model the actual diode switching behavior. The simulation results and comparisons are given.

Consider a one-dimensional, long  $p^+ - n$  diode with a  $p$ -type region much more heavily doped than the  $n$ -region. The diode parameters are  $\tau_p = 100 \text{ ns}$ ,  $D_p = 0.001 \text{ m}^2 / \text{s}$ ,  $p_{no} = 1 \times 10^{10} \text{ atom} / \text{m}^3$ ,  $A = 1 \times 10^{-9} \text{ m}^2$ , and  $V_T = 0.026 \text{ V}$ . A



voltage source, a resistance  $R=50\Omega$ , and a diode are connected in series as shown in Figure 4.2.

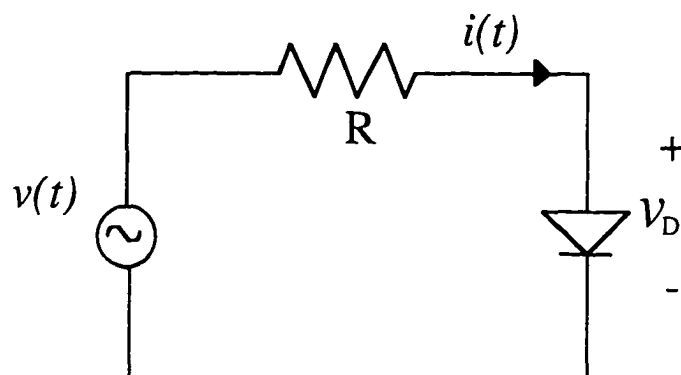


**Figure 4.2:** A biasing diode circuit.

Using Equation (4.18), the moments of hole concentration are calculated. The first eight actual moments along the scaled moments are given in Table 4.1. The moment values change very rapidly at a rate of  $\approx 10^{-7}$ . The actual computation of the coefficients of the polynomials in the Padé rational function using these moments is a classically ill-conditioned problem. Higher-order approximations cannot be obtained because of the large change in moment values which makes the corresponding coefficient matrix algorithmically singular. This problem is easily circumvented by using the ratio of the first two moments as the normalization factor. The scaled moments are of the same magnitude as shown in Table 4.1.

Once we obtain the normalized residues and poles, we have to scale them back to extract the actual residues and poles. The approximate residues and poles of the first, four-order approximations are given in Tables 4.2 and 4.3, respectively. A square waveform input is applied to forward bias the diode into the conducting state at  $t=2\text{ ns}$ , and then a reverse bias at  $t=11\text{ ns}$ , to instantaneously put the diode into reverse mode.

**Table 4.1:** Actual and scaled expansion moments.

| Order | Actual moments             | Scaled moments             |
|-------|----------------------------|----------------------------|
| $m_0$ | $1.60200 \times 10^{-16}$  | $1.60200 \times 10^{-16}$  |
| $m_1$ | $8.01000 \times 10^{-24}$  | $1.60200 \times 10^{-16}$  |
| $m_2$ | $-2.00250 \times 10^{-31}$ | $-8.01000 \times 10^{-17}$ |
| $m_3$ | $1.00125 \times 10^{-38}$  | $8.01000 \times 10^{-17}$  |
| $m_4$ | $-6.25781 \times 10^{-46}$ | $-1.00125 \times 10^{-16}$ |
| $m_5$ | $4.38047 \times 10^{-53}$  | $1.40175 \times 10^{-16}$  |
| $m_6$ | $-3.28535 \times 10^{-60}$ | $-2.10262 \times 10^{-16}$ |
| $m_7$ | $2.58135 \times 10^{-67}$  | $3.30412 \times 10^{-16}$  |
| $m_8$ | $-2.09734 \times 10^{-74}$ | $-5.36920 \times 10^{-16}$ |

**Table 4.2:** Approximate residues.

| Order | First order             | Second order             | Third order              | Fourth order             |
|-------|-------------------------|--------------------------|--------------------------|--------------------------|
| $k_0$ | $4.806 \times 10^{-16}$ | $8.010 \times 10^{-16}$  | $1.121 \times 10^{-15}$  | $1.442 \times 10^{-15}$  |
| $k_1$ | $-1.282 \times 10^{-8}$ | $-5.168 \times 10^{-10}$ | $-1.308 \times 10^{-10}$ | $-5.341 \times 10^{-11}$ |
| $k_2$ |                         | $-6.356 \times 10^{-8}$  | $-1.851 \times 10^{-9}$  | $-4.272 \times 10^{-10}$ |
| $k_3$ |                         |                          | $-1.774 \times 10^{-7}$  | $-4.272 \times 10^{-9}$  |
| $k_4$ |                         |                          |                          | $-3.793 \times 10^{-7}$  |

**Table 4.3:** Approximate poles.

| Order | First order          | Second order         | Third order          | Forth order          |
|-------|----------------------|----------------------|----------------------|----------------------|
| $p_1$ | $-4.000 \times 10^7$ | $-1.528 \times 10^7$ | $-1.308 \times 10^7$ | $-1.132 \times 10^7$ |
| $p_2$ |                      | $-1.047 \times 10^8$ | $-2.572 \times 10^7$ | $-1.704 \times 10^7$ |
| $p_3$ |                      |                      | $-2.020 \times 10^8$ | $-4.000 \times 10^7$ |
| $p_4$ |                      |                      |                      | $-3.316 \times 10^8$ |

During the first phase when the diode is in the forward conducting state, the hole-charge buildup due to the forward current, as time progresses, is shown in Figure 4.3. The vertical axis is the hole concentration in a logarithmic scale and the horizontal axis is the distance in microns from the  $p^+n$  junction. Each curve is a snapshot of the minority carrier concentration. When the input voltage waveform is suddenly switched to a reverse bias, the charge concentration at  $x = 0$  must drop to zero. Figure 4.4 illustrates the time progression of the excess charge removal.

The diode voltage and current waveforms are shown for a different order of approximations in Figures 4.5 and 4.6, respectively. The fourth-order approximation has only improved the third-order current waveform estimate by small details indicating convergence. The fourth-order approximation gives a more realistic prediction of the diode's storage time and reverse recovery times, similar to those for the exact numerical solutions in [90].

The conventional diode model [91] is not capable of accurately predicting the diode recovery effect because it cannot account for the finite time required for the stored charges to be removed from the junction region when the diode is suddenly reverse-biased after a steady forward bias. The charge-controlled capacitance element of the conventional model

cannot simulate this delay accurately. Distributed networks are needed to model the delay effect in the diffusion process. Figures 4.7 and 4.8 show the diode voltage and current responses using the conventional method and AWE technique, respectively. The conventional model underestimates the recovery time, while the AWE gives a more accurate solution for the storage and recovery times. The conventional simulation instantaneously switches to a steady-state value that predicts an unrealistic abrupt discharge of the residual stored charge.

The diode voltage and current predicted by the conventional model snaps to the nonconducting states are shown in Figures 4.7 and 4.8, respectively. The AWE model, on the other hand, predicts the smooth decay of the reverse-diode current observed in the diode recovery phenomenon. The conventional model predicts the reverse-recovery time, several orders of magnitude smaller than the actual. Thus, the conventional diode model is unsatisfactory for analyzing high-performance, high-power circuits.

It has been verified in [90] that 100 T-network sections are required for the ladder-network simulation of the diode recovery process with the same accuracy as that obtained using a ten-section lattice network. The results from the AWE analysis give a similar recovery time obtained with the mixed level simulation as reported in [90]. The AWE method also reduces the computer simulation time by a factor of more than two when compared to the simulation using SPICE-type analysis.

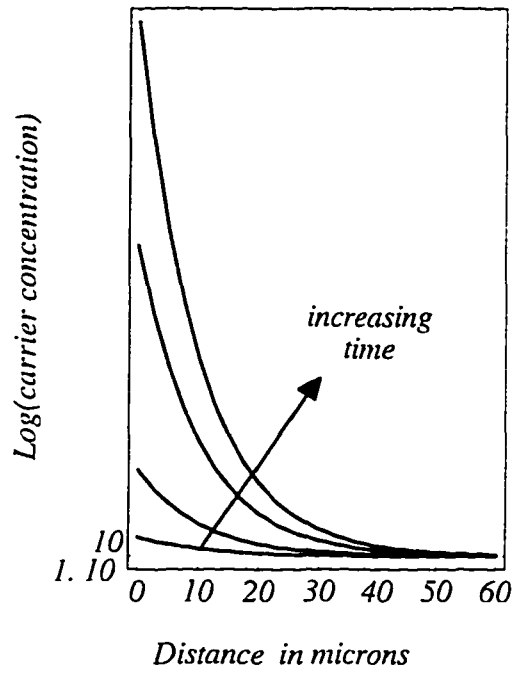


**Figure 4.3:** Charge buildup during turn-on phase.

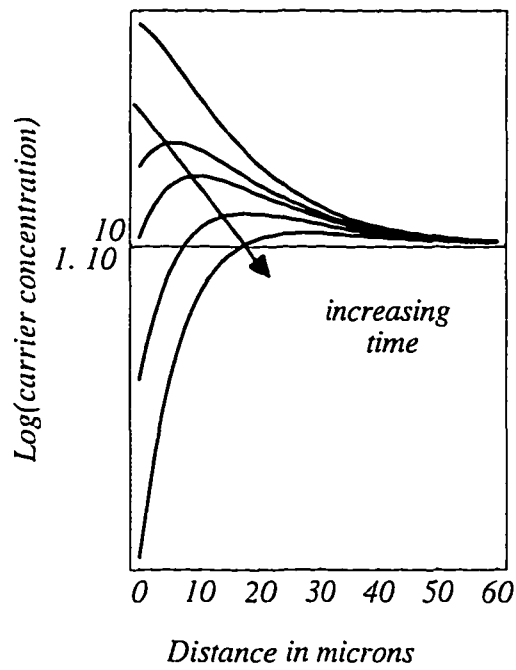


**Figure 4.4:** Stored charge decay during turn-off phase.

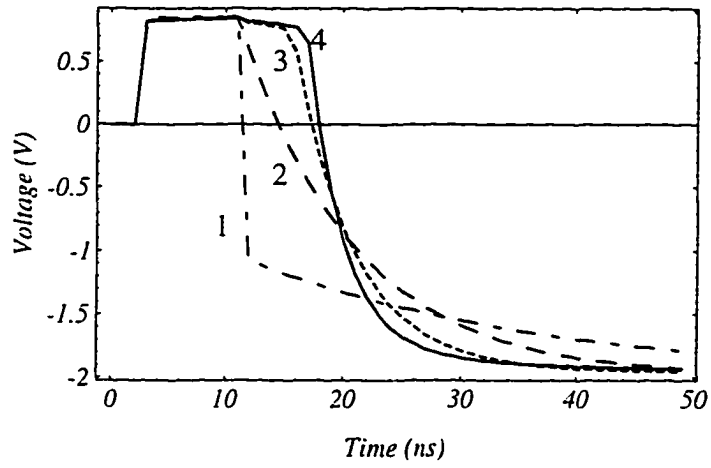


**Figure 4.5:** The diode voltage waveforms, one to four orders of approximations.

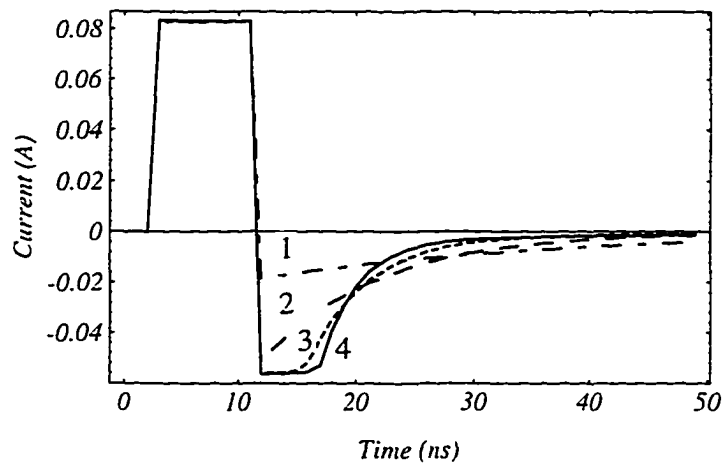


**Figure 4.6:** The diode current waveforms, one to four orders of approximations.

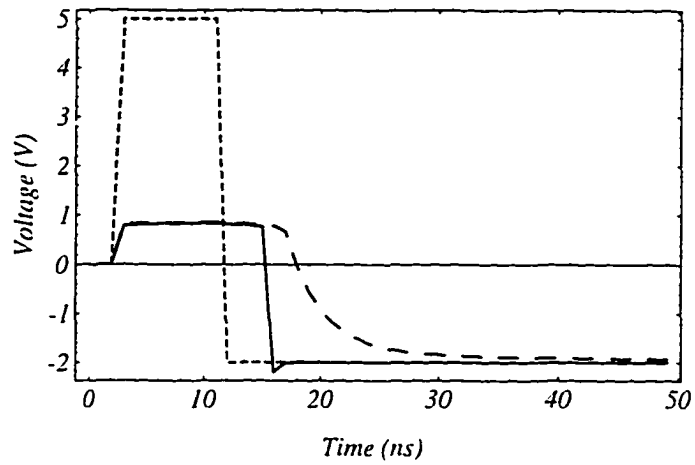


**Figure 4.7:** Input waveform and diode voltage response.  
 AWE method (---) versus conventional quasi-static model (—).

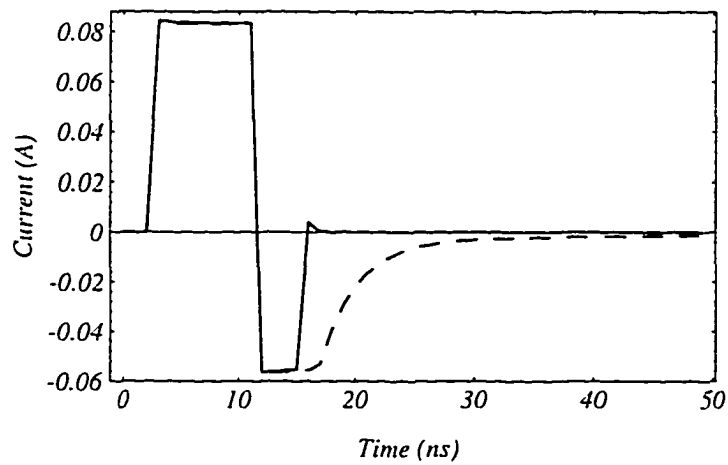


**Figure 4.8:** Diode current response.  
 AWE method (---) versus conventional quasi-static model (—).

## 4.4 Conclusion

Using asymptotic waveform evaluation, a reduced-order diode model has been derived for the efficient transient analysis of integrated, diode-switching circuits. Because the model is derived directly from the device physical operating principles, the method accurately represents the dynamics of the carrier redistribution process in the diode junction with the accuracy only achievable by device simulators. The model also avoids complex and time-consuming network synthesis and macro-modeling. Efficient recursive relationships are derived to generate the diode excess carrier-concentration moments rendering the computational cost associated with model constructions as negligible. Higher-order solutions are obtained with incremental costs by merely increasing the order of the approximation. Using a low-order model, the method accurately simulates the diode-switching behaviors; a more realistic time delay, storage, accurate recovery times of terminal currents and voltages, including time-varying charge distribution in the junction, have been calculated. The full potential and the correctness of the method have been verified using conventional methods and published results of the transient analysis of the diode-switching characteristics.



## CHAPTER 5

# FREQUENCY-DOMAIN MODELING AND SIMULATION TECHNIQUES

### 5.1 Introduction

As wiring density in high-performance packaging increases, the interconnect geometry becomes nonuniform and the cross-sectional dimensions become smaller. Consequently, the interconnect and dielectric losses, dispersions, and discontinuities have to be considered in the analysis of an electronic package. These frequency-dependent phenomena of an interconnect are most accurately characterized by measured or simulated data than by closed-form functionals [99]. For example, the skin effect of an interconnect is best characterized by frequency-domain measurements or full-wave electromagnetic simulation. The transient analysis of systems described in tabular forms cannot directly be performed using conventional simulators such as SPICE and ASTAP, or using methods based on order-reduction techniques, such as AWE, CFH, and PVL.

The incorporation of interconnects characterized by frequency-domain data obtained from measurements or full-wave electromagnetic solvers into circuit simulators is complex and computationally intensive. Because nearly all interconnects are driven or terminated by nonlinear devices, the method must combine the time-domain and frequency-domain descriptions [45], [100], [101]. The most straightforward approaches are to calculate the

impulse response of the measured network using the inverse Fourier transform (IFFT), and to apply the discrete time solution to solve the entire system for a given input waveform. Such an approach requires that at every simulation time step, the impulse response be convoluted with the entire computed input waveform. The IFFT used to transform frequency-domain data into time-domain data requires special attention to avoid aliasing. Extrapolation and low-pass filtering of the frequency-domain data are required to reduce the time-domain ripple associated with taking the IFFT. A very large number of samples is required for an adequate representation of the impulse functions, which increases the convolution computation time of the transient response. Although this method gives a reliable solution, it is not fast enough to provide results in an acceptable time interval.

Although order-reduction techniques, such as AWE, CFH and PVL are efficient methods to analyze linear systems, they are not quite suitable to handle networks characterized by tabular data, as the derivatives at selected expansions cannot accurately be calculated to find the moments. In [20], a hybrid technique is used by first approximating the function by calculating rational functions over partitioned frequency ranges, and then using the derivative of the rational functions to obtain the moments. However, the moments obtained using this method are order-dependent, violating the definition of the Taylor series. Several methods have been suggested to increase the versatility of AWE and CFH methods. In [16], [58], a methodology for incorporating subnetworks characterized by measured data is presented. The lumped-model-based subnetwork is reduced and the measured subnetworks are incorporated as submatrices in the MNA matrix, the formulation employed by conventional simulators of the global circuit to be solved at a set of frequency points. Then, IFFT is performed on the data points to obtain the response in the time domain.

In this chapter, we present an algorithm for accurate synthesis and efficient simulation of arbitrary networks. The method is based on network partitioning, robust rational interpolation and recursive convolution to generate macromodels that can be used

for time- and frequency-domain simulations. First, the network is partitioned into subnetworks. Then, if the pole-residue representation of each lumped-model subnetwork is found using a specific model-order reduction technique, a more accurate rational interpolation method can be applied for complex systems. Then, the pole-residue level representations of lumped-model-based and measured subnetworks are combined to form the global network. The pole-residue models are incorporated as submatrices into the system matrix of the global network using a recursive convolution formula, and then the entire system including the nonlinear devices is solved in the time domain. Thus, the size of the overall circuit to be simulated is reduced. The method does not require a numerical transform treatment or the smoothing and band-limiting filtering of a large number of points, which are often required in conventional methods.

In order to obtain an accurate rational approximation over a wide frequency range, frequency normalization and shift are used to optimally condition the Vandermonde-like approximation matrices and the Householder orthogonal triangularization to solve them. By utilizing the analytic properties of the network functions, the approximation algorithm efficiently generates stable, rational functions for high-order systems. The method can be integrated with reduced-order modeling techniques such as AWE, CFH and PVL, or conventional simulators such as SPICE and ASTAP for transient simulation of high-speed interconnect networks. Examples of linear and nonlinear networks are given to demonstrate the validity and accuracy of the method.

In Section 5.2, the formulation of a multiport network is presented. In Section 5.3, the rational approximation is discussed and the numerical properties of the approximation method are given. The modified, balanced transformation is used to reduce the approximating function in Section 5.4. In Section 5.5, the time-domain macromodels are generated from pole-residue representations using recursive convolution. Numerical results are shown in Section 5.6. Finally, the conclusion is given in Section 5.7.

## 5.2 Multiport Network

A general network can be partitioned into a number of subnetworks,  $N_1, N_2, \dots, N_n$ , as shown in Figure 5.1. Each subnetwork can be represented as a *multiport* network that can be characterized in terms of one of the following parameters: admittance, impedance, hybrid, transmission, or scattering parameters. The analysis of the global network,  $N$ , can be carried out by generating a pole-residue model for each subnetwork. The Padé synthesis can be used to efficiently compute the low-order approximation of the admittance matrix for the subnetworks characterized by a lumped or distributed model. The measured subnetwork, arbitrary linear electromagnetic system, is often characterized by frequency-domain data using scattering parameters.

Although either the characteristic impedance or admittance can be used to describe a network, impedance and admittance functions are difficult to derive, approximate or measure accurately for arbitrary interconnects. The impedance and admittance parameters can acquire extreme values at integer multiples of one-fourth of the wavelength. However, scattering parameters, in addition to their unique meaning, are stable parameters readily available from full-wave electromagnetic analysis or measurements. Scattering parameters of complex structures can be measured with high accuracy using one of the commercially available network analyzers. Scattering parameters can also be derived from *TEM*, *quasi-TEM* or frequency-dependent  $R$ ,  $L$ ,  $C$  and  $G$  parameters. The choice of an appropriate reference system to make the scattering parameters smooth function that is easy to approximate is discussed in Chapter 6.

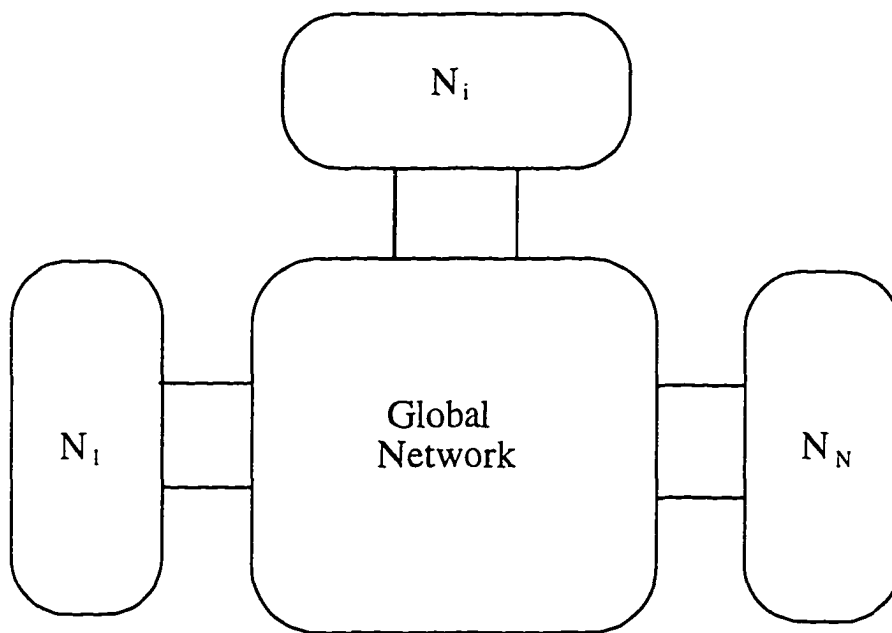


**Figure 5.1:** Partitioned multiport subnetworks.

Transfer function approximation is used to obtain the reduced-order model of the measured subnetwork. The transfer functions of port  $(i,j)$  can be given in a pole-residue form as

$$H_{ij}(j\omega) = k_{\infty} + \sum_{r=1}^q \frac{k_r}{(j\omega - p_r)} \quad (5.1)$$

where  $p_r$  and  $k_r$  are complex poles and residues, and  $k_{\infty}$  represents any direct coupling between the input and output. Once the pole-residue pairs are determined from the above equations, each subnetwork is treated as a multiterminal device in the MNA matrix of the global network.

In the following section, we will describe the method of approximating the scattering parameters of a subnetwork by a rational function over normalized and shifted frequencies.

### 5.3 Approximation

Polynomials are the simplest and most common means of approximating functions. Although the existence and uniqueness of polynomial interpolations of arbitrary data can be proved using the Weierstrass approximation theorem, polynomial functions are not used to approximate transfer functions of networks. Polynomials are not suitable to represent frequency responses of electrical networks, because polynomials do not work well in approximating the behavior of functions near their poles. In contrast, rational functions do capture the behavior of networks around the poles and their partial fraction expansions can readily be used to obtain the time-domain responses as sums of trigonometric and/or exponential functions. Hence, the transfer functions of electrical

networks can be approximated for the least maximum error by rational functions rather than by polynomial functions of comparable order.

The idea of approximating arbitrary functions using rational functions is quite an old problem [73], [102]-[105]. Rational function approximations in partial fraction expansion form, unlike polynomial approximations, are not linear spaces; the calculation of rational approximations is more difficult than the calculation of polynomial approximations. Determining network functions and the associated zeros and poles is not only time-consuming, but also subject to problems of great numerical inaccuracy. The computational procedures are numerically sensitive and limited by the precision of the computer. The approximation matrices are ill-conditioned, and the calculation of the polynomial coefficients involves costly nonlinear optimization.

The recent developments of new methods that are based on direct representation of lossy transmission lines using transfer functions have regenerated considerable interest in accurate and efficient techniques to determine the poles and zeros directly from the time-domain or frequency-domain responses [70]-[72].

In [20], [71] and [104], partitioned or section-by-section approximation over a smaller domain is proposed to avoid the numerical ill-conditioning of the rational approximation. The frequency range is partitioned into sections and a low-order approximation is applied in each section. Once an approximation is obtained in a section, the value of the approximation function is subtracted from the corresponding data, and the resulting data are again fitted using the next section. The procedure is repeated until the data in the last frequency section are approximated. Then, the entire procedure starting from the first section is repeated until the approximation converges. Although this method constructs better conditioned matrices, the process can introduce some erroneous dynamics when subtracting the results of already computed approximations from the exact data. Consequently, the convergence of the method can be extremely slow when the method is

applied to complex or periodic data. The method can be used to provide a good match with aperiodic data.

In [19], a rational interpolation algorithm is used for optimal transient simulation of transmission lines. The method is global in the sense that one rational approximation is used over the entire frequency range. The method is very efficient and gives good approximations for most practical problems. When higher-order approximations of complex systems are sought, however, the method has numerical inaccuracies due to the ill-conditioning of the matrices and the normal equation method the algorithm employs to obtain least-squares solutions. In this work, optimal conditioning, Householder orthogonal triangularization, and automatic adjustment of order approximation are introduced to guarantee the existence of a stable, rational approximation of a complex system over a wide approximation domain.

### 5.3.1 Interpolation by rational functions

A network function  $H(s)$  of a linear system can be approximated by a rational function that interpolates the given function at given points. The rational function can be in a pole-residue, pole-zero form or as a ratio of polynomials. Suppose the network function,  $F(s_i)$ , given either analytically or at given points  $\{s_i\}$ , is approximated by a rational function of degree  $(\xi, \vartheta)$

$$H_{\xi, \vartheta}(s) = \frac{Q_{\xi}(s_i)}{P_{\vartheta}(s_i)} = \frac{q_0 + q_1s + q_2s^2 + \dots + q_{\xi}s^{\xi}}{1 + p_1s + p_2s^2 + \dots + p_{\vartheta}s^{\vartheta}} \quad (5.2)$$

with  $p_0$  normalized to unity. Equation (5.2) contains  $n = \xi + \vartheta + 1$  free coefficients, hence, at most  $n$  independent parameters. The coefficients are determined so that the approximating function evaluated at the same frequency points gives close approximations to the function  $F(s)$ . For specified finite functional values  $y_i = F(s_i)$ , ( $i=0, \dots, k-1$ ) and  $k$  specified distinct points,  $s_i$ , the resulting equations give



$$\frac{Q_\xi(s_i)}{P_\vartheta(s_i)} - y_i = 0 \quad (5.3)$$

By canceling the denominators in (5.3), one obtains the linear homogenous system of  $k$  equations in  $n$  unknowns:

$$Q_\xi(s_i) - y_i P_\vartheta(s_i) = 0 \quad (5.4)$$

which can be written in a matrix form as

$$\underbrace{\begin{bmatrix} 1 & s_0 & s_0^2 & \cdots & s_0^\xi & -s_0 y_0 & -s_0^2 y_0 & \cdots & -s_0^\vartheta y_0 \\ 1 & s_1 & s_1^2 & \cdots & s_1^\xi & -s_1 y_1 & -s_1^2 y_1 & \cdots & -s_1^\vartheta y_1 \\ \vdots & \vdots & \vdots & \vdots & \vdots & \vdots & \vdots & \vdots & \vdots \\ 1 & s_{k-1} & s_{k-1}^2 & \cdots & s_{k-1}^\xi & -s_{k-1} y_{k-1} & -s_{k-1}^2 y_{k-1} & \cdots & -s_{k-1}^\vartheta y_{k-1} \end{bmatrix}}_V \underbrace{\begin{bmatrix} q_0 \\ q_1 \\ q_2 \\ \vdots \\ q_\xi \\ p_1 \\ p_2 \\ \vdots \\ p_\vartheta \end{bmatrix}}_X = \underbrace{\begin{bmatrix} y_0 \\ y_1 \\ \vdots \\ y_{k-1} \end{bmatrix}}_Y \quad (5.5)$$

The solution of the system is not guaranteed, in general. The linear problem in (5.5) is not necessarily equivalent to the interpolation problem in (5.3). The rational function does not necessarily satisfy the interpolation conditions if the denominator polynomial has a zero for one of the given abscissas  $s_i$ . As a consequence, the numerator polynomial must also have the same zero, so both polynomials have a common linear factor  $(s-s_i)$  that cancels. The resulting rational function will generally no longer satisfy the interpolation condition for  $s_i$ , as  $H(s_i) \neq y_i$ . Hence, the interpolation problem has no solution for the prescribed degrees  $\xi$  and  $\vartheta$  of the numerator and denominator polynomials, respectively. In this case, the order of approximation has to be adjusted to guarantee the existence of the solution.

To find the conditions under which a solution exists, it is important to point out that the columns of  $V$  form independent vectors; hence,  $V$  is full-rank. The rank of the matrix  $V \in R^{k \times n}$ , given by (5.5), is equal to  $\min(n, k)$ . There are two possible situations: (1)  $k \geq n$ ,

and (5.5) is a full-rank overdetermined system, (2)  $k < n$  and (5.5) is a full-rank underdetermined system.

The first case is an interpolation problem, and the case  $k > n$  can be reduced to the case  $k = n$  by writing (5.5) in an appropriate form. For the  $k = n$  problem, (5.5) is consistent for any  $Y \in R^n$ , and  $X = \hat{V}^{-1}Y$  is the unique solution, where  $\hat{V} \in R^{n \times n}$  is reformulated  $V$ . In the second case,  $k < n$ , there is, in general, an infinite number of solutions. The complete solution set is given by

$$X = V^T(VV^T)^{-1}Y + [I - V^T(VV^T)^{-1}V]b \quad (5.6)$$

where  $b$  is arbitrary.

For higher-order approximations over a wider approximation range, the system in (5.5) is highly ill-conditioned and nearly singular because of the large difference between the maximum and minimum frequencies raised to the order of approximation. Even with proper frequency normalization, the computational procedures are limited by the numerical range and precision of the computer. The numerical considerations are discussed in detail in Section 5.3.3.

### 5.3.2 Approximation of a network function

The approximation algorithm can be made more efficient and accurate by utilizing the special properties of network functions. For instance, constraints necessary to insure a physically realizable passive network require that the transfer function be a rational fraction of polynomials in  $s$ . The coefficients of these polynomials must be real, and all roots of the denominator polynomial must have negative or zero real parts.

In addition, network functions are analytic functions of a complex variable; hence, their real and imaginary parts are related by the Cauchy-Riemann equations. In an electrical network, some constraints remain between the frequency variations of resistance, reactance, conductance and susceptance, just as in the Kramers-Kronig relations between

real and imaginary parts of permittivity. The locations of zeros and poles of a passive network are constrained to the left-half complex frequency plane due to the analytical property of the network function. Thus, the response of a passive network can only decay in time from any transient initial state. The consequence of this property is that only the real part, imaginary part, angle, or magnitude of the network function have to be approximated and the network function itself can be found from the resulting approximation.

Next, we will discuss the procedure for determining a network function as a rational function of  $s$ , using the real parts of the function.

The real part of a network function (5.3) can be specified as the even part of  $H(s)$  replacing  $-s^2$  with  $\omega^2$ . The real part of the original function is fitted with the real rational polynomial function of the squared variable

$$\operatorname{Re}(H_{\xi, \vartheta}(s)) = \frac{c_0 + c_1 s^2 + c_2 s^4 + \dots + c_\xi s^{2\xi}}{1 + p_1 s^2 + p_2 s^4 + \dots + p_\vartheta s^{2\vartheta}} \quad (5.7)$$

Because the poles of the even function of  $F(s)$  are those of both  $F(s)$  and  $F(-s)$ , those belonging to  $F(s)$  lie in the left half-plane. Thus, the denominator coefficients of  $H(s)$  in (5.2) can be obtained from (5.7). The following system of equations results from matching the real parts of the original function with (5.7) at the set of frequencies

$$\begin{bmatrix} 1 & \omega_0^2 & \omega_0^4 & \dots & \omega_0^{2\xi} & -\omega_0^2 y_0^r & -\omega_0^4 y_0^r & \dots & -\omega_0^{2\vartheta} y_0^r \\ 1 & \omega_1^2 & \omega_1^4 & \dots & \omega_1^{2\xi} & -\omega_1^2 y_1^r & -\omega_1^4 y_1^r & \dots & -\omega_1^{2\vartheta} y_1^r \\ \vdots & \vdots & \vdots & \dots & \vdots & \vdots & \vdots & \dots & \vdots \\ 1 & \omega_{k-1}^2 & \omega_{k-1}^4 & \dots & \omega_{k-1}^{2\xi} & -\omega_{k-1}^2 y_{k-1}^r & -\omega_{k-1}^4 y_{k-1}^r & \dots & -\omega_{k-1}^{2\vartheta} y_{k-1}^r \end{bmatrix} \begin{bmatrix} c_0 \\ c_1 \\ c_2 \\ \vdots \\ c_\xi \\ p_1 \\ p_2 \\ \vdots \\ p_\vartheta \end{bmatrix} = \begin{bmatrix} y_0^r \\ y_1^r \\ \vdots \\ y_{k-1}^r \end{bmatrix} \quad (5.8)$$

where the superscript “ $r$ ” indicates the real part of a complex value.

The conditions for the existence of the solution are as stated in Section 5.3.1. Once the coefficients of the denominator polynomial are obtained from (5.8), the roots of the denominator are calculated from

$$1 + p_1\omega^2 + p_2\omega^4 + \dots + p_\vartheta\omega^{2\vartheta} = 0$$

The poles are assumed to be distinct. Repeated poles are not likely because of the nature of the problem and the fact that the poles are computed numerically. If repeated poles are obtained they can be modified to make them distinct.

Factoring the denominator and taking only the left half-plane roots, the partial fraction expansion of the transfer function is constructed. Not a single unstable (positive) pole is obtained, because the polynomial roots are determined in terms of the square poles. The purely imaginary single poles on the imaginary axis are rejected as spurious because the rational function in (5.8) has double poles. Hence, the order of the approximating function must be set to a value greater than or equal to the actual order sought. The remaining negative poles are used to formulate the stable partial fraction expansion of the transfer function as

$$H(s) = k_\infty + \sum_{i=1}^{\vartheta'} \frac{k_i}{s - p_i} \quad (5.9)$$

where  $\vartheta' \leq \vartheta$  and  $\vartheta - \vartheta'$  are the numbers of rejected, purely imaginary poles.

Solving for residues using only the stable poles gives a better approximation than the approach in [106] where the unstable poles with the associated residues are discarded at the final phase. No error is introduced in discarding the erroneous poles because the residues are calculated by matching the function using the remaining selected poles.

In the next section, a method for further reducing the remaining poles using the pole-clustering technique is discussed. The inverse distance-measure criterion is used to give more weight to the dominant poles closest to the  $j\omega$ -axis in each cluster.

Matching the real and imaginary parts of each element of the original matrix transfer function with the corresponding parts of the elements of (5.9) at the set of points leads to the following set of linear system equations

$$\underbrace{\begin{bmatrix} 1 & \frac{-p_1}{\omega_0^2 + p_1^2} & \dots & \frac{-p_\nu}{\omega_0^2 + p_\nu^2} \\ 1 & \frac{-p_1}{\omega_1^2 + p_1^2} & & \frac{-p_\nu}{\omega_1^2 + p_\nu^2} \\ \vdots & & & \\ 1 & \frac{-p_1}{\omega_{k-1}^2 + p_1^2} & \dots & \frac{-p_\nu}{\omega_{k-1}^2 + p_\nu^2} \\ 0 & \frac{-\omega_0}{\omega_0^2 + p_1^2} & & \frac{-\omega_0}{\omega_0^2 + p_\nu^2} \\ \vdots & & & \vdots \\ 0 & \frac{-\omega_{k-1}}{\omega_{k-1}^2 + p_1^2} & \dots & \frac{-\omega_{k-1}}{\omega_{k-1}^2 + p_\nu^2} \end{bmatrix}}_M \underbrace{\begin{bmatrix} k_\omega \\ k_1 \\ \vdots \\ k_\nu \end{bmatrix}}_K = \underbrace{\begin{bmatrix} y_0^r \\ y_1 \\ \vdots \\ y_{k-1}^r \\ y_1^i \\ \vdots \\ y_{k-1}^i \end{bmatrix}}_Y \quad (5.10)$$

where the superscripts “i” and “r” indicate the imaginary and real parts of a complex value, respectively. The solution of (5.10) gives the partial expansion coefficients,  $k_i$ 's. Arbitrary dc and steady-state values can be assigned prior to the approximation.

### 5.3.3. Numerical considerations

The transposed Vandermonde-like matrix in (5.8), even for moderate order, is notoriously ill-conditioned in the sense that the entries along each row are simple powers of the corresponding frequency values. If the span of the frequencies being considered is large, then the magnitudes of the entries on some of the rows will be much larger than those in rows corresponding to low frequency values. The application of a direct-elimination algorithm to solve the Vandermonde-type system in (5.8) produces unreliable results.

The unequal scale of the rows of  $V$  suggests that there is some artificial ill-conditioning in the problem. The artificial ill-conditioning can be removed. The condition number can be improved by normalizing the maximum frequency to unity. The condition number can still be uncomfortably large, though good enough for practical purposes, and intolerable for a wide frequency range or high-order approximation. This ill-conditioning is real and will not disappear with any further rescaling. On the other hand, posing the problem in a shifted basis using the transformation,

$$\omega' = \frac{2(\omega - \omega_{\min})}{\omega_{\max} - \omega_{\min}} - 1, \quad (5.11)$$

leads to a better-conditioned problem. Mapping the domain  $[\omega_{\min}, \omega_{\max}]$  to  $[-1, 1]$  normalizes the domain variable to the center within the numerical range of the computer and minimizes numerical inaccuracies in the solution process.

The minimum number of samples for the interpolation is  $k=n$ . Because the number of equations is often larger than the number of unknowns, Equation (5.8) can be transformed into a square matrix using the method of averages [19]. The method of averages is used to obtain a consistent system by adding consecutive equations from the system of equations in (5.8) into  $n$  groups. Due to numerical difficulties, solving the consistent equation obtained from (5.8) using the direct method, we need an alternative method that does not require a direct elimination method. We seek to transform the problem into a more numerically robust equivalent one, yet still produce the solution. Any matrix can be decomposed in the form  $V=QR$ , where  $Q$  is orthogonal and  $R$  is an upper-triangular matrix. For a general matrix, the decomposition is constructed by applying a series of Householder reflectors that zero out all elements in a given column to transform the matrix to a triangular form. Just as in an  $LU$  factorization, Householder  $QR$  factorization can be obtained in  $(n-1)$  steps. However, unlike the Gaussian elimination process, the

Householder  $QR$  decomposition can always be carried out to completion. Then, the solution of the following triangular system

$$R X = Q^T Y \quad (5.12)$$

is obtained more accurately.

The orthogonal-triangularization method is unconditionally stable; there is no *growth factor* to worry about, e.g., the growth of the elements in the reduced matrices, as in Gaussian elimination [107]. For the ill-conditioned problem, the orthogonal method gives an added measure of reliability. Even if the matrix is not full-rank or the system is near singular, the orthogonal factorization still exists. The decomposition of a matrix gives a nonsingular, upper-triangular matrix whenever the column vectors of  $V$  form a linearly independent sets of vectors. Thus, the triangular system (5.12) can be solved to high accuracy. The method is comparable with  $LU$  factorization in efficiency. It has a computational complexity of  $2n^3/3$ , and the cost for the triangular system is only  $O(n^2)$ . The right-hand side of (5.12) does not need  $Q$  explicitly; the Householder matrices are used to obtain  $Q^T Y$ .

The method is also known as the Golub-Householder method because the idea of solving the least-squares problem based on the  $QR$  factorization of  $V$  using the Householder transformation was first suggested by G. Golub [108]. For a matrix  $V \in R^{k \times n}$  with  $\text{rank}(V)=n$  and the vector matrix  $Y \in R^k$ , the Golub-Householder method computes the least-squares solution  $X \in R^n$  using Householder matrices  $H_1$  through  $H_n$ , with the cost of  $n^2(k - \frac{n}{3})$ . The matrix is decomposed as  $V = H_1 H_2 \dots H_{n-1} H_n R$ , and then the right-hand side is modified as  $Q^T Y = H_n H_{n-1} \dots H_2 H_1 Y$ . The pseudo-code for the Golub-Housholder method is given in Algorithm 5.1.

**Algorithm 5.1:** Golub-Householder method

***Golub\_Householder*** ( $V, Y$ )

*Step 1) Apply Householder factorization:*

$$V = H_1 H_2 \dots H_{n-1} H_n R$$

Step 2) Modify the right-hand side

$$H_n H_{n-1} \dots H_2 H_1 Y = \begin{bmatrix} Y_1 \\ Y_2 \end{bmatrix}$$

where  $Y_1 \in \mathbf{R}^n$ , and  $Y_2 \in \mathbf{R}^{k-n}$ .

Step 3) Solve  $R X = Y_1$ .

The residue calculation step does not have numerical problems. The system of equations in (5.8) is better conditioned, because the entries of the matrix are of the form  $-p_j(\omega_i^2 + p_j^2)^{-1}$ . In [19] and [109], the least-squares solution is obtained using the normal equation method. Because the normal equation method has numerical difficulties, the matrix  $M^T M$  is frequently ill-conditioned and influenced greatly by round-off errors. Instead, the solution of (5.10) is obtained using Householder  $QR$  orthogonalization.

The approximation problem is solved by building up and solving a linear system of equations. It is obvious that this requires only a small amount of *CPU*-time, especially because the system is rather small. The total computational complexity of the approximation method is one polynomial factorization, two Householder  $QR$  transformations, and two backsubstitutions. The algorithm is given in pseudo-code in Algorithm 5.2.

**Algorithm 5.2:** Rational interpolation.

***R\_Approximation*** ( $\omega, F, \xi, \vartheta$ )

Step 1) Normalize and shift frequency points

to map  $[\omega_{\min}, \omega_{\max}]$  into  $[-1, 1]$  using Equation (12).

Step 2) Construct real matrix of the real part of the function Equation (7):

$$V \in \mathbf{R}^{k \times n}, \quad X \in \mathbf{R}^n, \quad Y \in \mathbf{R}^k$$

Formulate square matrix using the method of averages:

$$\hat{V} \in \mathbf{R}^{n \times n}, \quad \hat{X}, \hat{Y} \in \mathbf{R}^n$$

Perform Householder  $QR$  factorization:  $\hat{V} = Q R$



$$\text{Solve: } \mathbf{R} X = \mathbf{Q}^T Y$$

*Step 3) If solution is not acceptable,*

*select new order of approximation ,  $\xi'$  and  $\vartheta'$ , and repeat Step 2.*

*Step 4) Factor denominator and filter the poles,*

*if the remaining poles are unacceptable, go to Step 3.*

*Step 5) Construct residue matrix Equation (9).*

*Perform Householder QR factorization:  $M=QR$*

$$\text{solve: } \mathbf{R} X = \mathbf{Q}^T Y$$

*Step 6) Return partial fraction expansion*

$$H(s) = k_{\infty} + \sum_{i=1}^{\nu'} \frac{k_i}{s - p_i}$$

## 5.4 Model-Order Reduction Using Pole-Clustering Technique

The system obtained from the approximation of a distributed system can have a higher order. The incorporation of such a large model into the global system matrix can result in a computationally expensive simulation. In most cases, the system in (5.9) can be reduced to a low-order model with slight degradation in accuracy. The approximation method described in Section 5.3, unlike the partitioned-approximation method proposed in [20], [71], and [106], rarely fits models of higher order. However, because the approximation method is a technique for fitting a function rather than simplifying models, the reduction steps can be necessary. One of the standard reduction methods can be used to obtain a low-order model.

Once the finite-partial expansion of the system function is determined, the system matrix corresponding to the approximating function can be realized by a linear time-invariant system as

$$\begin{aligned}\dot{x} &= Ax + Bu \\ y &= Cx + Du\end{aligned}\tag{5.13}$$

where

$$\begin{aligned}A &= \text{diag}(p_1, p_2, \dots, p_n) \\ B &= (\sqrt{|k_1|}, \sqrt{|k_2|}, \dots, \sqrt{|k_n|}) \\ C &= (\text{sign}(k_1)\sqrt{|k_1|}, \text{sign}(k_2)\sqrt{|k_2|}, \dots, \text{sign}(k_n)\sqrt{|k_n|}) \\ D &= k_\infty\end{aligned}\tag{5.14}$$

Then, the system matrix is further reduced by applying one of the standard techniques to obtain a low-order model [110]-[112].

The object of model reduction is to obtain the equations

$$\begin{aligned}\dot{x}_r &= A_r x_r + B_r u \\ y_r &= C_r x_r + Du\end{aligned}\quad r \ll n\tag{5.15}$$

where the matrices  $A_r$ ,  $B_r$ , and  $C_r$  are to be selected in such a manner that the model output  $y_r(t)$  is, in some predefined sense, a close approximation to  $y(t)$  for all admissible inputs  $u(t)$ . The reduced model of Equation (5.15) is chosen where the components of the system that make little contribution to the overall response of the system can be discarded. Although this can be done in several ways, perhaps the most common method is the balanced transformation, first introduced in control theory by Moore [110]. Here, the state vector is partitioned into a *slow* part and a *fast* part so that Equation (5.13) takes the following balanced realization form:

$$\begin{aligned}\begin{bmatrix} \dot{x}_1 \\ \dot{x}_2 \end{bmatrix} &= \begin{bmatrix} A_{11} & A_{12} \\ A_{21} & A_{22} \end{bmatrix} \begin{bmatrix} x_1 \\ x_2 \end{bmatrix} + \begin{bmatrix} B_1 \\ B_2 \end{bmatrix} u \\ \begin{bmatrix} y_1 \\ y_2 \end{bmatrix} &= \begin{bmatrix} C_1 & C_2 \end{bmatrix} \begin{bmatrix} x_1 \\ x_2 \end{bmatrix} + Du\end{aligned}\tag{5.16}$$

For a stable system, the *fast* modes decay much more quickly. The contributions of the fastest mode are important only at the beginning of the response; whereas, the retained dominant modes are important throughout the whole of the response that the system will have. Thus it is permissible to eliminate  $x_2$  to obtain a reduced-order model. In [106], this

approach is used to reduce the order of the intermediate system obtained from section-by-section approximation.

Although the balanced-matrix method is elegant and preserves the dominant eigenvalues of the original system, it does not always maintain the correct dc gain. It is also computationally intensive. It requires the solutions of two Lyapunov equations and the computation of the eigenvalues and eigenvectors of the intermediate system [113].

A less computationally intensive and a more accurate order-reduction method is based on pole-clustering techniques. The basic idea of the approach is that a low-order model is obtained by matching the frequency response of the original system. The poles of the low-order model approximate the effects of two or more clustered poles of the original system using the appropriate residues. The poles of the intermediate higher-order system that are clustered in certain areas can be grouped into several clusters. These clusters are then replaced by respective cluster-centers that are obtained by using an inverse distance measure criterion. This clustering is done only on the poles before determining the associated residues. After the cluster-centers are determined, the residues are calculated using Equation (5.10).

Recently, Sinha and Pal [114] used the inverse distance-measure (IDM) criterion for obtaining the cluster-centers of poles and zeros. The IDM gives larger weights to the poles near the  $j\omega$  axis in determining the cluster-centers because these poles have dominant effects on the system behavior.

The poles are first partitioned into clusters by identifying the larger jumps in the real and imaginary values of the poles. Separate partitions are formed for real poles and complex conjugate poles. Then, the complex conjugates of the cluster-centers are generated. The cluster-center for each partition is calculated as

$$P_o = \left\{ \frac{1}{r} \left( \sum_{i=1}^r \frac{1}{\text{Re}[p_i]} \right) \right\}^{-1} + j \left\{ \frac{1}{r} \left( \sum_{i=1}^r \frac{1}{\text{Im}[p_i]} \right) \right\}^{-1} \quad (5.17)$$

where  $P_o$  is the cluster-center, and  $p_i$ 's are the poles in each cluster.

The poles are replaced by the cluster-centers and the corresponding residues are calculated using Equation (5.10). The procedure for generating the cluster-centers are given in Algorithm 5.3. The poles of the original system and the cluster-centers are shown in Figure 5.2. The 26 poles of the original system are replaced by eight cluster centers.

**Algorithm 5.3:** Calculating cluster centers

- 1) Collect the real and complex poles in separate groups.
- 2) Calculate the distance between the poles.
- 3) Partition the poles into  $r$  clusters.
- 4) Using Equation (5.17), calculate the cluster centers

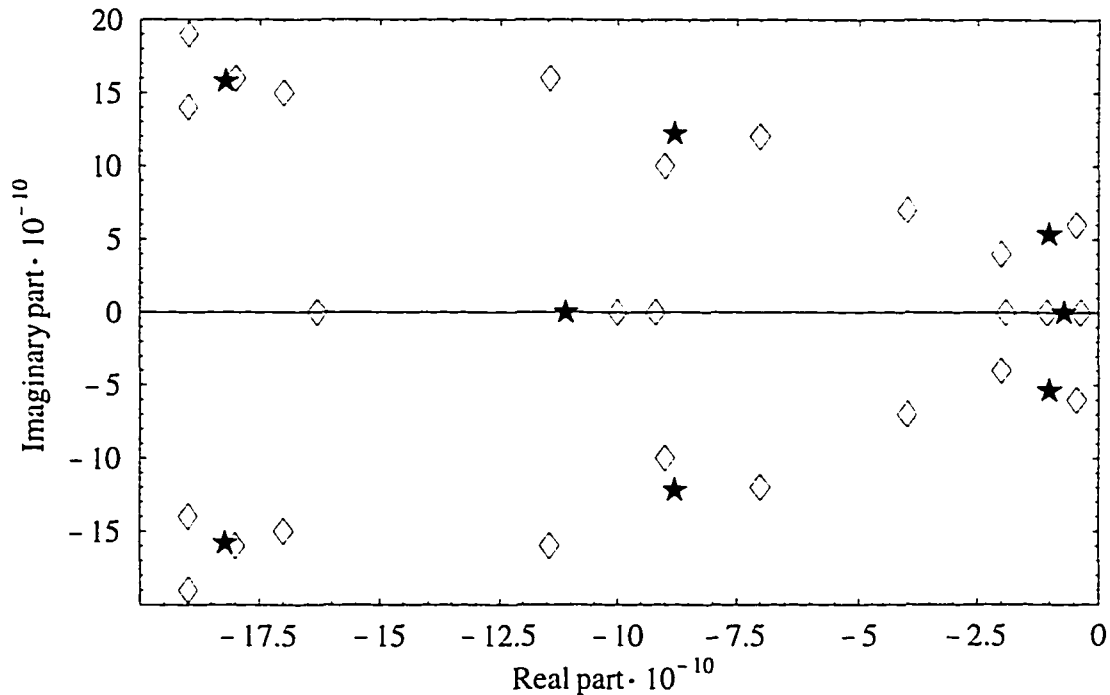


**Figure 5.2:** Locations of poles of original system (diamond) and the cluster-centers for reduced- order model (star) in the complex plane.

## 5.5 Recursive Convolution

We established the fact that the transient response of an electromagnetic system can be approximated by the exponential functions in the time domain or rational function in the frequency domain. In the preceding sections, we have successively derived a robust frequency-domain, rational-approximation method for the transfer functions of electromagnetic systems. The response of the system for arbitrary input is obtained in the form

$$Y(s) = \underbrace{\left( k_{\infty} + \sum_{i=1}^v \frac{k_i}{s - p_i} \right)}_{H(s)} X(s) \quad (5.18)$$

where  $X(s)$ ,  $Y(s)$  and  $H(s)$  are the Laplace domain input, output and transfer functions of the system, respectively. The time-domain response is obtained by calculating the convolution integral given as

$$y(t) = \int_0^{\infty} x(\tau) h(t - \tau) d\tau \quad (5.19)$$

where  $x(\tau)$  and  $y(\tau)$  are the input and output to the linear system, respectively,  $h(\tau)$  is the impulse-response or the kernel function of the system, and  $y(t)$  is the output. The convolution integral in (5.19) becomes progressively more expensive as the time-domain simulation time increases. For a total of  $N$  timepoints, the total cost of the convolutions is  $O(N^2)$ . Because the transfer function of the system is expressed as a sum of partial-fraction expansions (5.9), the time for the numerical convolution in (5.19) can be greatly reduced by taking advantage of the recursive convolution.

The advantage of a recursive convolution for calculating the switching response of frequency-dependent transmission lines was first recognized in the early 1970's by power and systems experts [115]. In 1975, Semlyen and Dabuleanu developed the recursive

convolution and showed its computational efficiency and usefulness [116]. In [[19], [57] [109], [116], recursive convolution is used as an efficient method for transient simulation of transmission lines.

Recursive convolution has linear time efficiency and reduces computation time by as much as one order of magnitude, while preserving the accuracy. In fact, recursive convolution improves accuracy, because it does not suffer from truncation errors as in the explicit convolution. The stability and convergence of recursive convolution depend on the system equation and the input.

### 5.5.1 Derivation of recursive-convolution equations

The efficiency of a recursive convolution comes from the fact that the impulse response of the system can be written as a series of exponential functions. For exponential kernel function, the convolution integral (5.19) at time  $t$  can be written as

$$y(t) = k_{\infty} x(t) + \sum_{i=1}^{\nu} \left( e^{p_i t} y(0) + \int_0^{\infty} k_i e^{p_i(t-\tau)} x(\tau) d\tau \right) \quad (5.20)$$

The convolution integral can be decomposed into

$$y(t) = k_{\infty} x(t) + \sum_{i=1}^{\nu} \left( e^{p_i \delta t} \underbrace{\left[ e^{p_i(t-\delta t)} y(0) + \int_0^{\delta t} k_i e^{p_i(t-\delta t-\tau)} x(\tau) d\tau \right]}_{\tilde{y}_i(t-\delta t)} + \int_{\delta t}^{\infty} k_i e^{p_i(t-\delta t-\tau)} x(\tau) d\tau \right)$$

where  $\tilde{y}_i$ 's are the values of the convolution integral associated with the pole  $p_i$ 's.

Therefore, Equation (5.20) can be written in terms of the last response and a single time-step convolution as

$$y(t) = k_{\infty} x(t) + \sum_{i=1}^{\nu} \left( e^{p_i \delta t} \tilde{y}_i(t-\delta t) + \int_0^{\infty} k_i e^{p_i t} x(t-\tau) d\tau \right) \quad (5.21)$$

The convolution integral in (5.21) can be calculated by adding the scaled values of the integral values corresponding to poles at previous timepoint and a single time step integration that can be reduced to algebraic equation. The cost of recursive convolution for

a total number of  $N$  timepoints is  $O(qN)$ . In general,  $N \gg q$ , the number of pole-residue pairs is much smaller than the number of time points in the total simulation time, the integration routine is linear in time, unlike the explicit convolution case which is quadratic in time.

Knowledge of the values of  $x(t)$  at a discrete number of points is not sufficient to specify  $y(t)$  uniquely by the above equation. It is necessary to make assumptions about the nature of  $x(t)$  such that its values at a discrete set of the points suffice to specify  $y(t)$  uniquely. In deriving the backward and forward Euler formulas, excitation is assumed to be a piecewise constant,  $x(t)=c$ , where  $t_{n-1} \leq t \leq t_n$ , and Equation (5.21) is solved using the values of the excitation at the current time interval as boundary conditions.

$$y(t_n) = k_\infty x(t_n) + \sum_{i=1}^q \tilde{y}_i(t_n) \quad (5.22)$$

where

$$\tilde{y}_i(t_n) = k_i (1 - e^{p_i \delta t_n}) x(t_n - \delta t_n) + e^{p_i \delta t_n} \tilde{y}_i(t_n - \delta t_n), \text{ and } \delta t_n = t_n - t_{n-1}.$$

If the excitation is assumed to be piecewise linear in  $t_{n-1} \leq t \leq t_n$  as in the well-known trapezoidal method in linear multistep methods, Equation (5.22) becomes

$$y(t_n) = k_\infty \left(1 - \frac{1 - e^{p_i \delta t_n}}{p_i \delta t_n}\right) x(t_n) + \sum_{i=1}^q \tilde{y}_i(t_n) \quad (5.23)$$

where

$$\tilde{y}_i(t_n) = k_i \left(\frac{1 - e^{p_i \delta t_n}}{p_i \delta t_n} + e^{p_i \delta t_n}\right) x(t_n - \delta t_n) + e^{p_i \delta t_n} \tilde{y}_i(t_n - \delta t_n)$$

The recursive convolution gives exact results if the assumption made about  $x(t)$  is valid; if not, the convolution formula has an error term. The local interpolation error is proportional to  $O(\delta t^{r+1})$  where  $r$  is the order of  $x(t)$ . The stability of the convolution method depends on the nature of the system impulse-response function,  $h(t)$ . The convergence of

the convolution is exactly the same as the convergence of the assumed input to the actual input as the time steps go to zero.

Each entry in the submatrix of the scattering parameters of the electromagnetic system is approximated by a rational function, and the inverse Laplace transform of the partial-fraction expansion or the pole-residue model is found symbolically. This corresponds to the macromodel stencils of the global MNA matrix conductance and current stencils. Equation (5.22) is implemented as a Norton-equivalent circuit consisting of a conductance of constant value,  $k_\infty$ , and a current source,  $-\sum_{i=1}^q \tilde{y}_i(t_n)$ , which is updated at each time-iteration based on the pole-residue pairs and the voltage at a previous time point. If Equation (5.23) is implemented, both the conductance and the current sources are time dependent.

## 5.6 Numerical Results

A strip-like interconnect with a V-shaped ground plane is characterized using a scattering matrix [125]. The scattering parameters are measured in the frequency range *45 MHz-10 GHz* with a *HP8510B* vector network analyzer. The measured scattering parameters of the interconnect are approximated over a frequency range using a rational function. Although the method is able to generate a stable, very high-order rational approximation, a *24th*- and a *27th*-order rational function are used to approximate  $S_{12}$  and  $S_{11}$ , respectively. The measured and approximated scattering parameters are shown in Figures 5.3 through 5.6. The magnitude and phase plots of  $S_{12}$  and  $S_{11}$  are almost indistinguishable.

A comparison of our method with the method of [19] is shown in Figure 5.7(a). A measure of the quality of the approximations is the normalized numerical difference between the measured data and the rational approximations. The maximum error of the



41st-order approximation, with respect to the original  $S_{11}$  data, is less than 0.8%. The order of approximation is limited to 41, because the direct-solution method of [19] becomes numerically unstable when the order approximation is increased beyond 41. The 41st-order of approximation of the proposed method is more accurate. The error in the 60th-order approximation of the proposed method is shown in Figure 5.7(b).

### 5.6.1 Example 5.1: Linear network

To illustrate the advantage of our method, the network shown in Figure 5.8 is analyzed. The network consists of a measured subnetwork characterized by the approximated scattering parameters. First, the measured  $S$ -parameters are extrapolated to low frequencies for the dc solution. Then, the scattering parameters are incorporated into the MNA matrix using conductances and dependent sources. Some of the implementation details associated with integrating the scattering matrix directly into circuit simulations are described in Chapter 6. The lumped-model subnetwork shown in Figure 5.8 is represented as a two-port network in the analysis. A twelfth-order Padé approximation of the admittance matrix of the lumped subnetwork is obtained using the Lanczos algorithm described in Chapter 3.

The network is excited by a pulse with rise and fall times of 0.3 ns and a pulse magnitude and width of 5 V and 4 ns, respectively. The transient responses of the network at nodes  $x$  and  $y$  are given in Figures 5.9 and 5.10. The proposed method is compared with the conventional approach in which the exact response is obtained via IFFT. In addition, the application of IFFT for the time-domain solution requires that the scattering parameters be band-limited. This is realized using rational-function extrapolations. The fact that the two responses are indistinguishable shows that an excellent match has been obtained.

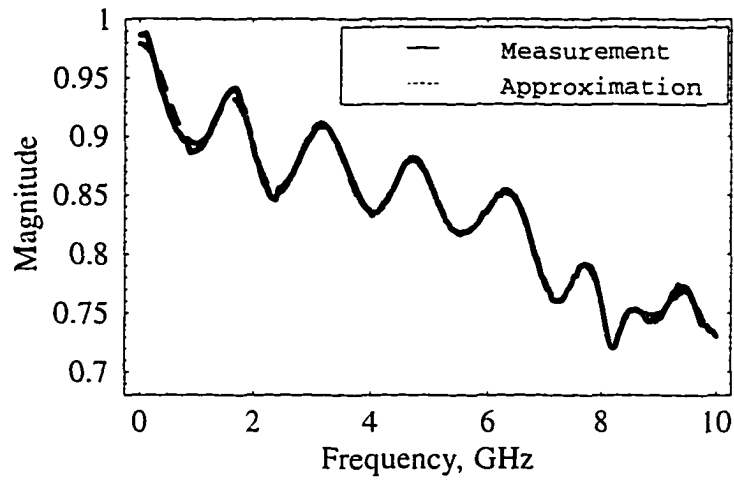


**Figure 5.3:** Magnitude plots of  $S_{12}$ , the measured data and the 24th-order rational approximation.

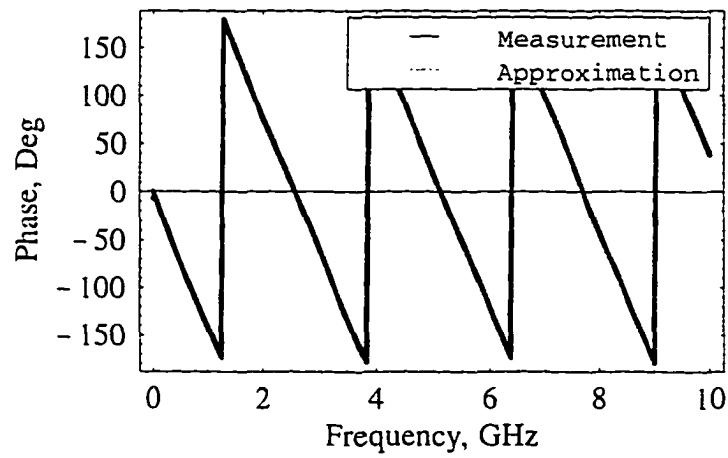


**Figure 5.4:** Phase plots of  $S_{12}$ , the measured data and the 24th-order rational approximation.

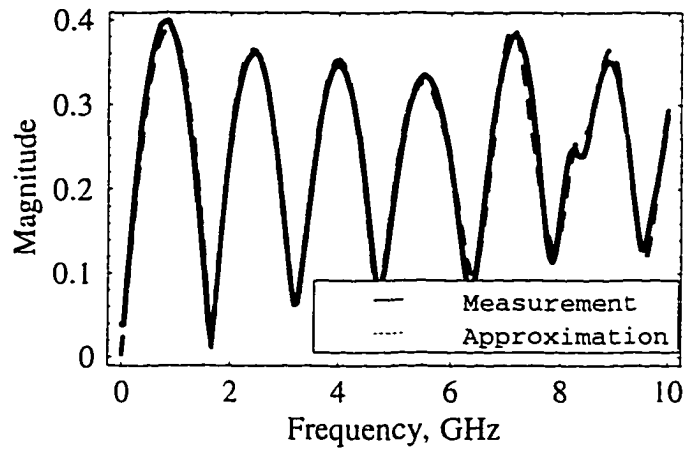


**Figure 5.5:** Magnitude plots of  $S_{11}$ , the measured data and the 27th-order rational approximation.

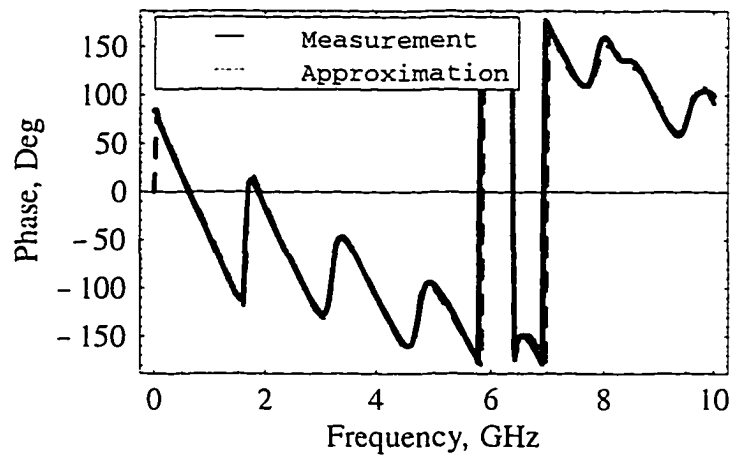
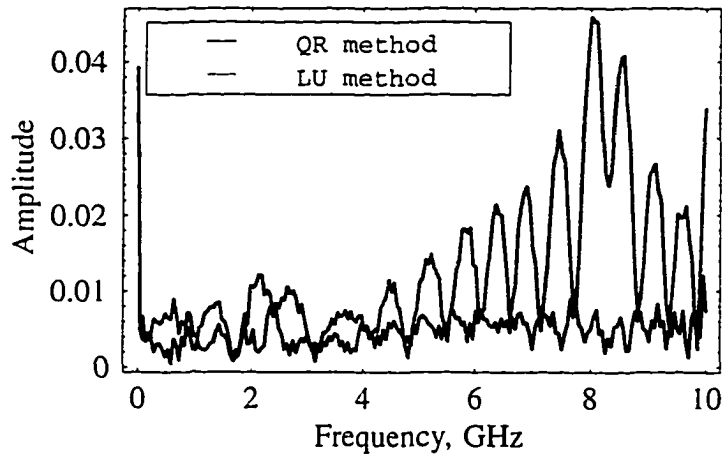
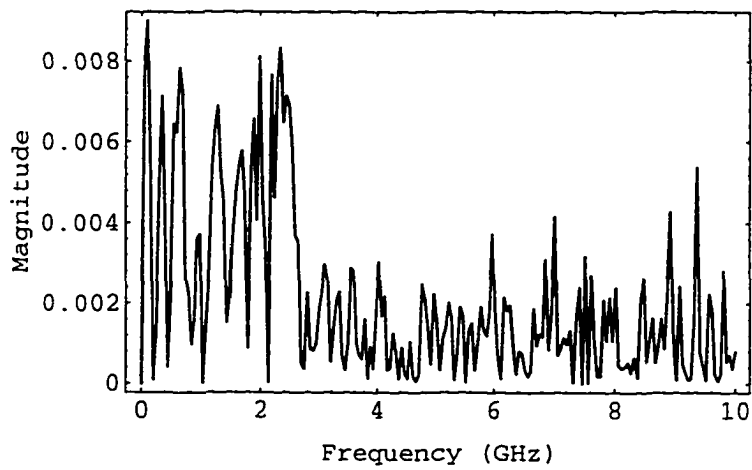


**Figure 5.6:** Phase plots of  $S_{11}$ , the measured data and the 27th-order rational approximation.



(a)



(b)

**Figure 5.7:** (a) Magnitude plot of the errors, the *41st*-order rational approximation using the method in [19] (gray line), and the proposed method (dark line), (b) magnitude plot of the errors, the *58th*-order rational approximation using the proposed method.

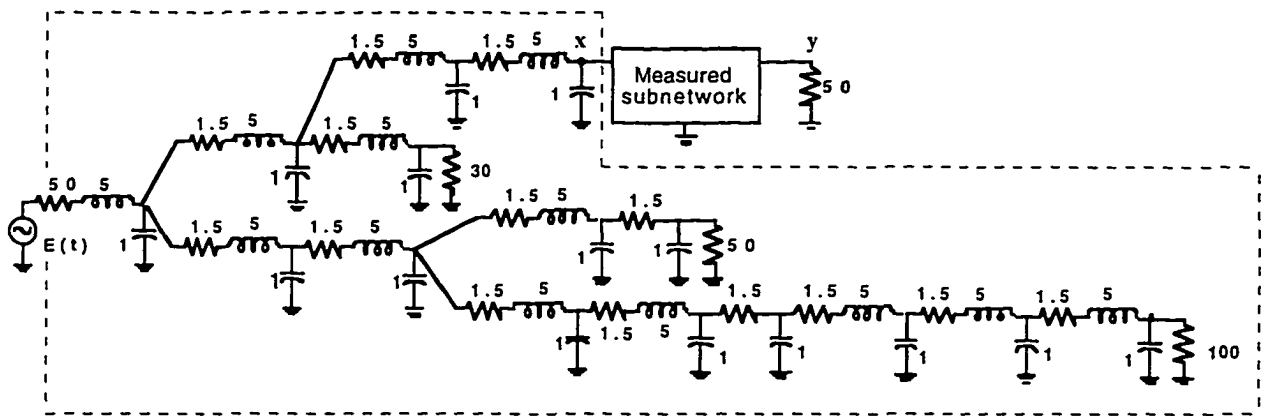
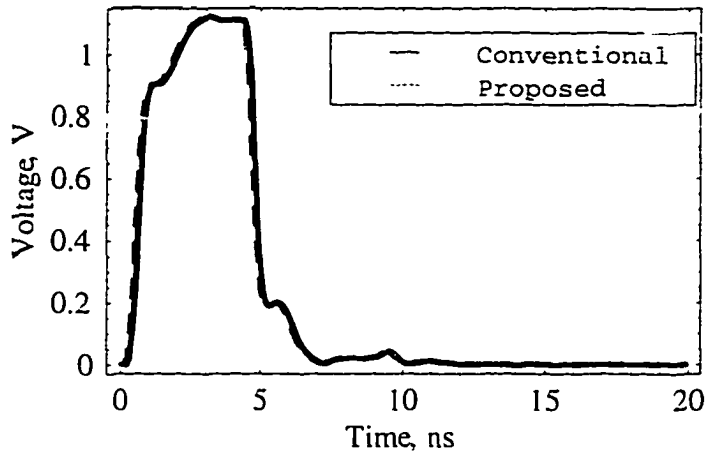
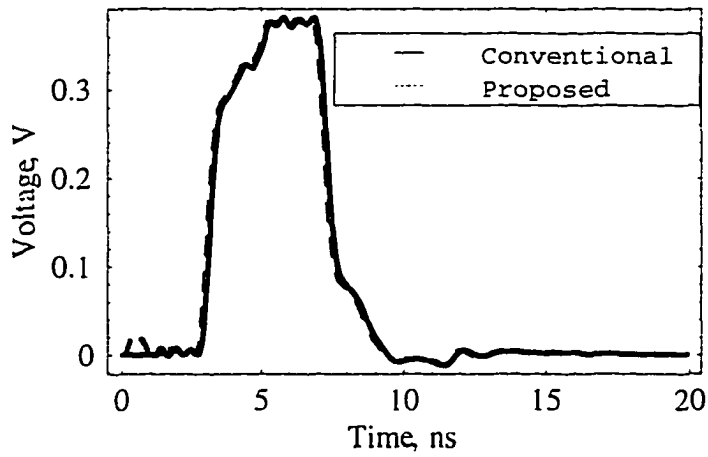


Figure 5.8: Example 5.1, interconnect network with measured component.



**Figure 5.9:** Example 5.1, transient response at node x.



**Figure 5.10:** Example 5.1, transient response at node y.

### 5.6.2 Example 5.2: Nonlinear network

In Example 5.2, the proposed method is used to study resistive and diode terminations. The network in Figure 5.11 consists of a measured subnetwork, a diode-pair termination and a resistive termination. For the measured subnetwork, the rational function approximation of the scattering parameters of Example 5.1 is used. The network is excited by a pulse with rise and fall times of  $0.3 \text{ ns}$  and pulse magnitude and width of  $5 \text{ V}$  and  $7 \text{ ns}$ , respectively. The network is simulated with the diode-pair termination and with the  $5K \Omega$  resistor replacing the diodes shown in Figure 5.11. The transient responses of the diode-pair termination at nodes  $x$  and  $y$  are compared to those of  $5K \Omega$  resistor termination. At the far-end, node  $y$ , the voltage response of the  $5K \Omega$  resistor shows voltage overshoots and undershoots while the diode-pair termination squelch the voltage overshoots, as shown in Figure 5.12. The voltage waveforms at the near-end, node  $x$ , for the two cases are almost identical as shown in Figure 5.13. Thus, time-domain analysis of a nonlinear network can be performed efficiently using the method.

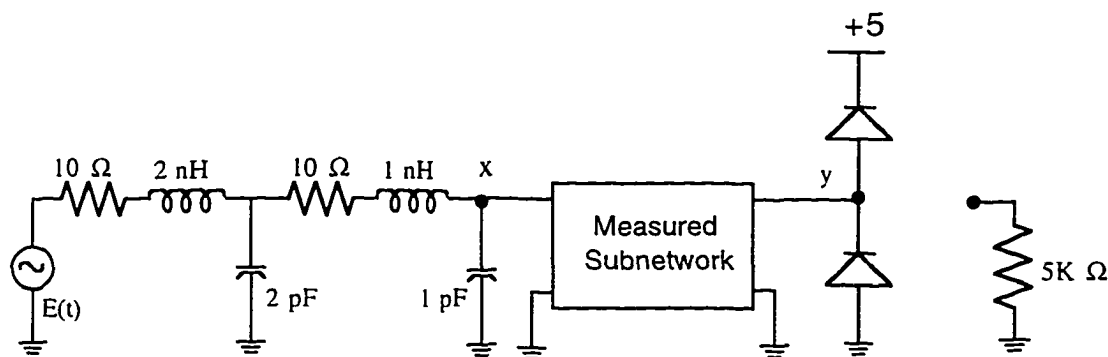


**Figure 5.11:** Example 5.2, diode-pair terminated network, (the  $5K \Omega$  resistor replaces the diode-pair).

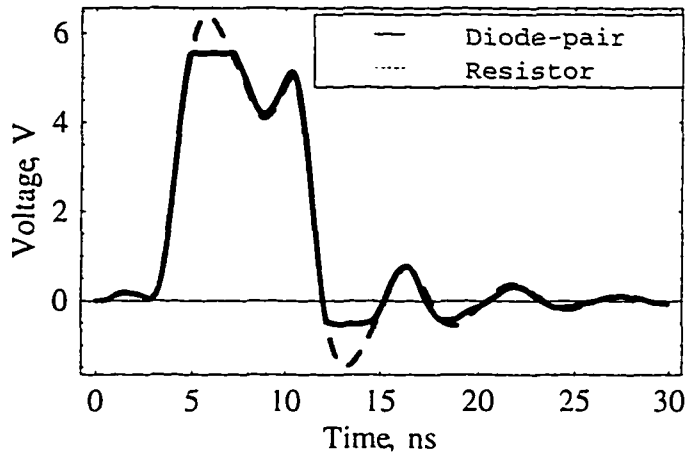


**Figure 5.12:** Example 5.2, transient response at node *y*.

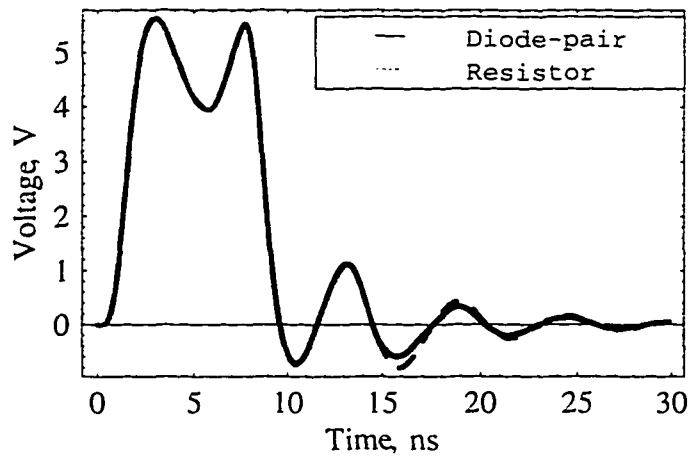


**Figure 5.13:** Example 5.2, transient response at node *x*.



## 5.7 Conclusions

In this chapter, a robust, rational-approximation algorithm is integrated with recursive convolution and network partitioning techniques for accurate and efficient transient simulations of arbitrary networks. Because of its stability and simplicity the scattering parameters are approximated by rational functions and incorporated directly into the network MNA matrix without converting them into other fundamental parameters or parasitic parameters. The analyticity of a scattering matrix is utilized to obtain stable pole-residue pairs using two linear solutions and one polynomial factorization. This leads to a significant reduction in the computational cost when compared to the costly nonlinear optimization used in traditional methods [51], [52]. Frequency normalization and shift, and Householder orthogonalization techniques are used to obtain accurate approximations. The necessary numerical considerations in the actual implementation of the algorithm are discussed. The intermediate model further reduced using modified balanced transformation. The transfer function can be used for time- or frequency-domain analysis of arbitrary networks. Recursive convolution is applied to obtain time-domain macromodels directly from the scattering matrix approximation. The method avoids the use of time-consuming explicit convolution, numerical transformation and artificial low-pass filtering of sampled data with a large number of frequency points. Thus, the method does not suffer from aliasing and numerical errors. The validity and accuracy of the method for the transient simulation of linear and nonlinear networks are shown by examples.

## CHAPTER 6

# ANALYSIS OF FREQUENCY-DEPENDENT COUPLED TRANSMISSION LINES

### 6.1 Introduction

The transient simulation of high-speed analog and digital integrated circuits require the analysis of frequency-dependent transmission lines. The frequency-dependent behaviors of transmission lines such as losses and dispersions are accurately represented in the frequency domain, while the determination of transmission line delays and noise requires the time-domain simulation of a nonlinear network often used as drivers and terminations. In order to resolve this dilemma, most analysis programs use numerical, inverse-transform techniques to go back and forth between frequency and time domains.

Traditionally, a transmission line is modeled by cascading a large number of resistors, inductors and capacitors. The method introduces a large number of nodes that greatly increases the simulation time. This equivalent-circuit based method introduces excessive ringing and can give accurate results only in a limited frequency range.

The lumped-element circuit models must be supplemented to account for frequency-dependent effects in transmission lines. The method of characteristics, introduced by Branin [37], can be used to simulate lossless transmission lines in the time domain.

The method transforms the telegrapher's equations into ordinary differential equations that can be easily solved [39], [40]. For lossless and distortionless transmission lines the ordinary differential equations can be integrated analytically [38]. In a distortionless transmission line, the ratio of the dc resistance and the dc conductance is equal to the square root of the characteristic impedance. The method is extended for lossy lines by using numerical techniques [41]. The method cannot be easily applied to analyze frequency-dependent behaviors such as the skin effect and dielectric losses. The most general approach for simulating transmission lines is based on the convolution method [42]-[45]. The impulse responses of transmission line systems are used to solve the nonlinear convolution equations governing the interconnects and nonlinear drivers and terminations [45], [118], [120]. The convolution requires the inverse transforms and band-limit filtering of a large number of points in order to minimize aliasing and unwanted ringing. The method is computationally expensive and cannot be used for large systems. When the convolution method is applied to low-loss or lossless transmission lines whose time-domain impulse response can be infinite in length, the Gibbs phenomena and aliasing errors can accumulate leading to convergence and numerical stability problems.

An efficient synthesis technique of the characteristics of distributed systems based on reduced-order rational approximation is presented in Chapter 5. The method generates finite-dimensional, reduced-order models of distributed systems using a combination of rational approximations of infinite-order systems and a modified balanced realization of the approximating finite-order systems. The distributed systems are represented as multiport, pole-residue models and are combined to form the system matrix to handle nonlinear elements. The equation describing the transmission line system is formulated using the scattering matrix and an optimal reference system. The scattering matrix is approximated using a rational function, and recursive convolution is applied to convert the rational functions into macromodels of multiterminal networks that can be used as system matrix stamps. The approach bypasses explicit convolution, inverse Fourier transforms, and

low-pass filtering of a large number of points in order to avoid aliasing and time-domain ripples associated with the transformation of data between the frequency and time domains. The circuit representations of the transmission line system using Norton-equivalent circuits with a conductance and a time-dependent current source are compatible with those of conventional time-domain simulators, such as SPICE and ASTAP or with methods based on reduced-order techniques such as AWE, CFH, and PVL.

In Section 6.2, the eigen-analysis of a transmission line equation is described. In Section 6.3, the scattering formulation of a transmission line system is presented. In Section 6.4, an efficient simulation technique using recursive convolution is presented. Examples of linear and nonlinear networks are given in Section 6.5. The conclusion is given in Section 6.6.

## 6.2 Transmission Lines Equations

The transmission lines, shown in Figure 6.1, are expressed with coupled partial differential equations relating the voltages and currents on the transmission lines given by

$$\begin{aligned}\frac{\partial}{\partial x} v(x,t) &= -R i(x,t) - L \frac{\partial}{\partial t} i(x,t) \\ \frac{\partial}{\partial x} i(x,t) &= -G v(x,t) - C \frac{\partial}{\partial t} v(x,t)\end{aligned}\tag{6.1}$$

where  $R$ ,  $L$ ,  $G$ , and  $C$  are the resistance, inductance, conductance and capacitance  $N \times N$  matrices per unit length, and  $v(x,t)$  and  $i(x,t)$  are  $N \times 1$  voltage and current vectors, respectively.

It is convenient to write Equation (6.1) as coupled, ordinary differential equations using Laplace transform as

$$\begin{aligned}\frac{\partial}{\partial x} V(x, s) &= -Z(s)I(x, s) \\ \frac{\partial}{\partial x} I(x, s) &= -Y(s)V(x, s)\end{aligned}\tag{6.2}$$

where  $Y(s)=G(s)+sC(s)$  and  $Z(s)=R(s)+sL(s)$  are the admittance and impedance per unit length,  $N \times N$  matrices of the transmission line systems, respectively. The frequency-dependent parameters of transmission lines can be described using Equation (6.2).

Combining the ordinary differential equations in (6.2) produces a set of second-order differential equations given by

$$\begin{aligned}\frac{\partial^2}{\partial x^2} V(x, s) &= Z(s)Y(s)V(x, s) \\ \frac{\partial^2}{\partial x^2} I(x, s) &= Y(s)Z(s)I(x, s)\end{aligned}\tag{6.3}$$

In general, Equation (6.3) has  $N$ -sets of possible solutions corresponding to  $N$ -propagation modes of the  $N$ -coupled transmission lines. These modes or the eigenvalues and eigenvectors associated with the solution are related as

$$\begin{aligned}EZY E^{-1} &= \Lambda_m^2 \\ HYZH^{-1} &= \Lambda_m^2\end{aligned}\tag{6.4}$$

where  $\Lambda_m$  is a diagonal matrix with the square root of the eigenvalues of  $ZY$  as diagonal entries, and  $E$  and  $H$  are the matrices of the associated eigenvectors of  $ZY$  and  $YZ$ , respectively. The eigenvectors are used to transform Equation (6.3) into decoupled equations as

$$\begin{aligned}\frac{\partial^2}{\partial x^2} V_m(x, s) &= \Lambda_m^2 V_m(x, s) \\ \frac{\partial^2}{\partial x^2} I_m(x, s) &= \Lambda_m^2 I_m(x, s)\end{aligned}\tag{6.5}$$

where  $V_m=EV$  and  $I_m=HI$  are the modal voltages and currents, respectively. Various approaches can be used to solve Equation (6.5). The general solution of Equation (6.5) can then be obtained as

$$\begin{aligned}
V_m(x) &= \psi(-x) A + \psi(x) B \\
I_m(x) &= Z_m^{-1} [\psi(-x) A - \psi(x) B]
\end{aligned}
\tag{6.6}$$

where  $\psi(x) = \text{diag}(e^{\beta_1 x}, e^{\beta_2 x}, \dots, e^{\beta_N x})$ ,  $\beta_i$  is the complex propagation constant associated with the  $i$ th mode and is the  $i$ th eigenvalue of  $ZY$ , and  $Z_m = \Lambda_m^{-1} E Z H^{-1}$  is the modal characteristic impedance of the transmission line system. The variables  $A$  and  $B$  are the coefficient vectors associated with the forward and backward traveling waves on the transmission lines. They are determined from the boundary conditions; the terminations at the ends of the lines.

### 6.3 Scattering Parameters Formulation

Transmission lines are often characterized by parasitic parameters such as resistance, inductance, capacitance and conductance per unit length. These parameters are difficult to approximate. The approximation of the characteristic impedance and admittance parameters are prone to numerical instability and acquire extreme values at integral multiples of one-fourth of the wavelength. For example, the impedance of a line with no shunt loss tends to infinity. An arbitrary transmission line system can be described in the frequency domain using scattering parameters. The magnitude of the scattering parameter is limited to one. Another advantage of the scattering-parameter formulation is that by choosing an appropriate reference system, the scattering function can be made smooth and simple enough to approximate with low-order, rational functions.

The analysis of  $N$ -coupled transmission lines characterized by scattering parameters is done using the following incident and reflected voltage wave definitions:

$$\begin{aligned}
A_i(j\omega) &= \frac{1}{2}(V_i(j\omega) + Z_{ref}I_i(j\omega)) \\
B_i(j\omega) &= \frac{1}{2}(V_i(j\omega) - Z_{ref}I_i(j\omega))
\end{aligned}
\tag{6.7}$$

The impedance matrix  $Z_{ref}$  describes the reference impedance of an  $N$ -port network and is used to describe the scattering parameters in the calculation or measurement of the scattering parameters. The scattering matrix relates the incident wave to the reflected wave matrix shown in Figure 6.2 as

$$\begin{aligned}
B_1 &= S_{11}A_1 + S_{12}A_2 \\
B_2 &= S_{21}A_1 + S_{22}A_2
\end{aligned}
\tag{6.8}$$

where  $S_{ij}$ 's are  $N \times N$  scattering matrices describing the transmission line system and  $A_i$ 's and  $B_i$ 's are the forward and backward waves, respectively. In order to be able to handle the nonlinear devices, the time-domain formulation can be obtained by inverting Equation (6.8) resulting with the convolution given as

$$\begin{aligned}
b_1(t) &= s_{11} * a_1(t) + s_{12} * a_2(t) \\
b_2(t) &= s_{21} * a_1(t) + s_{22} * a_2(t)
\end{aligned}
\tag{6.9}$$

where  $a_i$ 's and  $b_i$ 's are the time-domain wave vectors associated with  $A_i$ 's and  $B_i$ 's,  $s_{ij}$ 's are time-domain scattering matrices, and  $*$  is used to denote convolution.

The  $N$ -port scattering parameters of complex interconnect structures can be obtained from frequency-domain measurements with high accuracy by using one of the commercially available network analyzers. They are easier to measure over a wider frequency range using careful calibration techniques. The  $N$ -port, time-domain impulse response can also be obtained from reflection and transmission measurements using a high-speed oscilloscope with TDR and TDT options.

It is possible to calculate the scattering parameters of an arbitrary transmission line system using full-wave analysis techniques. For example, one FDTD simulation can generate the time-domain scattering matrix and eliminate the adverse effects from the imperfect boundary conditions. The corresponding frequency-domain scattering parameters

are defined in terms of the Fourier transforms of the time signatures of the incident, reflected and transmitted waves.

Scattering parameters of transmission can also be derived from TEM, quasi-TEM or frequency-dependent parasitic parameters, resistance  $R(j\omega)$ , conductance  $G(j\omega)$ , capacitance  $C(j\omega)$ , and inductance  $L(j\omega)$ , per unit length. The multiport scattering parameters can be obtained using the eigen-analysis described in [118]. By matching the line voltage wave vectors at the transition planes between the reference and transmission line system shown Figure 6.2, the scattering parameters are derived (also derived in Appendix A).

The line scattering matrices are given by

$$\begin{aligned} S_{11} = S_{22} &= T^{-1}(\Gamma - \Psi\Gamma\Psi)(1 - \Gamma\Psi\Gamma\Psi)^{-1}T \\ S_{12} = S_{21} &= 2E^{-1}(1 - \Gamma)\Psi(1 - \Gamma\Psi\Gamma\Psi)^{-1}T \end{aligned} \quad (6.10)$$

where

$$\begin{aligned} \Gamma &= (1 + EE_0^{-1}Z_0H_0H^{-1}Z_m^{-1})^{-1}(1 - EE_0^{-1}Z_0H_0H^{-1}Z_m^{-1}) \\ T &= (1 + EE_0^{-1}Z_0H_0H^{-1}Z_m^{-1})^{-1}E \\ \Psi &= \psi(-l) \end{aligned}$$

and  $Z_0$  is the modal impedance of the associated frequency-independent reference impedance given by  $Z_0 = \Lambda_0^{-1}E_0L_0H_0^{-1}$ , where  $\Lambda_0$  is a diagonal matrix with the square root of corresponding eigenvalues as diagonal entries and  $E_0$  and  $H_0$  are the matrices of the eigenvectors associated with  $L_0C_0$  and  $C_0L_0$  of the reference system. Because the reference system is an arbitrary nonphysical system, its parameters are selected to give smoother scattering parameters that are easy to approximate. The optimal choice for the inductance and capacitance per unit length of the reference line system is  $L_0=L$  and  $C_0=C$ , respectively. For example, the scattering parameters of a lossless coupled-line system can be simplified to

$$\begin{aligned} S_{11} = S_{22} &= 0 \\ S_{12} = S_{21} &= \Psi \end{aligned}$$



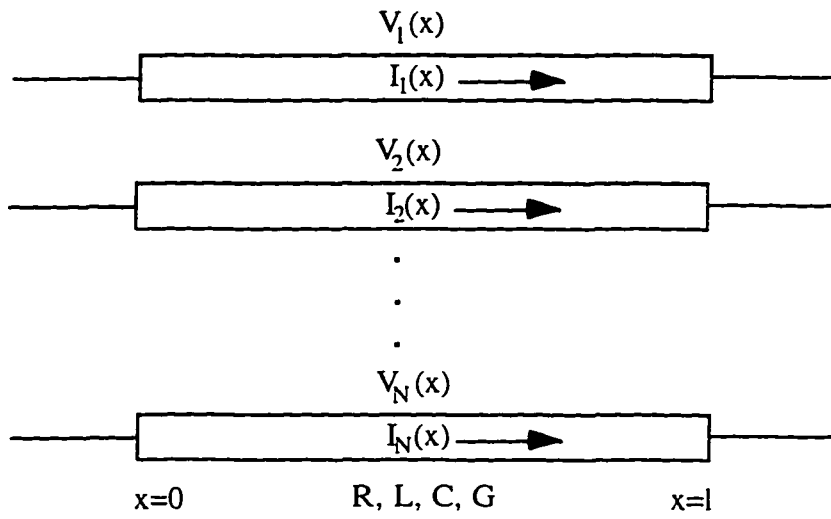


**Figure 6.1:** General representation of an  $n$ -coupled transmission line system.

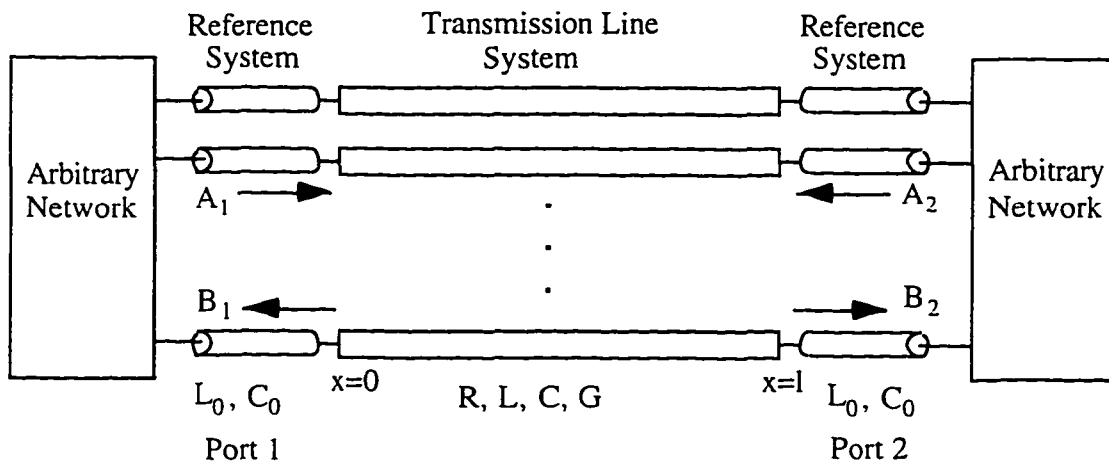


**Figure 6.2:** A network of  $n$ -coupled transmission line system, reference system, and arbitrary networks.

## 6.4 Simulation Techniques

Although the time-domain scattering parameters of an interconnect system can be approximated by a polynomial of exponential functions using such methods as Prony's or Pencil-of-function, the approximation procedures involve costly nonlinear optimization [121], [122]. Because interconnects are primarily linear and their parameters are simple functions of frequency, they are well-characterized in the frequency-domain. The frequency-domain approximation is more efficient and can give better results. Hence, the transfer functions of interconnect systems can be approximated by the least maximum error using rational functions described in Chapter 5.

The scattering parameters can be approximated by rational functions with high accuracy. The convolution in (6.10) can be done very efficiently using the recursive equation presented in Chapter 5. The convolution Equation (6.10) can be reduced into linear operation that involves a simple update of parameters at each time point. The relationship between  $a_i$ 's and  $b_i$ 's is described as

$$\begin{bmatrix} b_1 \\ b_2 \end{bmatrix}_n = \underbrace{\begin{bmatrix} k_{\infty}^{11} & k_{\infty}^{12} \\ k_{\infty}^{21} & k_{\infty}^{22} \end{bmatrix}}_{K_{\infty}} \begin{bmatrix} a_1 \\ a_2 \end{bmatrix}_n + \underbrace{\begin{bmatrix} \sum_{i=1}^q \tilde{b}_{11} + \sum_{i=1}^q \tilde{b}_{12} \\ \sum_{i=1}^q \tilde{b}_{21} + \sum_{i=1}^q \tilde{b}_{22} \end{bmatrix}}_{\tilde{b}_n} \quad (6.11)$$

where the matrix entries are the coefficients at time point  $t_n$  determined from the pole-residue models of the scattering parameters and the recursive convolution formula.

The terminal currents and voltages at the transmission line ports are obtained by writing the incident and reflected waves as

$$\begin{aligned}
 a_i &= \frac{1}{2}(v_i + Z_0 i_i) \\
 b_i &= \frac{1}{2}(v_i - Z_0 i_i)
 \end{aligned}
 \tag{6.12}$$

Substituting (6.12) into (6.11) at time point  $t_n$  gives the relationship between the terminal voltages and currents as

$$i(t_n) = Z_0^{-1}(1 + K_\infty)^{-1} (1 - K_\infty) v(t_n) - 2Z_0^{-1}(1 + K_\infty)^{-1} \bar{b}(t_n)
 \tag{6.13}$$

Equation (6.13) can be implemented into circuit simulators as conductance and time-dependent sources as shown in Figure 6.3. For a piecewise constant excitation, the conductance and time-dependent current values are given by:

$$\begin{aligned}
 G &= Z_0^{-1}(1 + K_\infty)^{-1} (1 - K_\infty) \\
 J_n &= 2Z_0^{-1}(1 + K_\infty)^{-1} \bar{b}(t_n)
 \end{aligned}
 \tag{6.14}$$

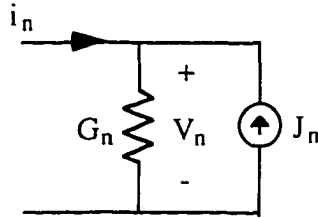


**Figure 6.3:** Norton-equivalent representation of Equation (6.13), at time  $t_n$ .

## 6.5 Numerical Results

To verify the capability and illustrate the advantages of the method, representative examples are presented. Some of the implementation details associated with the method are also described.

### 6.5.1 Example 6.1: Lossless coupled transmission lines

As mentioned in the introduction, methods based on convolution have problems dealing with low-loss lines. The situation can lead to an infinite response that results in expensive computation and numerical inaccuracies caused by the accumulation of errors from convolution and IFFT of a large number of points. An example of a three-conductor system taken from [39] and [73] is shown in Figure 6.4. The capacitance and inductance per unit length are, respectively,

$$C = \begin{bmatrix} 1.0413 & -0.3432 & -0.0140 \\ -0.3432 & 1.1987 & -0.3432 \\ -0.0140 & -0.3432 & 1.0413 \end{bmatrix} \text{ pF/cm}$$

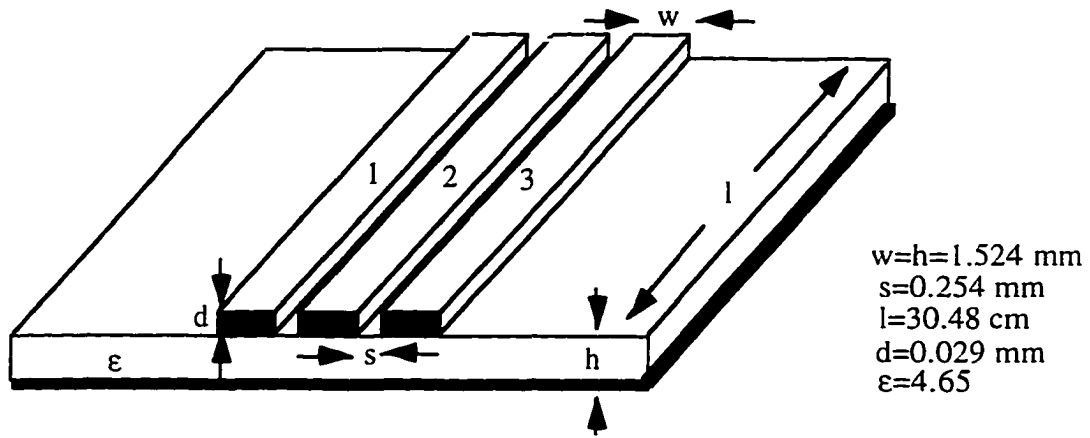
$$L = \begin{bmatrix} 3.8790 & 1.6238 & 0.8252 \\ 1.6328 & 3.7129 & 1.6238 \\ 0.8252 & 1.6238 & 3.8790 \end{bmatrix} \text{ nH/cm}$$

and simulated using the method developed above. The simulation results are compared with measurement results. The S-parameters are measured using an HP8510B network analyzer with a time-domain option. The  $6 \times 6$  time-domain, impulse-response matrix is integrated with time to obtain the step responses at each port. For simulation, the step response shown in Figure 6.5 is generated by

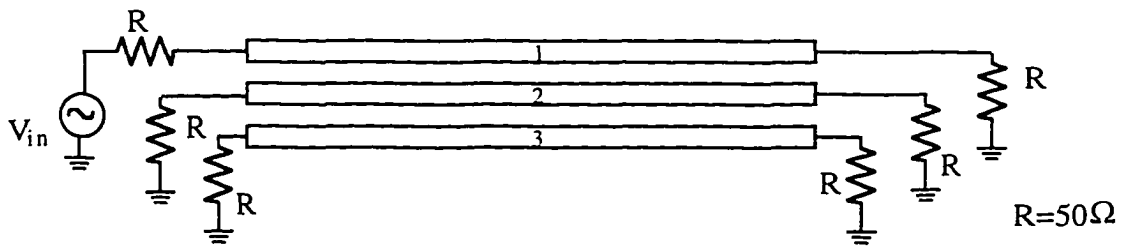
$$V_{in}(t) = \frac{1}{1 + e^{-\alpha(t-\tau)}} \quad (6.15)$$

where  $\alpha = 80 \times 10^9$  and  $\tau = 0.75 \times 10^{-9}$  seconds.

A very good match between the measurement and simulation for transient responses at near- and far-end of each line is obtained as shown in Figures 6.6-6.10. Some of the spikes are due to unaccounted parasitics of the measurement apparatus.



(a)



(b)

**Figure 6.4:** (a) Dimensions of a three-conductor microstrip system, (b) network of the three-conductor microstrip system.

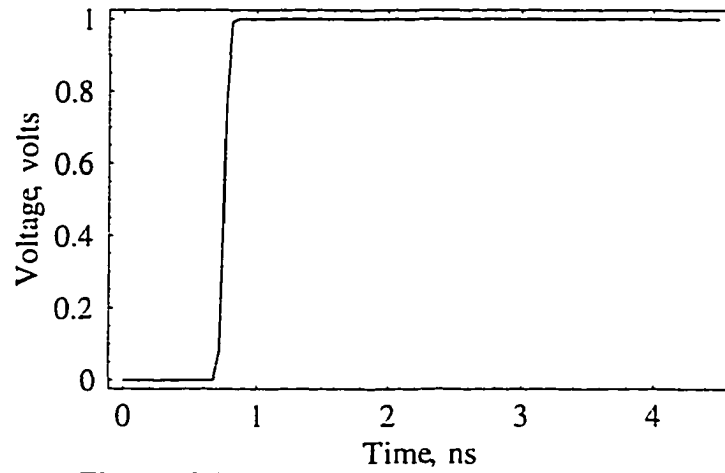


**Figure 6.5:** Approximated input waveform.

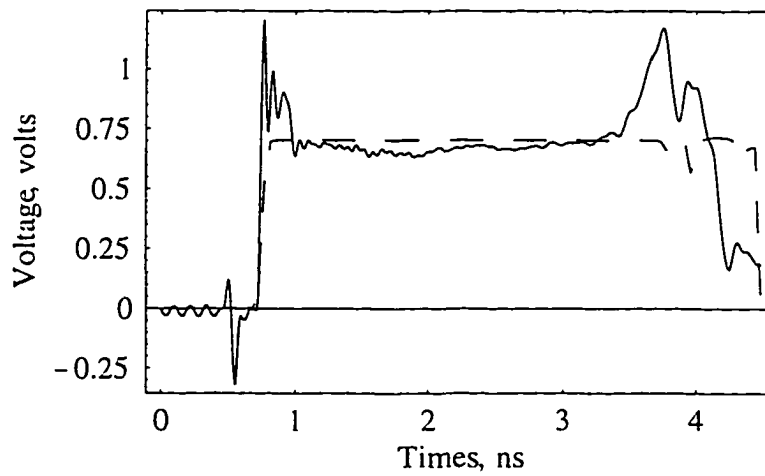


**Figure 6.6:** The near-end voltage transient waveform on conductor 1, measurements (solid ) and simulation (dashed).

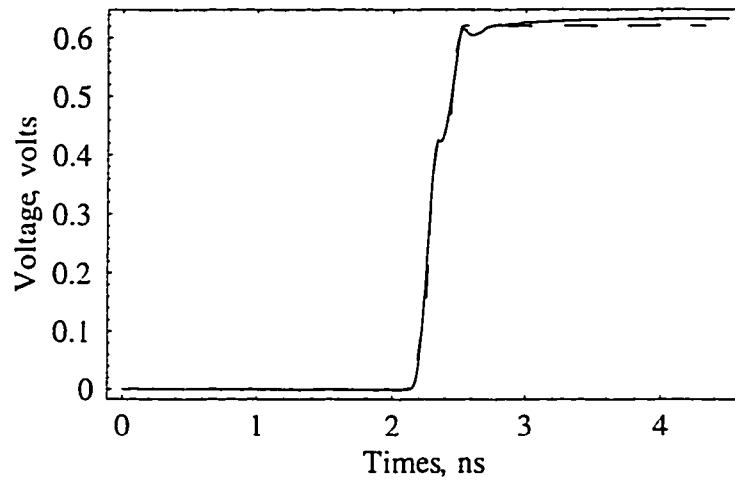


**Figure 6.7:** The far-end voltage transient waveform on conductor 1, measurements (solid ) and simulation (dashed).

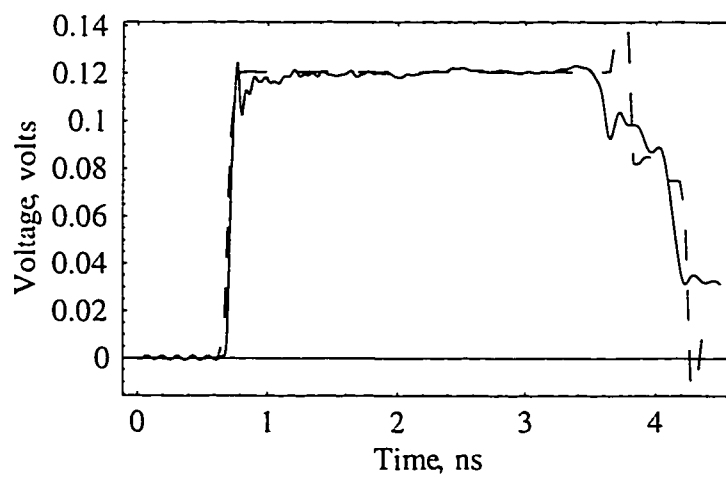


**Figure 6.8:** The near-end voltage transient waveform on conductor 2, measurements (solid ) and simulation (dashed).

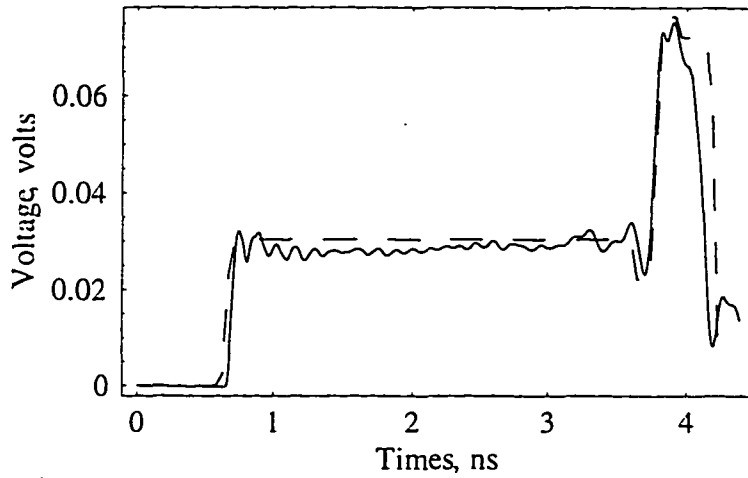


**Figure 6.9:** The near-end voltage transient waveform on conductor 3, measurements (solid ) and simulation (dashed).

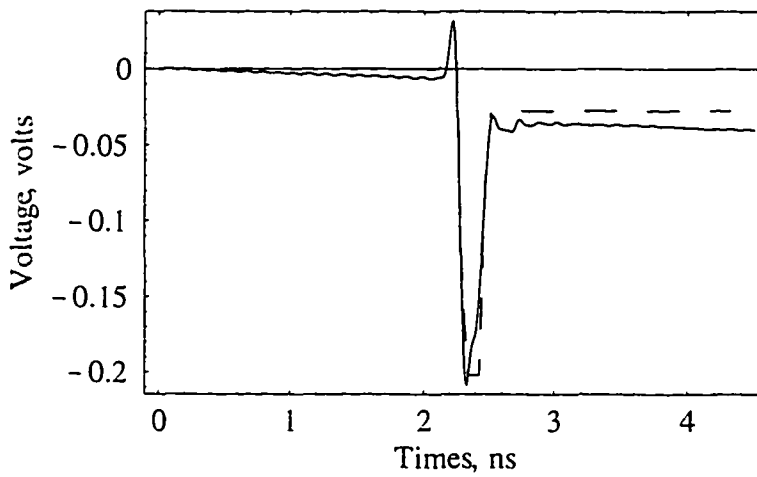


**Figure 6.10:** The far-end voltage transient waveform on conductor 3, measurements (solid ) and simulation (dashed).



### 6.5.2 Example 6.2: Coaxial cable with skin effect

To test the accuracy of the method, a lossy coaxial line simulated and waveforms are compared with measurements. A 100-m long coaxial cable, shown in Figure 6.11, has the following characteristic parameters of transmission line as the following  $L=476 \text{ nH/m}$ ,  $C=0.0476 \text{ nF/m}$ ,  $G=0$ , and the resistance is characterized with a skin effect model described in [85] as

$$R(s) = A + B(s)^\alpha$$

where  $R$  is the overall resistance in ohms per meter,  $A=0$ ,  $B= 15.384$ ,  $\alpha=0.48288$ , and  $s=j2\pi f$ , where  $f$  is the frequency in GHz. The line is not terminated at the far end. A 3 V pulse of 2 ns rise and fall time, and a duration of 58 ns is placed at the input.

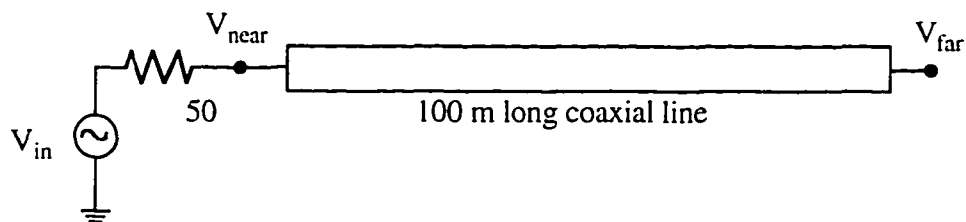


**Figure 6.11:** Example 6.2, a coaxial line.

For 100  $\Omega$  and 50  $\Omega$  reference impedances, the magnitude of  $S_{11}$  and  $S_{12}$  are shown in Figures 6.12 and 6.13, respectively. The optimal reference system used to calculate the response is  $\sqrt{L/C} = 100 \Omega$ . The solutions are compared to time-domain measurements. The simulation and measurement waveforms for the near-end port are shown in Figures 6.14 and 6.15, respectively. The far-end simulated and measured voltage waveforms are shown in Figures 6.16 and 6.17, respectively.

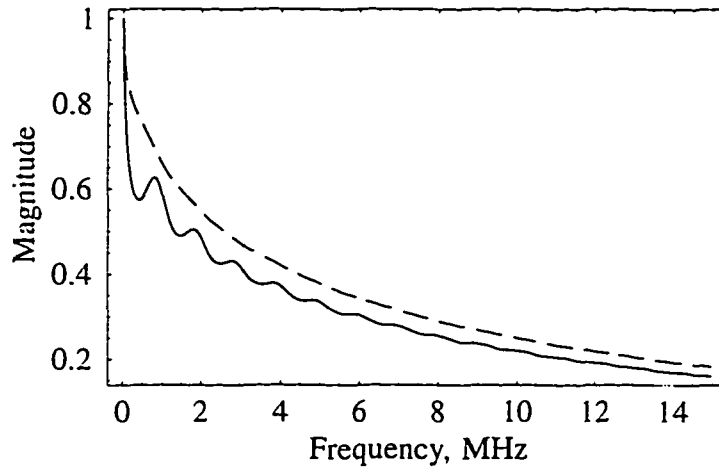


**Figure 6.12:** The magnitude of  $S_{12}$ , for  $50 \Omega$  (solid) and  $100 \Omega$  (dashed) reference impedances.

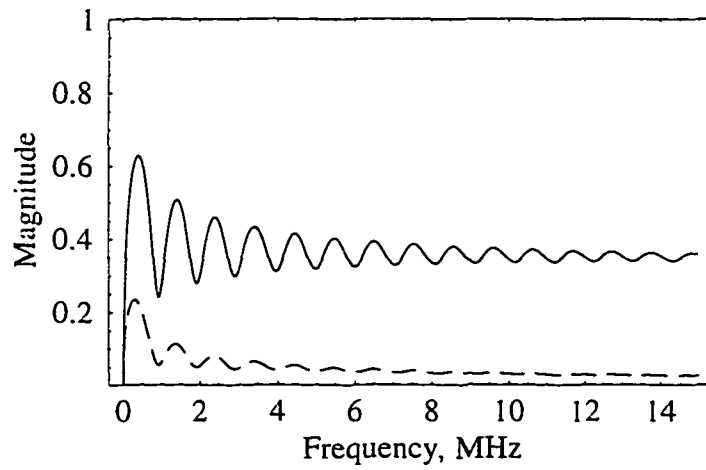


**Figure 6.13:** The magnitude of  $S_{11}$ , for  $50 \Omega$  (solid) and  $100 \Omega$  (dashed) reference impedances.

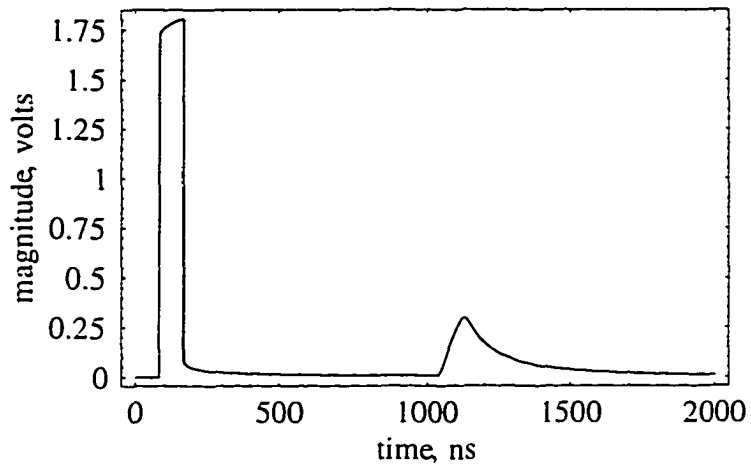


**Figure 6.14:** Example 6.2: Near-end simulated voltage waveform.

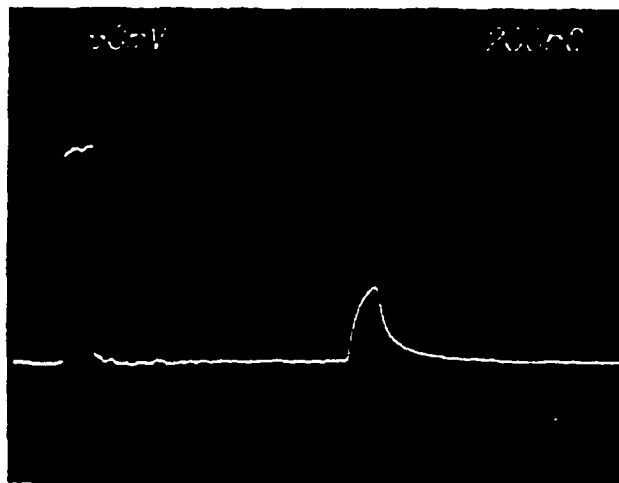


**Figure 6.15:** Example 6.2: Near-end measured voltage waveform.

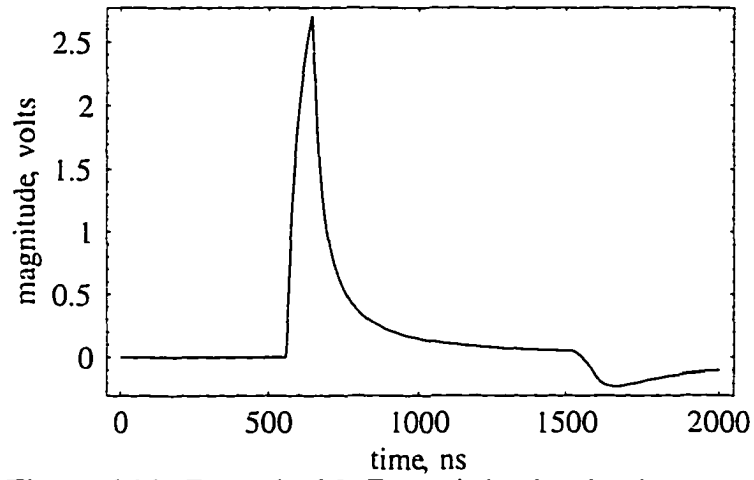


**Figure 6.16:** Example 6.2: Far-end simulated voltage waveform.

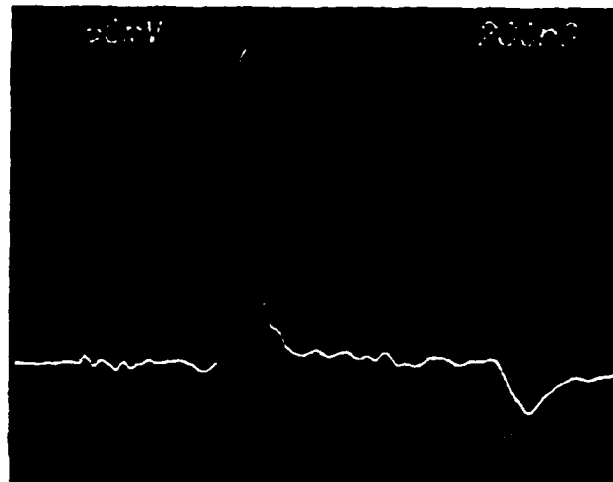


**Figure 6.17:** Example 6.2: Far-end measured voltage waveform.

## 6.6 Conclusions

An efficient analysis method of frequency-dependent, coupled transmission lines is presented. The frequency-dependent scattering matrix characterizing the transmission lines system is approximated by rational function, and recursive convolution is used to construct the macromodels and to incorporate them into time-domain nonlinear solvers. The MNA stamps corresponding to the transmission line systems are constructed as Norton-equivalent circuits of conductances and current sources that are updated at each time point. Nonlinear terminations are also handled efficiently by avoiding the overhead cost associated with FFT and other band-limiting processes, such as smoothing and filtering of a large number of points. The method does not suffer from nonphysical artificial filtering to band limit the impulse response of the system and the errors accumulated, due to filtering and numerical inversions. The algorithm enables the accurate modeling of complex interconnects that are often characterized in frequency-domain data obtained from measurement or electromagnetic analysis. Representative examples show that the method resolves the dilemma most analysis techniques encounter: the expedience of frequency-domain characterization of transmission lines and the indispensability of time-domain formulation of nonlinear drivers and receivers.

# CHAPTER 7

## CONCLUSIONS

### 7.1 Summary of Research

This dissertation extends the use of model order-reduction techniques for analog circuit simulation. The moment-matching, Krylov subspace and rational-interpolation techniques are investigated as efficient and accurate methods for simulating the transient response of circuits and interconnects. The order-reduction method provides a way to bring together the two conflicting needs in CAD tools: efficiency and accuracy. The method simplifies large networks using pole-residue models, while it provides a means to model higher-order effects. The carrier diffusion in diode and wave propagation in transmission lines are analyzed.

Conventional circuit simulation methods are reviewed in order to show that the traditional techniques are only good for lumped-element models, and that they are not suitable for distributed networks. Padé analysis is presented to demonstrate that a rational-function synthesis is a viable means to improve the simulation accuracy and efficiency of distributed systems. Although the Padé synthesis via Krylov subspace methods such as the Arnoldi and Lanczos techniques are superior to the moment-matching method, the presence of closed-form recursive formulas to generate the associated moment makes the

moment-matching method an efficient and suitable tool to generate reduced-order models of distributed effects that are smooth functions of frequency.

Based on these observations, the Padé synthesis is used to accurately model the carrier diffusion in  $p$ - $n$ -junction diodes. A recursive relation is derived for the first time to generate the moments of the carrier concentration efficiently. This new approach is more accurate than those of traditional methods that use simple, equivalent linearized-device models. The new method was able to accurately calculate the forward- and reverse-recovery effects in diode circuits. The results are favorably compared to recent work by Chang [90], who addressed the problem.

A robust rational interpolation algorithm that uses frequency scaling and shifting is introduced. Instead of normal equation method, Householder QR orthogonalization is used to solve the resulting over-determined and ill-conditioned linear systems. The rational interpolation is followed by a stable, pole-clustering technique to obtain a reduced-order model. The effects of the dominant poles that are close to the  $j\omega$ -axis are maintained by using inverse distance-measure criterion (IDM). The IDM automatically gives larger weights to the dominant poles. Furthermore, the recursive-convolution techniques are used to improve the computational cost to calculate the response of a system. The method is applied to model electromagnetic systems characterized by sampled data. The improvement over those recent methods that use the normal equation method is demonstrated by examples [19], [109].

The rational-interpolation method is used to analyze an arbitrary coupled transmission line system. The system is formulated using scattering parameters. Using an appropriate reference system, the scattering parameters are made smooth function of frequency, simple enough to be approximated by low-order rational functions. Using the analytical transforms of the partial-fraction expansions and recursive convolution, the response of the transmission line system for arbitrary terminations is calculated. The method bypasses numerical transforms and artificial low-pass filtering that the traditional

methods use to avoid aliasing and unwanted ringing. The method's accuracy is verified with measurement data.

## 7.2 Suggestions for Further Studies

This dissertation has presented, for the first time, the fundamentals necessary to use model order-reduction techniques for diode modeling. The work in Chapter 4 can be extended to analyze  $p$ - $n$  junction devices with arbitrary doping profiles. The spatial variation of doping profiles can be approximated using appropriate interpolating functions and similar order-reduction techniques can be applied. The extension of the method to field-effect devices, such as MOS, need to be investigated.

Padé approximation is notorious for generating unstable solutions. As discussed in Chapter 3, several techniques have been applied to circumvent these problems. However, almost all of these methods are heuristic, and there is no systematic way to choose expansion points that guarantee a stable solution. The work on rational Krylov methods [126]-[129] can shed some light on these problems. One important topic that merits further investigation is the relationship between the rational Krylov subspace method and the rational-interpolation method developed in Chapter 5.



# APPENDIX A

## Derivation of Scattering Parameters

The general solution of Equation (6.5) can be written as

$$\begin{aligned} V_m(x) &= \psi(-x) A + \psi(x) B \\ I_m(x) &= Z_m^{-1} [\psi(-x) A - \psi(x) B] \end{aligned} \quad (\text{A.1})$$

where  $A$  and  $B$  are determined from the boundary conditions. The modal incident and reflected wave vector pairs  $(A_1, B_1)$  and  $(A_2, B_2)$  at transition planes of Port 1 and Port 2, respectively, are defined as shown in Figure 6.2. The voltages and currents,  $V_1$  and  $I_1$ , are related to the incident and reflected waves at the reference system in Port 1 by

$$\begin{aligned} V_1(x) &= \psi_0(-x) A_1 + \psi_0(x) B_1 \\ I_1(x) &= Z_m^{-1} [\psi_0(-x) A_1 - \psi_0(x) B_1] \end{aligned} \quad (\text{A.2})$$

where  $\psi_0(x) = \text{diag}(e^{j\omega\lambda_1 x}, e^{j\omega\lambda_2 x}, \dots, e^{j\omega\lambda_n x})$  and  $\lambda_i$ 's are the square roots of the eigenvalues of  $L_0 C_0$

It is assumed that excitation is provided only at Port 1, which makes  $A_2=0$ . Because the line voltages and currents are equal to the reference and test systems on Port 1, we have

$$\begin{aligned} E_0^{-1} [A_1 + B_1] &= E^{-1} [A + B] \\ H_0^{-1} Z_0^{-1} [A_1 - B_1] &= H^{-1} Z_m^{-1} [A - B] \end{aligned} \quad (\text{A.3})$$

Also, by requiring that the line voltages and currents be continuous at the junction plane between the reference and test systems at Port 2, with  $A_2=0$ , we obtain

$$E^{-1}[\psi(-l)A + \psi(l)B] = E_0^{-1}Z_0^{-1}H_0H^{-1}Z_m^{-1}[\psi(-l)A - \psi(l)B] \quad (\text{A.4})$$

Solving (A.4) for  $B$  in terms of  $A$  and recalling  $\Psi = \psi(-l)$ , we have

$$B = -\Psi\Gamma\Psi A \quad (\text{A.5})$$

where

$$\Gamma = (1 + EE_0^{-1}Z_0H_0H^{-1}Z_m^{-1})^{-1} (1 - EE_0^{-1}Z_0H_0H^{-1}Z_m^{-1}) \quad (\text{A.6})$$

Then,  $A$  is expressed in terms of  $A_1$  as

$$A = 2(1 - \Gamma\Psi\Gamma\Psi)^{-1}TA_1 \quad (\text{A.7})$$

Finally, the relationship between  $B_1$  and  $A_1$  is given as

$$B_1 = T^{-1}(\Gamma - \Psi\Gamma\Psi)(1 - \Gamma\Psi\Gamma\Psi)^{-1}TA_1 \quad (\text{A.8})$$

where

$$T = (1 + EE_0^{-1}Z_0H_0H^{-1}Z_m^{-1})^{-1}EE_0^{-1} \quad (\text{A.9})$$

From the boundary conditions at junction plane of Port 2, we have

$$B_2 = E_0E^{-1}[\Psi A + \Psi^{-1}B] \quad (\text{A.10})$$

By using previous relations for  $A$  and  $B$  in terms of  $A_1$ , we get

$$B_2 = 2E_0E^{-1}(1 - \Gamma)\Psi(1 - \Gamma\Psi\Gamma\Psi)^{-1}TA_1 \quad (\text{A.11})$$

Therefore, the modal scattering parameters relating the line incident and reflected waves are given by

$$\tilde{S}_{11} = T^{-1}(\Gamma - \Psi\Gamma\Psi)(1 - \Gamma\Psi\Gamma\Psi)^{-1}T \quad (\text{A.12})$$

$$\tilde{S}_{21} = 2E_0E^{-1}(1 - \Gamma)\Psi(1 - \Gamma\Psi\Gamma\Psi)^{-1}T \quad (\text{A.13})$$

The actual scattering parameters of the test system are obtained from modal scattering parameters using the eigenvectors of the reference systems as

$$S_{11} = E_0^{-1} \tilde{S}_{11} E_0$$
$$S_{12} = E_0^{-1} \tilde{S}_{12} E_0$$

By symmetry, the  $2n \times 2n$  scattering matrix is given as

$$S = \begin{bmatrix} S_{11} & S_{12} \\ S_{21} & S_{22} \end{bmatrix} \quad (\text{A.14})$$

## REFERENCES

- [1] L. W. Nagel, "SPICE2: A computer program to simulate semiconductor circuits," University of California, Berkeley, CA, Technical Report ERL-M520, May 1975.
- [2] W. T. Weeks, A. J. Jininez, G. W. Mahoney, D. Mehta, H. Qassemzadeh, and T. R. Scott, "Algorithms for ASTAP-A network analysis program," *IEEE Transactions of Circuit Theory*, vol. CT-20, pp. 628-634, November 1973.
- [3] *Saber User's Guide*, Release 3.1a, Analogy Inc., Beaverton, OR, 1993.
- [4] L. O. Chua and C. C. Chang, "High-speed non-linear circuit models of  $p$ - $n$  junction diodes," *International Journal of Circuit Theory and Applications*, vol. 16, pp. 157-190, 1988.
- [5] Y. P. Tsividis, *Operation and Modeling of the MOS Transistor*. New York, NY: McGraw-Hill, 1987.
- [6] S. McCormick and J. Allen, "Waveform moment methods for improved interconnection analysis," in *Proceedings of 27th Design Automation Conference*, June 1990, pp. 406-412.
- [7] L. Pillage, C. Wolff, and R. Rohrer, "AWesim: Asymptotic waveform evaluation for timing analysis," in *Proceedings of the 26th Design Automation Conference*, 1989.
- [8] L. Pillage and R. Rohrer, "Asymptotic waveform evaluation for timing analysis," *IEEE Transactions on Computer-Aided Analysis*, vol. CAD-9, no. 4, pp. 352-366, April 1990.
- [9] J. Bracken, V. Raghavan, and R. Rohrer, "Interconnect simulation with asymptotic waveform evaluation (AWE)," *IEEE Transactions on Circuits and Systems*, vol. CAS-39, no. 11, pp. 869-878, November 1992.
- [10] T. Tang and M. Nakhla, "Analysis of lossy multiconductor transmission lines using the asymptotic waveform evaluation technique," *IEEE Transactions on Microwave Theory and Technology*, vol. 39, no. 12, pp. 2107-2116, December 1991.

- [11] E. Chiprout and M. S. Nakhla, "Transient waveform estimation of high-speed MCM networks using complex frequency hopping," in *Proceedings of Multi-Chip Module Conference (MCMC)*, March 1993, pp. 134-139.
- [12] E. Chiprout and M. S. Nakhla, *Asymptotic Waveform Evaluation and Moment Matching for Interconnect Analysis*. Boston, MA: Klumer Academic Publishers, 1994.
- [13] K. Gallivan, E. Grimme, and P. Van Dooren, "Asymptotic waveform evaluation via Lanczos methods," *Applied Mathematics Letters*, vol. 7, pp. 75-80, 1994.
- [14] K. Gallivan, E. Grimme, and P. Van Dooren, "Padé approximation of large-scale dynamic systems with Lanczos methods," in *Proceedings of the 33rd Conference on Decision and Control*, Lake Buena Vista, FL, December 1994.
- [15] P. Feldmann and R. W. Freund, "Efficient linear circuit analysis by Padé approximation via the Lanczos process," *IEEE Transactions on Computer-Aided Design of Integrated Circuits and Systems*, vol. 14, no. 5, May 1995.
- [16] R. Sanaie, E. Chiprout, M. S. Nakhla, and Q. J. Zhang, "Integrating subnetwork characterized by measured data into moment-matching simulations," in *Proceedings Multi-Chip Module Conference*, March 1994, pp. 114-119.
- [17] F. Y. Chang, "Transient simulation of nonuniform coupled lossy transmission lines characterized with frequency-dependent parameters, Part II: Discrete-time analysis," *IEEE Transactions on Circuits and Systems*, vol. 39, pp. 907-927, Nov. 1992.
- [18] C. E. Baumgartner, "On the representation of coupled lossy transmission lines using transfer functions," *Ninth Annual International Phoenix Conference on Computers and Communications*, Scottsdale, AZ, March 21-23, 1990.
- [19] D. B. Kuznetsov and J. E. Schutt-Ainé, "Optimal transient simulation of transmission lines," *IEEE Transactions on Circuits and Systems-I: Fundamental Theory and Applications*, vol. 43, no. 2, February 1996.
- [20] M. Celik and A. C. Cangellaris, "Efficient transient simulation of lossy packaging interconnects using moment-matching techniques," *IEEE Transactions of Components, Hybrids, and Manufacturing Technology-Part B*, vol. 19, no. 1, February 1996.
- [21] C. Ho, A. Ruehli, and P. Brennan, "The modified nodal approach to network analysis," *IEEE Transactions on Circuits and Systems*, vol. CAS-22, pp. 504-509, June 1975.

- [22] L. O. Chua and P. Lin, *Computer Aided Analysis of Electronic Circuits: Algorithms and Computational Techniques*. Englewood Cliffs, NJ: Prentice-Hall, 1975.
- [23] J. Vlach and K. Singhal, *Computer Methods for Circuits Analysis and Design*, Berkshire, England: Van Nostrand Reinhold, 1983.
- [24] B. Chawla, H. Gummel, and P. Kozak, "MOTIS-An MOS timing simulator," *IEEE Transactions on Circuits and Systems*, vol. CAS-22, pp. 901-910, December 1975.
- [25] A. Newton, "The simulation of large scale integrated circuits," *IEEE Transactions on Circuits and Systems*, vol. CAS-26, pp. 741-749, Sept. 1979.
- [26] G. Arnout and H. De Man, "The use of threshold functions and Boolean-controlled network elements for macromodeling of LSI circuits," *IEEE Journal of Solid State Circuits*, vol. SC-13, pp. 326-332, June 1978.
- [27] H. De Man et al, "DIANA: Mixed mode simulator with a hardware description language for hierarchical design of VLSI," in *Proceedings of IEEE ICCDC'80 Conference*, Rye, NY, October 1980, pp. 356-360.
- [28] Y. Shih and S. Kang. "ILLIADS: A new fast MOS timing simulator using direct equation-solving approach," in *Proceedings of 28th ACM/IEEE Design Automation Conference*, 1991, pp. 20-25.
- [29] G. Hachtel and A. Sangiovanni-Vincentelli, "A survey of third-generation simulation techniques," in *Proceedings of the IEEE*, vol. 69, no. 10, October 1981.
- [30] I. N. Hajj, "Sparsity considerations in network solution by tearing," *IEEE Transactions Circuits and Systems*, vol. CAS-27, no. 5, pp. 357-366, May 1980.
- [31] G. De Micheli, H. Y. Hsieh, and I. Hajj, "Decomposition techniques for large scale circuits analysis, and simulation," in *Circuit Analysis, Simulation and Design 2*, A. E. Ruehli, Ed., Amsterdam, Netherlands: North Holland, 1987, pp. 1-39.
- [32] E. Lelarasmee, A. Ruehli, and A. L. Sangiovanni-Vincentelli, "The waveform relaxation method for time-domain analysis of large scale integrated circuits," *IEEE Transactions of Computer-Aided Design*, vol. CAD-1, no. 3, pp. 131-145, July 1982.
- [33] J. White and A. Sangiovanni-Vincentelli, *Relaxation Techniques for the Simulation Of VLSI Circuits*. Boston, MA: Kluwer-Academic Publishers, 1987.

- [34] E. Lelarasmee and A. Sangiovanni-Vincentelli, "RELAX: A new circuit simulator for large scale MOS integrated circuits," Electronic Research Laboratory, Memo UCB/ERL-M82/6, University of California, Berkeley, February 1992.
- [35] F. Y. Chang, "Waveform relaxation analysis of RLGC transmission lines," *IEEE Transactions on Circuits and Systems*, vol. CAS-37, pp. 1394-1415, Nov. 1990.
- [36] W. F. Ames, *Nonlinear Partial Differential Equations in Engineering*. New York, NY: Academic Press, 1965.
- [37] F. H. Branin, "Transient analysis of lossless transmission lines," in *Proceedings of IEEE*, vol. 55, November 1967, pp. 2012-2013.
- [38] F. H. Branin, "Comments on 'Transient analysis of lossy transmission lines'," in *Proceedings of IEEE*, June 1971, pp. 1022-1023.
- [39] F. Y. Chang, "Transient analysis of lossless coupled transmission lines in nonhomogeneous dielectric medium," *IEEE Transactions on Microwave Theory and Technology*, vol. 18, pp. 616-626, September 1970.
- [40] C. W. Ho, "Theory and computer-aided analysis of lossless transmission lines," *IBM Journal of Research and Development*, vol. 17, 1973, pp. 249-255.
- [41] N. Orhanovic, and V. K. Tripathi, "Nonlinear transient analysis of coupled RLCG lines by the method of characteristics," *International Journal of Microwave and Millimeter-Wave CAE*, vol. 2, no. 2, pp. 108-115, 1992.
- [42] A. Djordjevic, T. Sarkar, and R. Harrington, "Analysis of lossy transmission lines with arbitrary nonlinear terminations," *IEEE Transactions on Microwave Theory and Technology*, vol. 34, no. 6, June 1986.
- [43] J. Schutt-Ainé and R. Mittra, "Scattering parameter transient analysis of transmission lines loaded with nonlinear terminations," *IEEE Transactions on Microwave Theory and Technology*, vol. 36, no. 3, March 1988.
- [44] Q. Gu, Y. E. Yang, and A. Kong, "Transient analysis of frequency-dependent transmission line systems terminated with nonlinear loads," *Journal of Electromagnetic Waves and Application*, vol. 3, pp. 183-197, 1989.
- [45] D. Winklestein, M. B. Steer, and R. Pomerleau, "Simulation of arbitrary transmission line networks with nonlinear terminations," *IEEE Transactions on Circuits and Systems*, vol. 38, no. 4, pp. 418-422, April 1991.

- [46] J. S. Roychowdhury and D. O. Pederson, "Efficient Transient Simulation of Lossy Interconnect," in *28th ACM/IEEE Design Automation Conference*, June 1991, pp. 740-745.
- [47] T. Shibata, "Circuit simulations combined with electromagnetic field analysis," *IEEE Transactions on Microwave Theory and Techniques*, vol. 39, no. 11, pp. 1862-1868, November 1991.
- [48] P. B. Johns and M. O'Brien, "Use of the transmission line modelling (T.L.M.) method to solve nonlinear lumped networks," *Radio Electronic Engineering*, vol. 50, nos. 1-2, pp. 59-70, January-February 1980.
- [49] R. Voelker and R. Lomax, "A finite-difference transmission matrix method incorporating a nonlinear device," *IEEE Transactions on Microwave Theory and Techniques*, vol. 38, no. 3, pp. 302-312, March 1990.
- [50] W. Sui, D. A. Christensen, and C. H. Durney, "Extending the two-dimensional FDTD method to hybrid electromagnetic systems with active and passive lumped elements," *IEEE Transactions on Microwave Theory and Techniques*, vol. 40, no. 4, pp. 724-730, April 1992.
- [51] Y. Chen, P. Harms, R. Mittra, and W. Beyene, "Analysis of complex electronic packages using FDTD / TOUCHSTONE hybrid technique," *Microwave and Optical Technology Letters*, vol. 12, no. 6, pp. 313-315, August 1996.
- [52] S. D. Corey, K. J. Kerns, and A. T. Yang, "Automatic measurement-based characterization of lossy MCM line using lumped elements," *IEEE 5th Topical Meeting on Electrical Performance of Electrical Packaging*, Napa, CA, October 28-30, 1996.
- [53] W. T. Beyene and J. E. Schutt-Ainé, "Efficient transient simulation of high-speed interconnects characterized by sampled data," in *Proceedings of the 5th Tropical Meeting on Electrical Performance of Electrical Packaging*, Nappa, CA, October 28-30, 1997.
- [54] W. T. Beyene and J. E. Schutt-Ainé, "Integrating data obtained from electromagnetic field analysis into frequency- and time-domain circuit simulations," *13th Annual of Progress in Applied Computational Electromagnetics*, Monterey, CA, March 17-21, 1997.
- [55] T. Tang and M. Nakhla, "Analysis of high-speed VLSI interconnects using the asymptotic waveform evaluation technique," *IEEE Transactions on Computer-Aided Design*, vol. 11, no. 3, pp. 341-352, April 1992.



- [56] J. E. Bracken, V. Raghavan, and R. A. Rohrer, "Simulating distributed elements with asymptotic waveform evaluation," *IEEE MTT-s Digest*, pp. 1337-1340, September 1992.
- [57] S. Lin and E. Kuh, "Transient simulation of lossy interconnects based on the recursive convolution formulation," *IEEE Transactions on Circuits and Systems*, vol. CAS -39, no. 11, pp. 879-892, November 1992.
- [58] R. Sanaie and M. Nakhla, "A fast method for frequency and time domain Simulation of high-speed VLSI interconnects," *IEEE Transactions on Microwave Theory and Technology*, vol. 42, no. 12, pp. 2562-2571, December 1994.
- [59] M. Celik and A. C. Cangellaris, "Simulation of dispersive multiconductor transmission Lines by Padé approximation via the Lanczos process," *IEEE Transactions on Microwave Theory and Technology*, vol. 44, no. 12, pp. 2525-2535, December 1996.
- [60] W. C. Elmore, "The transient response of damped linear networks with particular regard to wide-band amplifiers," *Journal of Applied Physics*, vol. 19, no. 1, pp. 55-63, January 1948.
- [61] J. Rubinstein, P. Penfield, Jr., and M. A. Horowitz, "Signal delay in RC tree networks," *IEEE Transactions on Computer-Aided Design*, vol. CAD-2, no. 1, pp. 202-211, July 1983.
- [62] T. Lin and C.A. Mead, "Signal delay in general RC network," *IEEE Transactions on Computer- Aided Design*, vol. CAD-3, pp. 331-349, October 1984.
- [63] J. L. Wyatt, Jr. "Signal delay in RC mesh networks," *IEEE Transactions on Circuits and Systems*, vol. CAS-32, no. 5, pp. 507-510, May 1985.
- [64] C. Zukowski, *The Bounding Approach to VLSI Circuit Simulation*. Boston, MA: Kluwer Publishers, 1986.
- [65] Q. Yu, J. L. Wyatt, Jr., C. Zukowski, H. N. Tan, and P. O'Brien, "Improved bounds on signal delay in linear RC models for MOS interconnect," in *Proceedings of 1985 International Symposium on Circuits and Systems*, Kyoto, Japan, June 1985, pp. 903-906.
- [66] M. R. Hestenes and E. Stiefel, "Methods of conjugate gradients for solving linear systems," *Journal of Research of the National Bureau of Standards*, vol. 49, no. 6, pp. 409-439, December 1952.

- [67] M. H. Gutknecht, "A completed theory of the unsymmetric Lanczos process and related algorithms. Part I." *SIAM Matrix Analysis and Applications*, vol. 13, no. 2, pp. 594-639, April 1992.
- [68] Y. Saad, *Iterative Methods for Sparse Linear Systems*. Boston, MA: PWS Publishing Company, 1996.
- [69] F. Y. Chang, "Transient simulation of nonuniform coupled lossy transmission lines characterized with frequency-dependent parameters, Part II: Discrete-time analysis," *IEEE Transactions on Circuits and Systems*, vol. 39, pp. 907-927, November 1992.
- [70] R. J. Bowman and C. C. Brewster, "Determining the zeros and poles of linear circuit networks using function approximation," *IEEE Transactions on Computer-Aided Design*, vol. CAD-6, no. 4, pp. 678-689, July 1987.
- [71] C. E. Baumgartner, "On the representation of coupled lossy transmission lines using transfer functions," *Ninth Annual International Phoenix Conference on Computers and Communications*, Scottsdale, AZ, March 21-23, 1990.
- [72] A. J. Gruodis and C. S. Chang, "Coupled lossy transmission line characterization and simulation," *IBM Journal of Research and Development*, vol. 25, pp. 25-41, January 1981.
- [73] E. C. Levy, "Complex curve-fitting," *IRE Transactions on Automatic Control*, vol. AC-4, pp. 37-44, May 1959.
- [74] P. Van Dooren, "Numerical linear algebra techniques for large scale matrix problems in systems and control," in *Proceedings of the 31st Conference on Decision and Control*, Tucson, AZ, December 1992.
- [75] C. De Villemaigne and R. E. Skelton, "Model reductions using a projection formulation," *International Journal of Control*, vol. 46, no. 6, pp. 2141-2169, 1987.
- [76] I. M. Jaimoukha and E. M. Kasenally, "Oblique projection methods for large scale model reduction," *SIAM Journal of Matrix Analysis and Applications*, vol. 16, no. 2, pp. 602-627, April 1995.
- [77] D. L. Boley, "Krylov space methods on state-space control models," Department of Computer Science, University of Minnesota, Minneapolis, MN, Report No. TR92-18, March 1992.
- [78] C. Lanczos, "An iteration method for the solution of the eigenvalue problem for linear differential and integral operators," *Journal of Research of the National Bureau of Standards*, vol. 45, pp. 255-282, 1950.

- [79] W. E. Arnoldi, "The principle of minimized iterations in the solution of the matrix eigenvalue problem," *Quarterly Applied Mathematics*, vol. 9, no. 1, pp. 17-29, 1951.
- [80] Y. Saad, "Variations on Arnoldi's method for computing eigenelements of large unsymmetric matrices," *Linear Algebra and its Applications*, vol. 34, pp. 268-295, 1980.
- [81] D. L. Boley and G. H. Golub, "The Lanczos-Arnoldi algorithm and controllability," *Systems and Control Letters*, vol. 4, pp. 317-324, September 1984.
- [82] G. A. Baker, Jr. and P. Graves-Morris, "Padé Approximants," in *Encyclopedia of Mathematics and its Applications*, G. Rota, Ed., vols. 13-14. Reading, MA: Addison-Wesley, 1981.
- [83] C. T. Chen, *Linear System Theory and Design*. New York, NY: Holt, Rinehart and Winston, Inc., 1970.
- [84] F. R. Gantmacher, *The Theory of Matrices, Vol. I*. New York, NY: Chelsea Publishing Company, 1960.
- [85] N. S. Nahman and D. R. Holt, "Transient analysis of coaxial cables using skin effect approximation,  $A + B\sqrt{s}$ ," *IEEE Transactions on Circuit Theory*, vol. CT-19, pp. 443-451, September, 1972.
- [86] D. M. Triesenberg, "An efficient state variable transmission line model," *IEEE Transactions on Power Apparatus and Systems*, vol. PAS-98, no. 2, March/April 1979.
- [87] O. A. Palusinski and A. Lee, "Analysis of transients in nonuniform and uniform multiconductor transmission lines," *IEEE Transactions on Microwave Theory and Technology*, vol. 37, no. 1, January 1989.
- [88] J. G. Linvill, *models of transistors and diodes*. New York, NY: McGraw-Hill, 1963.
- [89] P. P Wang and F. H. Branin, "Multi-section network modeling of junction diodes," in *Proceedings 4th Annual Pittsburgh Conference on Modeling and Simulation*, Pittsburgh, PA, 1973, pp. 470-474.
- [90] F. Y. Chang, "Transient analysis of diode switching circuits including charge storage effects," *IEEE Transactions on Circuits and Systems-I: Fundamental Theory and Applications*, vol. 43, no. 3, March 1996.

- [91] P. Antognetti and G. Massobrio, *Semiconductor Device Modeling with SPICE*. New York, NY: McGraw-Hall, 1988.
- [92] J. L. Moll, S. Krakauer, and R. Shen, "P-N junction charge-storage diodes," in *Proceedings of the IRE*, January, 1962, pp. 43-53.
- [93] R. H. Kingston, "Switching time in junction diodes and junction transistors," in *Proceedings of the IRE*, vol. 42, May 1954, pp. 829-834.
- [94] B. Lax and S. F. Neustadter, "Transient response of a *p-n* junction," *Journal of Applied Physics*, vol. 25, pp. 1148-1154, September 1954.
- [95] Y. Liang and V. J. Gosbell, "Diode forward and reverse recovery model for power electronic SPICE simulations," *IEEE Transactions on Power Electronics*, vol. 5, pp. 356, July 1990.
- [96] P. O. Lauritzen and C. L. Ma, "A simple diode model with reverse recovery model," *IEEE Transactions on Power Electronics*, vol. 6, no. 2, pp. 188-191, April 1991.
- [97] A. T. Yang, Y. L. Liu and J. T. Yao, "An efficient nonquasi-static diode model for circuit simulation," *IEEE Transactions on Computer-Aided Design*, vol. 13, no. 2, pp. 231-239, February 1994.
- [98] W. T. Beyene and J. E. Schutt-Ainé, "Accurate diode forward and reverse recovery model using asymptotic waveform evaluation," in *Proceedings of International Symposium on Circuits and Systems*, Atlanta, GA, May 12-15, 1996, vol. I, pp. 625-628.
- [99] S. B. Goldberg, M. B. Steer, P. D. Franson, and J. S. Kasten, "Experimental electrical characterization of interconnects and discontinuities in high-speed digital systems," *IEEE Transactions of Components, Hybrids, and Manufacturing Technology*, vol. 14, no. 4, December 1991.
- [100] R. Wang and O. Wing, "Analysis of VLSI multiconductor systems by bi-level waveform relaxation," in *Proceedings of IEEE International Conference CAD*, October 1990, pp. 166-169.
- [101] W. T. Beyene, "Bi-level waveform relaxation analysis of package interconnects using scattering parameters," in *Proceedings of International Symposium on Microelectronics*, San Francisco, CA, 1992.
- [102] C. K. Sanathanan and J. Koerner, "Transfer function synthesis as a ratio of two complex polynomials," *IEEE Transactions on Automatic Control*, vol. AC-6, no. 1, pp. 56-58, January 1963.

- [103] E. J. Davison, "A method for simplifying linear dynamic systems," *IEEE Transactions on Automatic Control*, vol. AC-11, no. 1, January, 1966.
- [104] D. L. Fletcher and C. N. Weygandt, "A digital method of transfer function calculation," *IEEE Transactions on Circuit Theory*, vol. CT-18, pp. 185-187, January 1971.
- [105] M. J. Bosley and F. P. Lees, "A survey of simple transfer-function derivations from higher-order state-variable models," *Automatica*, vol. 8, pp. 765-775, Pergamon Press, 1972.
- [106] M. Silveira, I. Elfadel, J. White, M. Chilukuri, and K. Kenneth, "Efficient frequency-domain modeling and circuit simulation of transmission lines," *IEEE Transactions of Components, Hybrids, and Manufacturing Technology-Part B*, vol. 17, no. 4, Nov. 1994.
- [107] G. W. Stewart, *Introduction to Matrix Computations*. New York, NY: Academic Press, Inc., 1973.
- [108] G. Golub, "Numerical methods for solving linear least squares problems," *Numerische Mathematik*, vol. 7, pp. 206-216, 1965.
- [109] E. C. Chang and S. Kang, "Transient simulation of lossy coupled transmission lines using iterative linear least square fitting and piecewise recursive convolution," *IEEE Transactions on Circuits and Systems-1*, vol. 43, no. 11, November 1996.
- [110] B. C. Moore, "Principal component analysis in linear systems: Controllability, observability, and model reduction," *IEEE Transactions of Automatic Control*, AC-26, pp. 17-32, 1981.
- [111] Y. Jang, J. Kong, and J. H. Seo, "Balanced model reduction with guarantee performance in frequency range," in *Proceedings of the 33rd Conference on Decision and Control*, Lake Buena Vista, FL, December 1994.
- [112] K. Glover, "All optimal hankel-norm approximations of linear multivariable systems and their L-error bounds," *International Journal of Control*, vol. 39, pp. 1115-1193, June 1984.
- [113] R. H. Bartels and G. W. Stewart, "Solution of the Matrix Equation  $AX+XB=C$ ," *Communication of the ACM*, vol. 15, no. 9, pp. 820-826, September 1972.
- [114] A. K. Sinha and J. Pal, "Simulation based reduced order modelling using clustering technique," *Computers and Electrical Engineering*, vol. 16, no. 3, pp. 159-169, 1990.

- [115] J. Umoto and T. Hara, "A new digital analysis of surge performance in electric power networks utilizing the convolution integral," *Journal of the Institute of Electrical Engineers in Japan*, vol. 91, no. 3, pp. 48-57, 1971.
- [116] A. Semlyen and A. Dabuleanu, "Fast and accurate switching transient calculations on transmission lines with ground return using recursive convolutions," *IEEE Transactions on Power Apparatus and Systems*, vol. PAS-94, no. 2, March/April 1975.
- [117] F. Y. Chang, "Transient simulation of frequency-dependent nonuniform coupled lossy transmission lines with double orthogonal expansions and recursive convolution integrations," *1993 Multi-Chip Module Conference*, Santa Cruz, CA, March 1993.
- [118] J. E. Schutt-Ainé and R. Mittra, "Nonlinear transient analysis of coupled transmission lines," *IEEE Transactions on Circuits and Systems*, vol. 36, no. 7, pp. 959-967, July 1989.
- [119] J. Schutt-Ainé and R. Mittra, "Scattering parameter transient analysis of transmission lines loaded with nonlinear terminations," *IEEE Transactions on Microwave Theory and Techniques*, vol. 36, no. 3, March 1988.
- [120] T. K. Liu and F. M. Tesche, "Analysis of antennas and scattering with nonlinear loads," *IEEE Transactions on Antennas and Propagation*, vol. AP-24, pp. 131-139, March 1976.
- [121] M. L. Van Blaricum and R. Mittra, "A technique for extracting the poles and residues of a system directly from its transient response," *IEEE Transactions on Antennas Propagation*, vol. AP-23, no. 6, pp. 777-781, November 1975.
- [122] T. K. Sarkar, D. D. Weiner, and V. K. Jain, "Suboptimal approximation/identification of transient waveforms from electromagnetic systems by pencil-of-function method," *IEEE Transactions on Antennas Propagation*, vol. AC-28, no. 6, pp. 928-933, November 1980.
- [123] J. E. Schutt-Ainé, "Static analysis of V transmission lines," *IEEE Transactions on Microwave Theory and Techniques*, vol. 40, no. 4, April 1992.
- [124] S. B. Haley, "The generalized eigenproblem: Pole-zero computation," *Proceedings of the IEEE*, vol. 76, no. 2, February 1988.
- [125] E. Grimme, D. Sorensen, and P. Van Dooren, "Model reduction of state space systems via an implicitly restarted Lanczos method," *Numerical Algorithms*, vol. 12, 1996.

- [126] A. Ruhe, "Rational Krylov sequence methods for eigenvalue computation," *Linear Algebra and Its Applications*, vol. 58, pp. 391-405, 1984.
- [127] A. Ruhe, "The Rational Krylov algorithm for nonsymmetric eigenvalue problems II: Matrix pairs," *Linear Algebra and Its Applications*, vol. 197, pp. 283-295, 1994.
- [128] A. Ruhe, "The Rational Krylov algorithm for nonsymmetric eigenvalue problems III: Complex shifts for real matrices," *BIT*, vol. 34, pp. 165-176, 1994.
- [129] K. Gallivan and E. Grimme, "A rational algorithm for model reduction," *Numerical Algorithms*, vol. 12, pp. 33-63, 1996.

## CURRICULUM VITAE

Wendemagegnehu Tsegaye Beyene received his elementary and secondary education in Addis Ababa, Ethiopia, graduating from Misrak Comprehensive High School in 1981. While attending high school, he played soccer at a national level as a member of the Ethiopian Youth National Soccer Team and later, as a member of the Ethiopian National Soccer Team. In 1983, he went to Budapest, Hungary, to pursue a higher education. After attending Budapest Technical University for two semesters, and spending six months in Rome, Italy, he came to the United States. He attended Columbia University in New York City where he received the B.S. degree in Electrical Engineering in May 1988. From July 1988 to February 1995, he was with the Intentional Business Machine Microelectronics division in East Fishkill, New York, where he worked on the electrical analysis of advanced electronic packages. While working at IBM, he obtained an M.S. degree in Electrical Engineering from Columbia University in May 1991. He has held a professional trainee position at the Ford Research Laboratory in Dearborn, Michigan in the summer of 1994. Since 1994, he has held a teaching and research assistant position at the University of Illinois at Urbana-Champaign, while pursuing a doctoral degree in the department of Electrical and Computer Engineering.

Dr. Beyene is a member of Eta Kappa Nu, Tau Beta Pi, the Institute of Electrical and Electronics Engineers, and the Society of Industrial and Applied Mathematics. He is a licensed soccer coach registered with the United States Soccer Federation. He is the co-author of the following publications.

1. W. Beyene, H. Hamel, and S. Kadakia, "Design and measurement techniques for packages requiring equal net delays," *Electronic Packaging ITL Conference*, San Jose, CA, 1991.



2. S. Kadakia, W. Beyene, and H. Bhatia, "Repair and EC technique for advanced packaging application," *Electronic Packaging ITL Conference*, San Jose, CA, 1991.
3. W. T. Beyene, "Characterization of advanced package interconnects using scattering parameters," IBM East Fishkill, NY, Technical Report TR 22-362, 1992.
4. W. T. Beyene, S. D. Kadakia, and S. P. Antippas, "Reliability of a multichip carrier mounted on a large glass substrate," *Electronic Packaging ITL Conference*, Endicott, NY 1992.
5. W. T. Beyene, "Bi-level waveform relaxation analysis of package interconnects using scattering parameters," in *Proceedings of International Symposium on Microelectronics*, San Francisco, CA, 1992.
6. S. Kadakia, W. Beyene, T. Donovan, and H. Bhatia, "Advanced design and modeling for manufacturability of a hybrid package," in *Proceedings of the International Conference and Exhibition on Multichip Modules*, Denver, CO, April 14-16, 1993.
7. W. T. Beyene and J. E. Schutt-Ainé, "Accurate diode forward and reverse recovery model using asymptotic waveform evaluation," in *Proceedings of International Symposium on Circuits and Systems*, Atlanta, GA, May 12-15, 1996.
8. Y. Chen, P. Harms, R. Mitra, and W. Beyene, "Analysis of complex electronic packages using FDTD-TOUCHSTONE hybrid technique," *Microwave and Optical Technology Letter*, August 20, 1996.
9. W. T. Beyene and J. E. Schutt-Ainé, "Krylov subspace based model-order reduction techniques for circuit simulation," in *Proceedings of 39th Midwest Symposium on Circuits and Systems*, Ames, IA, August 18-21, 1996.
10. W. T. Beyene and J. E. Schutt-Ainé, "Efficient transient simulation of high speed interconnects characterized by sampled data," *5th Topical Meeting on Electrical Performance of Electronic Packaging*, Napa, CA, October 28-30, 1996.
11. Y. Chen, R. Mitra, P. Harms, and W. Beyene, "A technique for deriving the equivalent circuit of an SOP package using the FDTD in conjunction with TOUCHSTONE hybrid technique for equivalent circuits modeling of electronic packages," *5th Topical Meeting on Electrical Performance of Electronic Packaging*, Napa, CA, October 28-30, 1996.
12. W. T. Beyene and J. E. Schutt-Ainé, "Transient analysis of diode switching circuits using asymptotic waveform evaluation," submitted to *IEEE Transactions on Computer-Aided Design of Integrated Circuits and Systems*.

13. Y. Chen, P. Harms, R. Mittra, and W. Beyene, "A FDTD-TOUCHSTONE hybrid technique for equivalent circuits modeling of electronic packages," submitted to *IEEE Transactions on components, Packaging, and Manufacturing Technology-Part B: Advanced Packaging*.
14. W. T. Beyene and J. E. Schutt-Ainé, "Efficient transient simulation of high-speed interconnects characterized by sampled data," submitted to *IEEE Transactions on components, Packaging, and Manufacturing Technology-Part B: Advanced Packaging*.
15. W. T. Beyene and J. E. Schutt-Ainé, "Accurate frequency-domain modeling and efficient circuit simulation of high-speed packaging interconnects" submitted to *IEEE Transactions on Microwave Theory and Techniques*.
16. W. T. Beyene and J. E. Schutt-Ainé, "Nonlinear analysis of arbitrary coupled transmission lines using robust low-order rational approximations," to be submitted to *IEEE Transactions on Circuits and Systems-1*.
17. W. T. Beyene and J. E. Schutt-Ainé, "Integrating data obtained from electromagnetic field analysis into circuit simulations," in *13th Annual Review of Progress in Applied Computational Electromagnetic*, Monterey, CA, March 17-21, 1997.
18. W. T. Beyene and J. E. Schutt-Ainé, "Order-reduction techniques for packaging and interconnect simulation," in *Progress in Electromagnetics Research Symposium*, Boston, MA, July 17-21, 1997.
19. W. T. Beyene and J. E. Schutt-Ainé, "Analysis of frequency-dependent transmission lines using rational approximation and recursive convolution," in *Workshop on Signal Propagation on Interconnects*, Trarmsünde, Germany, May 14-16, 1997.
20. W. T. Beyene and J. E. Schutt-Ainé, "Model-order reduction techniques for circuits and interconnects simulation," University of Illinois at Urbana-Champaign, Electromagnetics Laboratory Technical Report No. 97-1, February 1997